October 2019

Designing Ion-Containing Polymers with Controlled Structure and Dynamics

Joshua Enokida

DESIGNING ION-CONTAINING POLYMERS WITH CONTROLLED STRUCTURE AND DYNAMICS

A Dissertation Presented

by

JOSHUA S. ENOKIDA

Submitted to the Graduate School of the
University of Massachusetts Amherst in partial fulfillment
of the requirements for the degree of

DOCTOR OF PHILOSOPHY

September 2019

Polymer Science and Engineering

DESIGNING ION-CONTAINING POLYMERS WITH CONTROLLED STRUCTURE AND DYNAMICS

A Dissertation Presented

by

JOSHUA S. ENOKIDA

Approved as to style and content by:

_____
E. Bryan Coughlin, Chair

_____
David A. Hoagland, Member

_____
Sarah L. Perry, Member

_____
E. Bryan Coughlin, Department Head
Polymer Science and Engineering

ACKNOWLEDGMENTS

Foremost, I would like to thank my advisor, Professor Bryan Coughlin. Without his guidance and support, I would not have become the scientist I am today. He is a great mentor, both academically and professionally, and I have gained much wisdom from our time together these last five years. I look forward to our future correspondence and applying what I have learned from you to my upcoming endeavors.

I would also like to thank my committee members Professor David Hoagland and Professor Sarah Perry for contributing their insight and feedback to my work. I greatly appreciated the time and effort they have spent evaluating my science, and I have thoroughly enjoyed our discussions. Your thought-provoking questions and willingness to challenge me have compelled me to become a better scientist and presenter.

I have had the great pleasure of working with several exceptional scientists throughout my time in graduate school. Without their assistance, I would not have been able to complete my research projects. I would specifically like to thank Dr. Vijesh Tanna, Dr. Huagao Fang, and Professor Henning Winter for their help with the rheology experiments and analysis, Dr. Weiguo Hu for his help with the solid-state NMR, Dr. Rick Beyer and Dr. Brian Morgan at ARL for their assistance with SAXS, and the Department of Defense for financial support of my work through the National Defense Science and Engineering Graduate Fellowship.

Of course, I have to thank the Coughlin Research group. Throughout the years, I have been surrounded by awesome groupmates. I would like to thank Dr. Patrick Homyak, Dr. Piril Ertem, Dr. Xiaohui Liu, Dr. WenXu Zhang, Dr. Brian Cromer, and Katie Williams for their excellent mentorship during my first few years, and Dr. Rohit Gupta and Dr.

Chinomso Nwosu for their friendship, intellectual discussions, and frequent Blue Wall lunches. I also have to thank the current group, Huyen Vu, Christian Steinmetz, Yifeng Du, and Ria Ghosh. The last few years have been great largely due to our light-hearted office antics and impromptu group lunches. Additionally, I would like to thank the past visiting Mainz students Dr. Rebeccca Klein, Nico Alleva and Matay Kaplan and my former undergraduate researcher, Andreas Muller.

Throughout my time in graduate school, I have had two amazing sets of roommates: Dr. Vijesh Tanna, Dr. Nick Posey, Dr. Ben Yavitt, and Dr. Cristiam Santa; Dan Camarda and Huyen Vu. You all truly made my graduate school experience special and will always be some of my dearest friends.

A big thanks goes out to the Class of 2014. It has been great going through the different stages of graduate school with you all, and I can't wait to see what the future holds for everyone. I would like to specifically thank Dr. Matt Lampe, Dr. Mike Kwansy, and Dr. Marcus Cole for their friendships. I would also like to acknowledge the entire PSE community. I really enjoyed interacting with everyone throughout Conte. A few people I would like to mention include Dr. George Chang, Dr. Jack Ly, Dr. Ryan Selhorst, Dr. Kara Martin, Steve Rosa, Chris Hango, Robert Enright, Marcel Brown, the game night crew (Hazel Davis, Zach Fink, and Emily Maling), and the Renegades softball team. I will always look back at our times together fondly.

Lastly, I would like to thank my family. Without your love and support, none of this would be possible. Your belief in me has kept me going through all stages of my life. I would specifically like to thank my Grandpa who was the first one to encouraged me to pursue my doctorate.

ABSTRACT

DESIGNING ION-CONTAINING POLYMERS WITH CONTROLLED STRUCTURE AND DYNAMICS

SEPTEMBER 2019

JOSHUA S. ENOKIDA, B.S., VIRGINIA POLYTECHNIC INSTITUE AND STATE AND UNIVERSITY

M.S., UNIVERSITY OF MASSACHUSETTS AMHERST

Ph.D., UNIVERSITY OF MASSACHUSETTS AMHERST

Directed by: Professor E. Bryan Coughlin

Ion-containing polymers are a unique class of materials for which strong electrostatic interactions dictate physical properties. By altering molecular parameters, such as the backbone chemical structure, the ion content, and the ion-pair identity, the structure and dynamics of these polymers can be altered. Further investigation of the molecular parameters that govern their structure-property relationships is critical for the future development of these polymeric materials. Particularly, the incorporation of ammonium-based counterions into these polymers offers a facile method to tune their electrostatic interactions and hydrophobicity. Applying this concept, a bulky dimethyloctylammonium (DMOA) counterion was used to modify the organic solubility of styrenesulfonate in order to facilitate its direct solution copolymerization with isoprene. With these poly(isoprene-*ran*-styrenesulfonate) (P(I-*ran*-SS)) copolymers the effect of ion content and the counterion identity on the structure and dynamics were evaluated.

In the first project, poly(isoprene-*ran*-dimethyloctylammonium styrenesulfonate) (P(I-*ran*-DMOASS)) copolymers with high molecular weights and dimethyloctylammonium styrenesulfonate (DMOASS) compositions ranging between 8

and 40 mol% (30 - 77 wt%) were synthesized via nitroxide-mediated polymerization. Thermal and viscoelastic characterization revealed distinct behaviors for the low (30 - 51 wt%) and high (56 - 77 wt%) DMOASS content copolymers. Three structural regimes were identified: ion clusters (30 wt% DMOASS), continuous ionic phase (56 - 77 wt% DMOASS), and the coexistence of the two (42 - 51 wt% DMOASS). As DMOASS content increased, small angle X-ray scattering revealed a gradual transition from the characteristic ion cluster structure to a smaller, more regular backbone-backbone structure associated with a continuous ionic phase. The ion clusters acted as physical crosslinks and introduced additional elasticity into the low DMOASS content copolymer, while the continuous ionic phase showed restricted flow behavior and the disappearance of a definitive plateau modulus. Dynamic mechanical analysis revealed two distinct T_g's at intermediate DMOASS content, indicating the coexistence of both structures.

In the second project, the role of counterion sterics on the structure and dynamics of a low glass transition temperature, amorphous P(I-*ran*-SS) at low ion contents (7 mol%) was investigated using a series of symmetric, tetraalkylammonium counterions with methyl (TMA), ethyl (TEA), propyl (TPA), and butyl (TBA) pendent groups in addition to a sodium cation control. A detailed analysis of the aggregate structure was achieved by fitting the X-ray scattering profiles with a modified hard sphere model. Increasing the counterion sterics from sodium to TEA resulted in slight changes to the aggregates with some ionic groups present in the isoprene matrix. For the more sterically hindered TPA and TBA counterions, considerable disruption of the structure occurs. Using solid-state NMR, dynamic mechanical analysis, and rheology, the effect of the counterion sterics on the copolymer dynamics was determined. The larger counterions exhibited an increase in

the dynamic moduli at high frequency while decreasing the dynamic moduli at lower frequencies in addition to possessing faster molecular dynamics. These two observations correspond to the incorporation of more ionic groups into the isoprene matrix and weakening of the dipole-dipole interactions, respectively.

Lastly, binary mixtures of TMA and TBA ammonium counterions were employed in these P(I-*ran*-SS) copolymers. The P(I-*ran*-SS) ionomers with TMA:TBA weight ratios of 100:0, 75:25, 50:50, 25:75, and 0:100 were prepared through solution blending. The SAXS profiles and Kinning-Thomas fitting showed only slight structural changes between 100:0 and 50:50, while major modification of the structure appears once the ratio reaches 75:25 and above. The alterations of the structure also indicated a mixed counterion aggregate structure. The linear viscoelastic characterization of the mixed counterion ionomers showed an increase in the polymer dynamics at low frequencies with increasing TBA weight percentages. Additionally, preliminary tensile tests were collected that showed increased mechanical properties with the stronger electrostatic interaction associated with TMA counterions. Thus, the structure and properties of these low T_g, amorphous ionomers can be specifically tuned by using multiple counterions.

Through these studies, the role of both ion content and counterion identity on the structure and dynamics of low T_g, amorphous P(I-*ran*-SS) copolymers have been elucidated. Furthermore, ammonium-based cations have been shown to offer a versatile means to modify both the ion aggregate structure and interaction strength of an ionomer. Appropriate selection of the pendent groups and mixture of different counterions allow for the properties of the ionomer to be freely tuned.

TABLE OF CONTENTS

Page

LIST OF TABLES

Table Page

LIST OF FIGURES

LIST OF ABBREVIATIONS

ATR-IR	Attenuated total reflectance infrared
ATRP	Atom transfer radical polymerization
CP	Cross polarization
DMA	Dynamic mechanical analysis
DMOA	Dimethyloctylammonium
DMOASS	Dimethyloctylammonium styrenesulfonate
DP	Degree of polymerization
DSC	Differential scanning calorimetry
HAADF-STEM	High-angle annular dark-field scanning transmission electron microscopy
K-T	Kinning-Thomas
MAXS	Medium-angle X-ray scattering
MWCO	Molecular weight cut-off
Na-SPS	Sodium neutralized sulfonated polystyrene
Na^+	Sodium cation
NMP	Nitroxide-mediated polymerization
NMR	Nuclear magnetic resonance
P(I-*ran*-DMOASS)	Poly(isoprene-*ran*-dimethyloctylammonium styrenesulfonate)
P(I-*ran*-SS)	Poly(isoprene-*ran*-styrenesulfonate)
PDMOASS	Poly(dimethyloctylammonium styrenesulfonate)
PI	Polyisoprene
R_I	Radius of ion aggregate
R_{ca}	Radius of closest approach
SAOS	Small-angle oscillatory shear
SAXS	Small-angle X-ray scattering
SPS	Sulfonated polystyrene
SS	Styrenesulfonate
TBA	Tetrabutylammonium
TEA	Tetraethylammonium
T_g	Glass transition temperature
TGA	Thermogravimetric analysis
TMA	Tetramethylammonium
TPA	Tetrapropylammonium
TTS	Time-temperature superposition
V_p	Volume of sample per aggregate
WLF	Williams-Landel-Ferry

CHAPTER 1

INTRODUCTION

With the growing demand for new polymeric materials to accommodate modern technologies, ion-containing polymers have attracted a considerable attention due to their unique bulk and solution properties.[1,2] These properties stem from the incorporation of covalently-bound ionic groups along the polymer chain. These ionic groups introduce strong electrostatic interactions into the polymeric materials that directly alter their physical properties. In the bulk, beneficial properties such as improved mechanical strength,[3] increased polymer-polymer miscibility,[4] and ability to facilitate ion transport[5] have been observed. These properties make ion-containing polymers compelling materials for applications such as new polymer composites,[6] self-healing materials,[7] actuators,[8,9] water purification membranes,[10] and ion exchange membranes for fuel cells and batteries.[5,11] A substantial literature already exists on these material, but a better understanding of their structure-property relationship is still necessary to further develop these materials for advanced applications.

1.1. Introduction to Ion-Containing Polymers

Ion-containing polymers encompass a broad range of polymeric materials. As the term implies, these polymers possess some quantity of ionic groups within their chemical structure, and in this dissertation, specifically refers to polymers where the ionic groups are covalently attached to the polymer backbone (thus polymers containing dissolved salts will not be considered). This classification can be further divided into various sub-categories based on characteristics such as ion content (ionomer versus polyelectrolyte), ionic group identity (polycation, polyanion, or polyzwitterion), and ionic group placement (ionene).

The work presented in this chapter, and throughout the dissertation, will focus mainly on ionomers with pendent ionic groups and will provide a detailed overview of the structure-property relationship of these polymers.

1.1.1. Polyelectrolytes versus Ionomers

As alluded to previously, a predominant method to distinguish different ion-containing polymers is through the quantity of ionic repeat units present in the polymer chain. Based on this metric, these polymers can then be classified into two categories, polyelectrolytes and ionomers. It important to note that while the ion content can be used to differentiate between these two categories, there is not a definitive ion content that separates these two groups. Due to this ambiguity, the corresponding physical properties of the polymer also need to be considered.[1,12] A depiction of a polyelectrolyte and an ionomer is shown in Figure 1.1a and 1.1b, respectively.

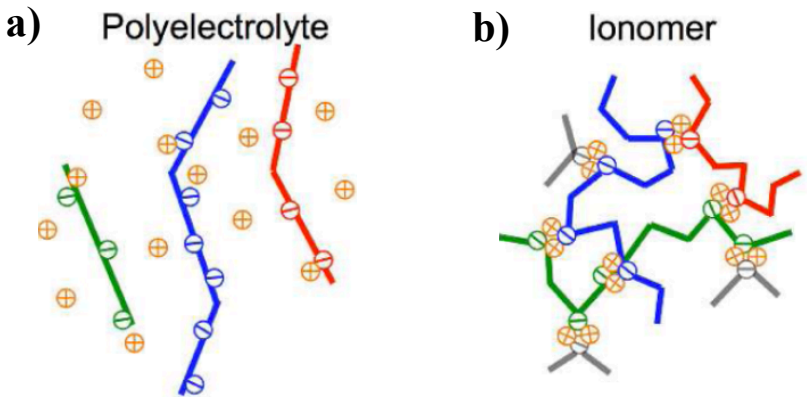

Figure 1.1. Depiction of a) polyelectrolytes and b) ionomers (image taken from ref. 12)

In general, polyelectrolytes are typically defined by higher quantities of ionic groups which dissociated when dissolved in high dielectric constant solvents. Thus, their properties are dictated by electrostatic interactions. These electrostatic interactions correlate over larger distances compared to their uncharged counterparts and produce an

extend chain configuration when no additional salt is present (Figure 1.1a).[2,12,13] From a practical standpoint, the ionic groups in polyelectrolytes offer advantageous interactions that are often used to control the flow and stability of various multi-component solution-based products (e.g. cosmetics) and processes (e.g. flocculation agents for water purification).[14]

Ionomers, on the other hand, possess a low fraction of ionic groups (classically < 20 mol %) and produce mechanically robust materials. The ionic groups in these polymers microphase-separate into nanoscale aggregates known as "ion clusters" (Figure 1.1b).[1,12,13] These structures greatly alter the overall physical behavior of these copolymer, acting as thermoreversible physical crosslinks between the polymer chains. The strength and dynamics of these ionic structures confers upon these polymers improved mechanical strength, melt viscosity, and puncture/scratch resistance.[1,15] As the research field has progressed, the definition of ionomers has been expanded to include all ionic polymers that contain this characteristic ion cluster structure and their resulting physical properties.[12]

1.1.2. Molecular Variables for Designing Ionomers

A broad range of polymers fall into the ionomer sub-category, and several aspects of the ionomer molecular structure can be altered to obtain desired properties. Specifically, four noteworthy molecular variables will be discussed: (1) the backbone chemical structure, (2) the ion content, (3) the ionic group identity, and (4) the counterion identity. Figure 1.2 further elaborates on these variables and shows several examples within the different groups. These variations in chemical structure control the overall properties of the ionomer by changing the characteristics of the matrix, the structure of the ion aggregates, and the strength of the ionic interactions within the aggregates.

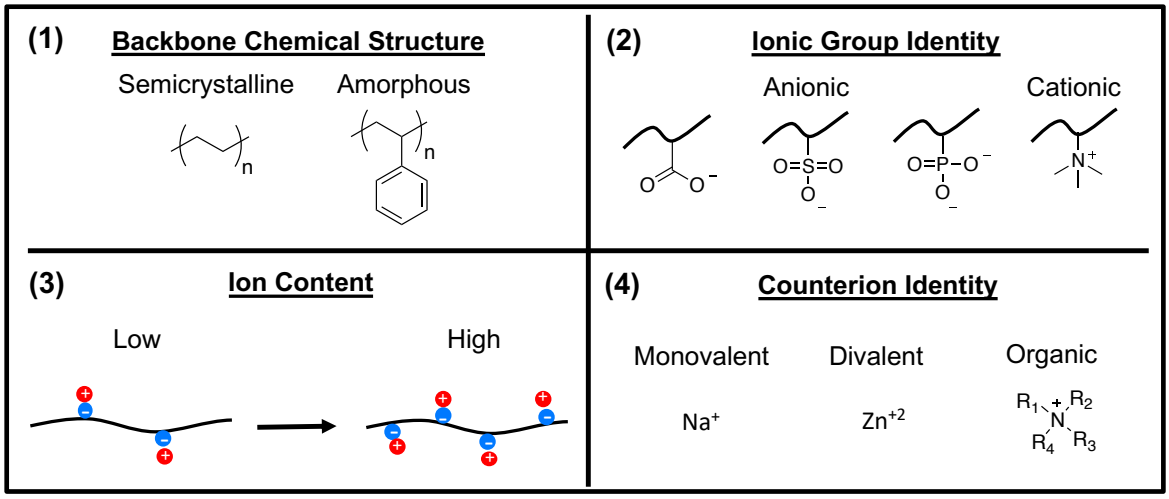

Figure 1.2. Graphical representation of the molecular design variables for ionomers

For instance, the chemical structure of the polymer backbone dictates the physical properties of the polymer matrix, which can be either semicrystalline or amorphous with a glass transition temperature above (high T_g) or below (low T_g) room temperature. These matrix characteristics also affect the size and shape of the ion cluster structures, which will be discussed in a later section. When increasing the ion content of an ionomer, by changing either the number of ionizable units or the degree of neutralization, an increased number density of ion aggregates occurs, and as long as the characteristic ion cluster structure remains, the copolymer is still categorized as an ionomer. The ionic group identity can be varied between ionic groups such as carboxylate and sulfonates or even cationic groups such as quaternary ammonium and phosphoniums. This parameter alters the strength of the dipole-dipole interactions that will in turn affect the organization of the ionic groups and association-dissociation lifetime of the ionic groups. Similar effects can also be achieved by altering the corresponding counterion in these ionomers. A full discussion of all of these different parameters will be presented in the context of their synthesis, structure and corresponding dynamics.

1.2. Synthetic Strategies to Afford Ionomers

The synthesis and characterization of ionomers has proven to be challenging due to the contrasting polarities of the hydrophilic ionic monomer and hydrophobic comonomer. To overcome this chemical mismatch, alternative synthetic methods have been developed to obtain various ionomer structures. In this section, the conventional methods for the synthesis of ionomer possessing covalently-bound anionic groups, such as carboxylate and sulfonates, will be discussed in addition to recent synthetic advances that have expanded the scope of accessible ionomer chemical structures.

1.2.1. Conventional Synthesis of Ionomers

In the early development of ionomer synthesis, polymer chemists relied on acrylic acid monomers as the ionizable group.[16–20] These acrylic acid monomers provide an uncharged precursor that can be copolymerized with a variety of hydrophobic comonomers. Following polymerization, neutralizing of the carboxylic acid functional groups with an inorganic base, in solution or the melt, converts the copolymer into the corresponding ionomer. This methodology has been successfully used to synthesize the commercially relevant metal neutralized poly(ethylene-*co*-acrylic acid) ionomer (Surlyn®). As shown in Figure 1.3, the synthesis of this ionomer proceeds through a high pressure, free radical copolymerization of ethylene with (meth)acrylic acid.[21] Controlling the copolymer's composition and degree of neutralization allows for the facile synthesis of ionomer with targeted thermal and mechanical properties. This synthetic methodology, however, is limited to carboxylic acid groups due to problematic side reactions when using stronger acids.

Neutralized Carboxylic Acid Copolymers

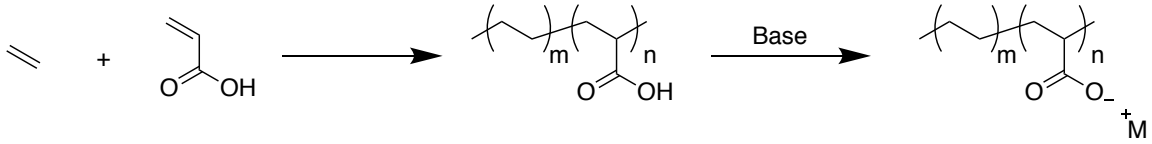

Post-Polymerization Sulfonation

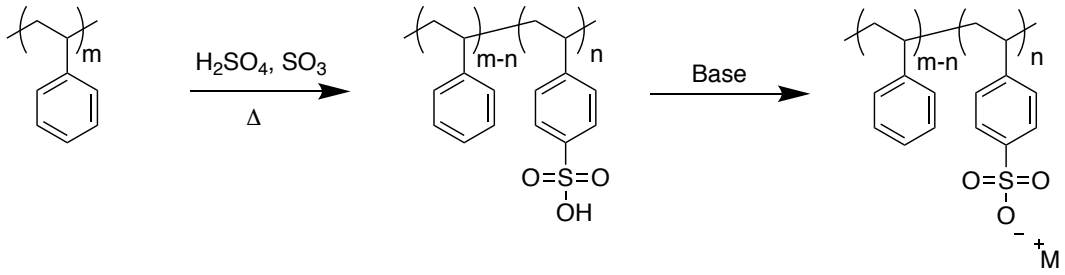

Figure 1.3. Conventional synthetic routes to afford ionomers

As the field progressed, ionomers containing stronger acidic groups such as sulfonates were desired. These sulfonate groups provide stronger electrostatic interactions compared to their carboxylate counterparts;[1] however, the synthesis of these sulfonated polymer is more difficult due to the instability of the unionized sulfonic acid monomers. Thus, synthesizing these copolymers can be achieved by either 1) direct copolymerizing the neutralized sulfonate with the hydrophobic comonomer via an emulsion polymerization or 2) performing a post-polymerization sulfonation reaction to add the sulfonate group onto the polymer backbone.

In the direct synthesis via an emulsion polymerization, the two phases provide a pathway to overcome the limitations of the contrasting monomer polarities, and copolymers containing low compositions of ionic monomers can be synthesized.[22] This synthetic methodology has been used to copolymerize sodium styrenesulfonate with a

variety of comonomers, such as styrene,[23] butadiene,[24,25] and isoprene.[25] Still, the emulsion polymerization method does not allow for the desired macromolecular precision of these ionomers. For instance, Siadat found that the composition of the copolymer synthesized could be controlled, but styrenesulfonate conversion showed a significant dependence on the reaction conversion in which the percent of styrene sulfonate incorporation decreased with the overall monomer conversion. Additionally, previous studies show evidence of heterogeneous incorporation of sodium styrenesulfonate into the polymer chain that alters the structure,[26] solubility,[24] and thermal properties of the ionomer.[27]

The synthetic challenges that plague the emulsion polymerization strategy can be overcome by employing a post-polymerization sulfonation technique (Figure 1.3). This synthesis route avoids the initial problem of monomer incompatibility by incorporating charged functionality into the polymer backbone after polymerization.[5,22] The addition of the sulfonate group results from an electrophilic substitution of a sulfonating reagent (sulfuric acid, sulfur trioxide, acetyl sulfate, etc.) onto an aromatic ring or double bond located along, or pendent to, the polymer backbone. This synthetic strategy has been used to produced sulfonated polystyrenesulfonate[28–32] and incorporate ionic groups on various engineering polymer such as poly(aryl ether ether ketones), poly(aryl ether sulfones), and poly(imides).[5] Additionally, post-polymerization sulfonation of ethylene-propylene-diene monomer rubbers to afford elastomeric ionomers. The harsh reaction conditions limits the sulfonation approach to select aromatic and double bond-containing polymers and also suffers from a lack of control over sulfonation placement.[33] Furthermore, polymers with a high quantity of double bonds, such as polydienes, undergo various side reactions, which

lead to the formation of chemical crosslinks and cyclized polymers.[22,34] Thus, new approaches are necessary to synthesize polymer with these structures.

1.2.2. New Approaches for Ionomer Synthesis

With advances in both monomer and polymer synthesis, alternative synthetic routes have been developed that offer access to an expanded library of ionomers. Specifically, for sulfonated ionomers, two new methods exist that allow for the direct solution copolymerization of these sulfonated monomer with hydrophobic comonomers. The first method involves using protecting groups to convert the sulfonate into an uncharged precursor monomer. The most common protected sulfonate monomers used in literature are styrenesulfonate esters.[35–37] In these studies, the sodium styrenesulfonate is first converted to styrenesulfonyl chloride using a chlorinating agent such as thionyl chloride. The styrenesulfonyl chloride is then reacted with a primary alcohol in the presence of a weak base to obtain the sulfonate ester. These sulfonate ester monomers have been successfully polymerized using free radical,[35] atom transfer radical polymerization (ATRP),[36] and nitroxide-mediated polymerization (NMP).[38] Following the copolymerization, treating the polymer with a base hydrolyzes the sulfonate ester and recovers the ionic sulfonate functionality. While this method does work, the additional synthetic steps to afford the nonionic sulfonated monomer leaves opportunity to develop simplified monomer modification chemistries.

An alternative, less laborious synthetic approach that has recently been used is the counterion exchange modification, which has been recently reviewed by Cavicchi.[39] The counterion exchange method relies on bulky ammonium counterions to improve the hydrophobicity of the sulfonated monomer and allow for their copolymerization with

nonpolar comonomers in organic solvents. Figure 1.4 shows different sulfonate monomers with various ionic liquid counterions that have been explored in literature.[39] Various controlled radical polymerizations have been investigated using this synthetic method and has permitted access to a breadth of new polymer chemical structures and architectures as shown in Figure 1.4. [39–42]

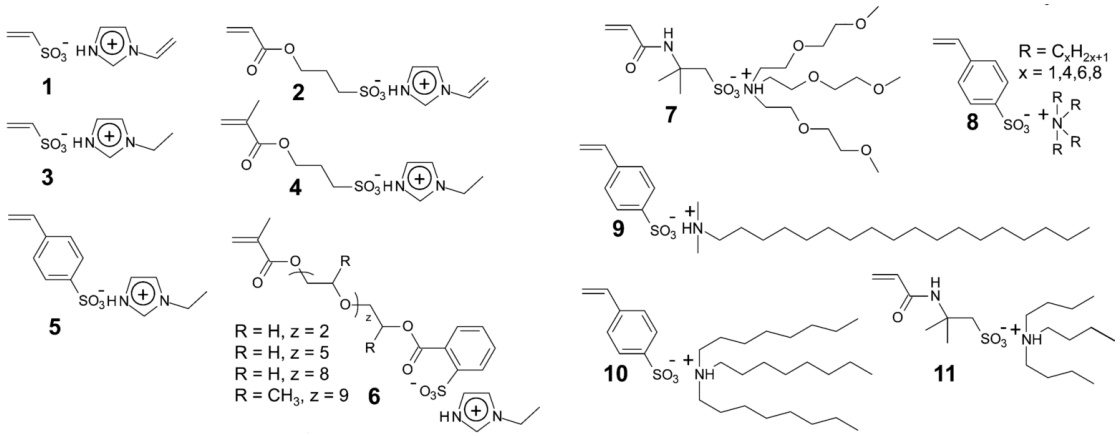

Figure 1.4. Overview of the various ion exchanged monomers in presented literature
(image taken from ref. 39)

1.3. Ion Aggregation in Ionomers

As previously mentioned, the ionic groups in the ionomer assembly into a characteristic, nanophase-separated structure known as "ion clusters". The formation of these clusters is driven by two phenomena: 1) the strong dipole-dipole interactions between the ionic groups and 2) the contrasting dielectric constants of the ionic groups relative to the polymer backbone.[43] The exact shape and size of these ionic clusters still remains unclear and highly debated.[6]

Small angle X-ray scattering has proved to be the most useful tool for the observation of these structure. In these scattering profiles, these clusters typically appear as a broad asymmetric scattering peak in the high q region (0.04 – 0.4 $Å^{-1}$), shown in Figure

1.2a.[44] The q value of the peak maximum can be converted into a domain spacing that corresponds to an approximate inter-cluster distance; however, the lack of higher order peaks prevents a complete understanding and depiction of these clusters. In an attempt to elucidate this structure, researchers have proposed various models to fit the ionomer SAXS peak such as the hard-sphere model,[44] the core-shell model,[45] and the multiplet-cluster model.[43] These conventional models all ascribe the scattering feature to spherical ion clusters in a liquid-like arrangement (Figure 1.2b) and use multiple adjustable parameter to provide the best fit.[44,46] Still, none of these models have provided definitive representation of the ion cluster structure. In addition, experimental results have shown that the cluster structure depends significantly on the polymer chemical structure, the ionic group, and the counterion, thus an all-encompassing, one-size-fits-all ionomer model may not be attainable.

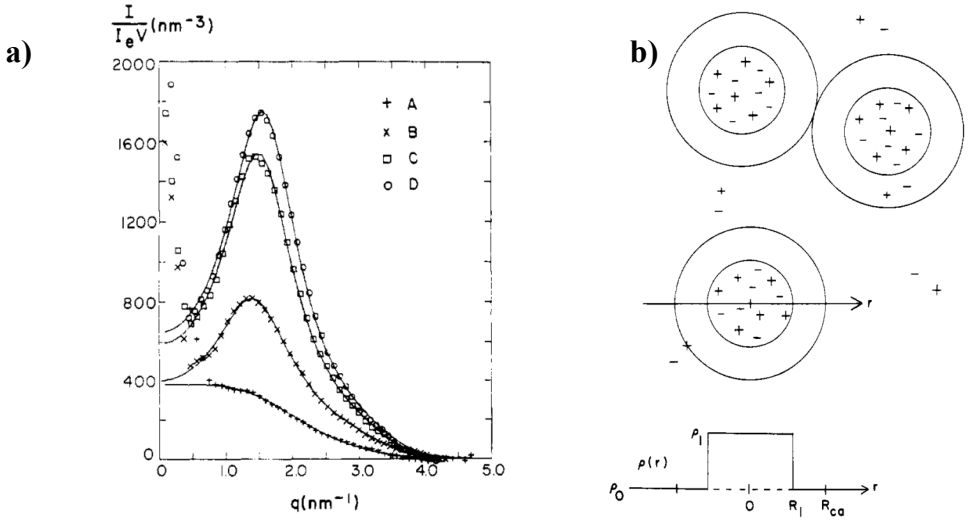

Figure 1.5. a) Ion cluster feature in SAXS scattering profile and b) depiction of the hard sphere model in liquid-like arrangement (image taken from ref. 44)

With improvements in electron microscopy techniques, aggregate structures with length scales of a few nanometers have been directly observed; however, the structure's

shape varies depending on the ionomer system, and the exact organization of the ionic groups within these structures cannot be definitively determined.[6] Currently, the majority of the investigated ionomers have exhibited a structure with spherical ion clusters in a liquid-like arrangement.[47,48] The dimensions and spacing of these structures depend heavily on factors such as the chemical structure of the polymer backbone, the concentration of the ionic groups, and the chemical identity of the ionic group and their corresponding counterions.

A variety of ionomer systems have been investigated to elucidate the complex structure-property relationships within these materials. The most common ionomers studies consist of polystyrene- (high T_g, amorphous) and polyethylene-based (low T_g, semicrystalline) backbones containing either acrylic or sulfonic acid groups neutralized with various metal counterions. In both ionomer systems, Winey and coworkers have reconciled the SAXS patterns with high-angle annular dark-field scanning transmission electron microscopy (HAADF-STEM).[49,50] In the sulfonated polystyrene (SPS) ionomers, spherical ion clusters with diameters of ~ 2 nm have been observed, and the size of the cluster appears to be independent of the degree of sulfonation, degree of neutralization, and counterion identity.[7] Compared to SPS, neutralized poly(styrene-*co*-methacrylic acid) and neutralized poly(ethylene-*co*-methacrylic acid) ionomers contain slightly smaller ion clusters (~ 1.5 nm) and slightly larger ion clusters (~ 2.5 - 2.8 nm),[47] respectively. This finding suggests that the chemical nature of the polymer backbone and covalently bound ionic group plays a more significant role in dictating the size of the ion cluster structure;[51] however, it is important to note that the presence of polar, unneutralized acid groups in acrylic acid-based ionomers plays a role in the structure and dynamics of these systems.

1.4. Thermal and Viscoelastic Properties of Ionomers

Even with the ambiguity behind the ion cluster structure, thorough investigations of the relationship between ionic group incorporation and the corresponding thermal and viscoelastic properties have contributed to a better understanding of these materials. These studies have mainly focused on the effect of ionic group concentration and counterions identity on the glass transition and polymer melts behavior using characterization techniques such as differential scanning calorimetry (DSC), dynamic mechanical analysis (DMA), and rheology. Some of the polymers that have been investigated include: neutralized poly(ethyl acrylate-*co*-acrylic acid),[16] poly(styrene-*co*-sodium methacrylate),[17–20] sulfonated polystyrene,[28–32] neutralized poly(ethylene-*co*-methacrylic acid),[52–55] sulfonated polyesters,[56] and poly(oligo(ethylene glycol) methyl ether methacrylate-*co*-styrenesulfonate).[13]

The ionic groups in these ionomers have been shown to significantly alter the overall physical behavior compared to their uncharged analogs. In the glassy state, these ionic group produce an increase in the T_g of the polymer due to chain mobility restrictions caused by the strong electrostatic interactions.[16,28] As the ionomer is heated above its T_g, the inhibited chain mobility results in a new plateau modulus. This plateau is a consequence of the ion clusters acting as physical crosslinks between polymer chains, effectively increasing the polymer-polymer connectivity and prolonging their characteristic relaxation times.[29,57] In addition, the new ionic plateau modulus exhibit an increase in modulus value with ion concentration. These electrostatic interactions are dynamic with a dissociation-association lifetime corresponding to the ion pair's mobility between clusters (ion hopping). This phenomena affects the polymer's linear viscoelastic

response and can be captured when the material is probed at appropriate time scales as seen in Figure 1.6.[29–31,56,58–60]

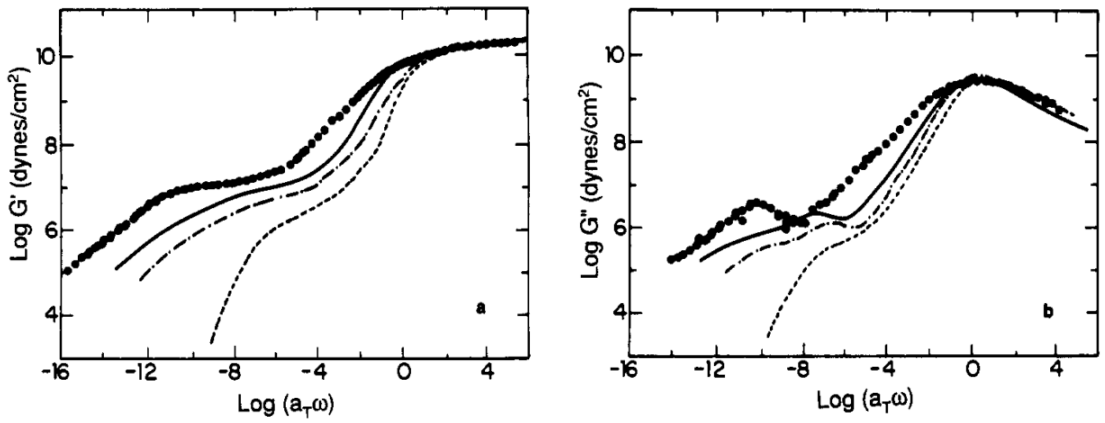

Figure 1.6. G' and G" master curves of (---) PS, (-•-) 1.82 Na-SPS, (—) 3.44 Na-SPS, and (•) 5.81 Na-SPS referenced to their T_g (image taken from ref. 29)

The counterion size and identity can be used to alter these interactions. The majority of studies have focused on inorganic counterions such as alkali, alkaline earth, and transition metals. [16,28,54,61,62] For lower T_g, higher dielectric constant ionomers, such as neutralized poly(ethyl acrylate-*co*-acrylic acid), the T_g of the polymer matrix corresponds to the counterion charge to distance of closest approach ratio (q_c/a).[16] For higher T_g, lower dielectric constant ionomers, however, the T_g of the matrix has been shown to be independent of q_c/a.[28] The reason for this trend is still not completely understood. Presumably, the T_g versus q_c/a dependence is influenced by both the number of ion clusters and their size and only appears in ionomer in which ion hopping begins to play a role in the segmental mobility.[1] For the ionic plateau modulus, the characteristic times correlate with the counterion charge and size with high charge, smaller molecules extending the plateau to longer times.[61,62]

Some studies have also investigated organic counterions such as alkyl ammoniums. By incorporating these bulkier ions, these electrostatic interactions can be partially screened through steric hindrance, which allows for ion cluster dissociation and flow at lower temperatures.[63] Recently, Colby investigated the dynamics of ionic liquid counterions in sulfonated polyesters and demonstrated improved ion conductivity and polymer mobility.[64] Furthermore, Weiss investigated the rheological properties of styrenic ionomers with ammonium counterions possessing alkyl chains of varying number of carbons.[65] With increased alky chain length, a reduction of the glass transition temperature (T_g) and melt viscosity was observed. Further investigation of these organic counterions and their effect on the structure and dynamics in ionomers would be useful and could extend their capabilities by offering a method to tune their interaction strength.

1.5. Ionomers for Advanced Material Applications

The impact of ionomers was first realized upon the commercialization of partially neutralized poly(ethylene-*co*-methacrylic acid) by DuPont under the name Surlyn®. This copolymer possessed superior mechanical toughness compared to its uncharged precursor, and could be fabricated into flexible, optically clear films for applications in packaging and coating.[66] Other early proposed applications of these polymers include membranes, fertilizers, adhesives, impact resistant materials, and additives for oil drilling.[1] Limited commercial success has been realized by these copolymers; however, renewed interest has developed as a result of the recent scientific trends with specific interest in ionomers for self-healing, shape memory, and tough elastomer applications.[7,67]

A self-healing material possesses the ability to recover load bearing properties after damage has occurred. The appeal of ionomers for this advanced application arises due

to the dynamic nature of these ionic bonds and the supramolecular structure of the ion clusters.[7] These two factors offer a self-healing mechanism in which the polymer can repair fracture sites as a result of the disruption and reformation of the ionic supramolecular structure.[7,68–70] The most prevalent example of a self-healing ionomer is the previously discussed neutralized poly(ethylene-*co*-methacrylic acid). Several studies have investigated the self-healing properties of this ionomer when damaged using a ballistic projectile test.[71–73] These tests have shown a need for balancing the elastic and viscoelastic behaviors in order for the puncture to rebound and then seal, respectively. Elastomeric ionomer systems are of particular interest for self-healing materials due to their low T_g and high polymer chain mobility. Some system that have recently been explored include: imidazole-modified butyl rubber (Figure 1.5),[74] natural rubber-based ionomers,[75] and functionalized poly(butadiene).[76]

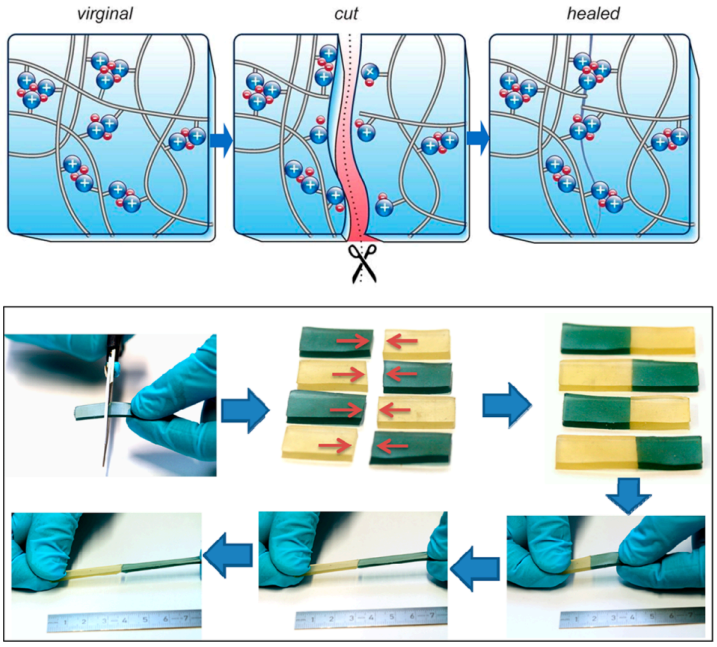

Figure 1.7. Schematic (top) and experimental demonstration (bottom) of the ionic association and self-healing behavior of imidazolium-modified bromobutyl rubber (image taken from ref. 71)

On a similar note, the shape-memory materials and tough elastomers build off of related concepts and mechanisms. The main distinctions of these materials compared to the self-healing materials are the necessity for a covalently crosslinked system. These polymers depend on the permanent crosslinked network to retain its original shape while the non-covalent, physical crosslinks enable programming of temporary shapes or provide the additional interactions to increase the elastomer's toughness and modulus.[7] The added ionic group in the covalently crosslinked network takes advantage of the dynamic ionic clusters that will dissociate when sufficient stress or thermal energy is applied to the system. Winey recently addressed this concept of toughened elastomers using ionomers as a strategy to reconcile the elastomer's toughness and modulus with its extensibility, using Filippidi's earlier work on catechol-iron complexes as a framework.[67,77]

An area not yet discussed but of significant interest for ionomers is their application as ion exchange membranes for applications in fuel cells and batteries.[5,78,79] These membranes require high ion conductivity in addition to good mechanical and chemical stability. Achieving these three design criteria has proven difficult and requires the appropriate design of new polymers. For ionomers, the ionic portions of these polymer chains offer the necessary sites for ion transport, while the uncharged portion provide mechanical stability. A trade-off exists between the mechanical integrity of the membrane and the ion conductivity, thus optimization of the ion content is necessary to balance these two desirable properties. The current benchmark material for these applications is a fluoropolymer developed by DuPont under the name Nafion®, which has shown excellent conductivity and chemical stability. The disadvantage of this membrane is the high cost to

fabricate and the lower than desired operational temperature range; thus, further research in polymer development is needed.

1.6. Dissertation Objectives

Using the existing studies on ion-containing copolymers as a framework, this dissertation aims to further the current understanding of the structure-property relationship of ionomers. Specifically, the presented work focuses on the role of the ionomer chemical structure on both the organization of the ionic groups and the dynamics for a low T_g, amorphous poly(isoprene-*ran*-styrenesulfonate) ionomers containing bulky organic, ammonium-based counterions. First, the effect of the ion content on the structure when transitioning from classical ionomer to polyelectrolytes will be explored in Chapter 2. Chapter 3 will evaluate and discuss the role of the counterion sterics on the ion aggregate structure and their implications on the molecular and macroscopic dynamics of the ionomer system. Building from the previous chapter, Chapter 4 then focuses on counterion selection as a method to tailor the ionic interactions and control their bulk properties, specifically their structure, dynamics and mechanical properties. Finally, Chapter 5 will summarizes the conclusions of the presented work and detail an updated picture of the ionomer structure. Additionally, this chapter will outline future directions in the field of ionomers.

1.7. References

(1) Eisenberg, A.; Kim, J.-S. *Introduction to Ionomers*; Wiley: New York, 1998.

(2) Dobrynin, A. V.; Rubinstein, M. Theory of Polyelectrolytes in Solutions and at Surfaces. *Prog. Polym. Sci.* **2005**, *30* (11), 1049–1118.

(3) Ward, T. C.; Tobolsky, A. V. Viscoelastic Study of Ionomers. *J. Appl. Polym. Sci.* **1967**, *11* (12), 2403–2415.

(4) Capek, I. Dispersions of Polymer Ionomers: I. *Adv. Colloid Interface Sci.* **2004**, *112* (1–3), 1–29.

(5) Hickner, M. A.; Ghassemi, H.; Kim, Y. S.; Einsla, B. R.; McGrath, J. E. Alternative Polymer Systems for Proton Exchange Membranes (PEMs). *Chem. Rev.* **2004**, *104*, 4587–4611.

(6) Grady, B. P. Review and Critical Analysis of the Morphology of Random Ionomers Across Many Length Scales. *Polym. Eng. Sci.* **2008**, *48* (6), 1029–1051.

(7) Zhang, L.; Brostowitz, N. R.; Cavicchi, K. A.; Weiss, R. A. Perspective : Ionomer Research and Applications. *Macromol. React. Eng.* **2014**, *8*, 81–99.

(8) Ricks-Laskoski, H. L.; Snow, A. W. Synthesis and Electric Field Actuation of an Ionic Liquid Polymer. *J. Am. Chem. Soc.* **2006**, *128* (38), 12402–12403.

(9) Jo, C.; Pugal, D.; Oh, I. K.; Kim, K. J.; Asaka, K. Recent Advances in Ionic Polymer-Metal Composite Actuators and Their Modeling and Applications. *Prog. Polym. Sci.* **2013**, *38* (7), 1037–1066.

(10) Geise, G. M.; Freeman, B. D.; Paul, D. R. Characterization of a Sulfonated Pentablock Copolymer for Desalination Applications. *Polymer.* **2010**, *51* (24), 5815–5822.

(11) Hickner, M. a.; Herring, A. M.; Coughlin, E. B. Anion Exchange Membranes: Current Status and Moving Forward. *J. Polym. Sci. Part B Polym. Phys.* **2013**, *51* (24), 1727–1735.

(12) Eisenberg, A.; Rinaudo, M. Polymer Bulletin. *Polym. Bull.* **1990**, *24*, 671.

(13) Chen, Q.; Bao, N.; Wang, J. H.; Tunic, T.; Liang, S.; Colby, R. H. Linear Viscoelasticity and Dielectric Spectroscopy of Ionomer / Plasticizer Mixtures : A Transition from Ionomer to Polyelectrolyte. *Macromolecules* **2015**, *48*, 8240–8252.

(14) Mortimer, D. A. Synthetic Polyelect Rolytes-A Review. *Polym. Int.* **1991**, *25*, 29–41.

(15) *Ionomers: Synthesis, Structure, Properties and Applications*; Tant, M. R., Mauritz, K. A., Wilkes, G. L., Eds.; Chapman & Hall: New York, 1997.

(16) Matsuura, H.; Eisenberg, A. Glass Transitions of Ethyl Acrylate-Based Ionomers. *J. Polym. Sci. Polym. Phys. Ed.* **1976**, *14* (7), 1201–1209.

(17) Kim, J.; Jackman, R. J.; Eisenberg, A. Filler and Percolation Behavior. *Macromolecules* **1994**, *27* (10), 2789–2803.

(18) Eisenberg, A.; Navratil, M. Ion Clustering and Viscoelastic Relaxation in Styrene-Based Ionomers. II. Effect of Ion Concentration. *Macromolecules* **1973**, *6* (4), 604–612.

(19) Navratil, M.; Eisenberg, A. Ion Clustering and Viscoelastic Relaxation in Styrene-Based Ionomers. III. Effect of Counterions, Carboxylic Groups, and Plasticizers. *Macromolecules* **1973**, *7* (1), 84–89.

(20) Eisenberg, A.; Navratil, M. Ion Clustering and Viscoelastic Relaxation in Styrene-Based Ionomers. IV. X-Ray and Dynamic Mechanical Studies. *Macromolecules* **1974**, *7* (1), 90–94.

(21) Jerome, R.; Mazurek, M. Synthesis and Characterization of Molecular Structure. In

Ionomers: Synthesis, Structure, Properties and Applications; Tant, M. R., Mauritz, K. A., Wilkes, G. L., Eds.; Chapman & Hall: New York, 1997; pp 1–31.

(22) Fitzgerald, J. J.; Weiss, R. A. Synthesis, Properties, and Structure of Sulfonate Ionomers. *J. Macromol. Sci. Part C Polym. Rev.* **1988**, *28* (1), 99–185.

(23) Turner, S. R.; Weiss, R. A.; Lundberg, R. D. The Emulsion Copolymerization of Styrene and Sodium Styrene Sulfonate. *J. Polym. Sci. Polym. Chem. Ed.* **1985**, *23* (2), 535–548.

(24) Weiss, R. A.; Lundberg, R. D.; Werner, A. The Synthesis of Sulfonated Polymers by Free Radical Copolymerization. Poly(Butadiene-Co-Sodium Styrene Sulfonate). *J. Polym. Sci. Polym. Chem. Ed.* **1980**, *18* (12), 3427–3439.

(25) Siadat, B.; Oster, B.; Lenz, R. W. Preparation of Ion-Containing Elastomers by Emulsion Copolymerization of Dienes with Olefinic Sulfonic Acid Salts. *J. Appl. Polym. Sci.* **1981**, *26*, 1027–1037.

(26) Blosch, S. E.; Orler, E. B.; Talley, S. J.; Moore, R. B.; Turner, S. R. Effect of Ion Concentration on the Properties of Polyisoprene-Sodium Styrene Sulfonate Elastomeric Ionomers Prepared by Emulsion Polymerization. *Polymer.* **2019**, *172*, 126–132.

(27) Weiss, R. A.; Lundberg, R. D.; Turner, S. R. Comparisons of Styrene Ionomers Prepared by Sulfonating Polystyrene and Copolymerizing Styrene with Styrene Sulfonate. *J. Polym. Sci. Polym. Chem. Ed.* **1985**, *23* (2), 549–568.

(28) Yang, S.; Sun, K.; Risen, W. M. Preparation and Thermal Characterization of the Glass Transition Temperatures of Sulfonated Polystyrene-metal Ionomers. *J. Polym. Sci. Part B Polym. Phys.* **1990**, *28* (10), 1685–1697.

(29) Weiss, R. A.; Fitzgerald, J. J.; Kim, D. Viscoelastic Behavior of Lightly Sulfonated Polystyrene Ionomers. *Macromolecules* **1991**, *24* (5), 1071–1076.

(30) Weiss, R. A.; Yu, W. Viscoelastic Behavior of Very Lightly Sulfonated Polystyrene Ionomers. *Macromolecules* **2007**, *40* (10), 3640–3643.

(31) Weiss, R. A.; Zhao, H. Rheological Behavior of Oligomeric Ionomers. *J. Rheol.* **2009**, *53* (1), 191–213.

(32) Hird, B.; Eisenberg, a. Sizes and Stabilities of Multiplets and Clusters in Carboxylated and Sulfonated Styrene Ionomers. *Macromolecules* **1992**, *25*, 6466–6474.

(33) Kucera, F.; Jancar, J. Homogeneous and Heterogeneous Sulfonation of Polymers: A Review. *Polym. Eng. Sci.* **1998**, *38* (5), 783–792.

(34) Zhou, Z. L.; Eisenberg, A. Dynamic Mechanial Properties of Sulfonated Cyclized Cis-1,4-polyisoprene. *J. Appl. Polym. Sci.* **1982**, *27* (2), 657–671.

(35) Woeste, G.; Meyer, W. H.; Wegner, G. Copolymers of Ethyl P-Vinylbenzenesulfonate for the Preparation of Polyelectrolytes of Reproducible Ion Content. *Makromol. Chemie* **1993**, *194*, 1237–1248.

(36) Chen, L.; Hallinan, D. T.; Elabd, Y. A.; Hillmyer, M. A. Highly Selective Polymer

Electrolyte Membranes from Reactive Block Polymers. *Macromolecules* **2009**, *42* (16), 6075–6085.

(37) Chang, Y.; Brunello, G. F.; Fuller, J.; Hawley, M.; Kim, Y. S.; Disabb-Miller, M.; Hickner, M. a.; Jang, S. S.; Bae, C. Aromatic Ionomers with Highly Acidic Sulfonate Groups: Acidity, Hydration, and Proton Conductivity. *Macromolecules* **2011**, *44* (21), 8458–8469.

(38) Okamura, H.; Takatori, Y.; Tsunooka, M.; Shirai, M. Synthesis of Random and Block Copolymers of Styrene and Styrenesulfonic Acid with Low Polydispersity Using Nitroxide-Mediated Living Radical Polymerization Technique. *Polymer.* **2002**, *43* (11), 3155–3162.

(39) Cavicchi, K. A. Synthesis and Polymerization of Substituted Ammonium Sulfonate Monomers for Advanced Materials Applications. *ACS Appl. Mater. Interfaces* **2012**, *4* (2), 518–526.

(40) McCullough, L. A.; Dufour, B.; Matyjaszewski, K. Incorporation of Poly(2-Acryloamido-2-Methyl-N-Propanesulfonic Acid) Segments into Block and Brush Copolymers by ATRP. *J. Polym. Sci. Part A Polym. Chem.* **2009**, *47* (20), 5386–5396.

(41) Consolante, V.; Marić, M. Nitroxide-Mediated Polymerization of an Organo-Soluble Protected Styrene Sulfonate: Development of Homo- and Random Copolymers. *Macromol. React. Eng.* **2011**, *5* (11–12), 575–586.

(42) Liu, Y.; Pollock, K. L.; Cavicchi, K. A. Synthesis of Poly(Trioctylammonium p-Styrenesulfonate) Homopolymers and Block Copolymers by RAFT Polymerization. *Polymer.* **2009**, *50* (26), 6212–6217.

(43) Eisenberg, A.; Hird, B.; Moore, R. B. A New Multiplet-Cluster Model for the Morphology of Random Ionomers. *Macromolecules* **1990**, *23* (18), 4098–4107.

(44) Yarusso, D. J.; Cooper, S. L. Microstructure of Ionomers: Interpretation of Small-Angle X-Ray Scattering Data. *Macromolecules* **1983**, *16* (12), 1871–1880.

(45) MacKnight, W. J.; Taggart, W. P.; Stein, R. S. A Model for the Structure of Ionomers. *J. Polym. Sci. Symp.* **1974**, *45* (45), 113–128.

(46) Kinning, D. J.; Thomas, E. L. Hard-Sphere Interactions between Spherical Domains in Diblock Copolymers. *Macromolecules* **1984**, *17* (9), 1712–1718.

(47) Winey, K. I.; Laurer, J. H.; Kirkmeyer, B. P. Ionic Aggregates in Partially Zn-Neutralized Poly(Ethylene-Ran-Methacrylic Acid) Ionomers: Shape, Size, and Size Distribution. *Macromolecules* **2000**, *33* (2), 507–513.

(48) Benetatos, N. M.; Chan, C. D.; Winey, K. I. Quantitative Morphology Study of Cu-Neutralized Poly(Styrene-Ran- Methacrylic Acid) Ionomers: STEM Imaging, X-Ray Scattering, and Real-Space Structural Modeling. *Macromolecules* **2007**, *40* (4), 1081–1088.

(49) Taubert, A.; Winey, K. I. Imaging and X-Ray Microanalysis of a Poly(Ethylene-*ran*-Methacrylic Acid) Ionomer Melt Neutralized with Sodium. *Macromolecules* **2002**, *35* (19), 7419–7426.

(50) Zhou, N. C.; Chan, C. D.; Winey, K. I. Reconciling STEM and X-Ray Scattering Data To Determine the Nanoscale Ionic Aggregate Morphology in Sulfonated Polystyrene. *Macromolecules* **2008**, *41* (16), 6134–6140.

(51) Castagna, A. M.; Wang, W.; Winey, K. I.; Runt, J. Influence of Cation Type on Structure and Dynamics in Sulfonated Polystyrene Ionomers. *Macromolecules* **2011**, *44* (13), 5420–5426.

(52) Read, B. B. E.; Carter, E. A.; Connor, T. M.; Macknightt, W. J. Structure and Properties of Ethylene-Methacrylic Acid Copolymers and Their Sodium Salts: Dielectric and Proton Magnetic Relaxation Studies. *Br. Polym. J.* **1969**, *1*, 123–131.

(53) Tadano, K.; Hirasawa, E.; Yamamoto, H.; Yano, S. Order—Disorder Transition of Ionic Clusters in Ionomers. *Macromolecules* **1989**, *22* (1), 226–233.

(54) Hirasawa, E.; Yamamoto, Y.; Tadano, K.; Yano, S. Effect of Metal Cation Type on the Structure and Properties of Ethylene Ionomers. *J. Appl. Polym. Sci.* **1991**, *42*, 351–362.

(55) Tachino, H.; Hara, H.; Hirasawa, E.; Kutsumizu, S.; Tadano, K.; Yano, S. Dynamic Mechanical Relaxations of Ethylene Ionomers. *Macromolecules* **1993**, *26* (4), 752–757.

(56) Chen, Q.; Tudryn, G. J.; Colby, R. H. Ionomer Dynamics and the Sticky Rouse Model. *J. Rheol.* **2013**, *57* (5), 1441–1462.

(57) Kim, J. S.; Yoshikawa, K.; Eisenberg, A. Molecular Weight Dependence of the Viscoelastic Properties of Polystyrene-Based Ionomers. *Macromolecules* **1994**, *27* (22), 6347–6357.

(58) Tierney, N. K.; Register, R. A. Synthesis and Melt Dynamics of Model Sulfonated Ionomers. *Macromolecules* **2003**, *36* (4), 1170–1177.

(59) Leibler, L.; Rubinstein, M.; Colby, R. H. Dynamics of Reversible Networks. *Macromolecules* **1991**, *24* (16), 4701–4707.

(60) Hall, L. M.; Stevens, M. J.; Frischknecht, A. L. Dynamics of Model Ionomer Melts of Various Architectures. *Macromolecules* **2012**, *45* (19), 8097–8108.

(61) Hara, M.; Jar, P.; Sauer, J. A. Dynamic Mechanical Properties of Sulfonated Polystyrene Ionomers. *Polymer.* **1991**, *32*, 1622–1626.

(62) Lefelar, J. A.; Weiss, R. A. Concentration and Counterion Dependence of Cluster Formation in Sulfonated Polystyrene. *Macromolecules* **1984**, *17* (6), 1145–1148.

(63) Chen, Q.; Liang, S.; Shiau, H. S.; Colby, R. H. Linear Viscoelastic and Dielectric Properties of Phosphonium Siloxane Ionomers. *ACS Macro Lett.* **2013**, *2* (11), 970–974.

(64) Tudryn, G. J.; Liu, W.; Wang, S. W.; Colby, R. H. Counterion Dynamics in Polyester-Sulfonate Ionomers with Ionic Liquid Counterions. *Macromolecules* **2011**, *44* (9), 3572–3582.

(65) Weiss, R. A.; Agarwal, P. K.; Lundberg, R. D. Control of Ionic Interactions in Sulfonated Polystyrene Ionomers by the Use of Alkyl- Substituted Ammonium

Counterions. *J. Appl. Polym. Sci.* **1984**, *29*, 2719–2734.

(66) Rees, R. W.; Vaughan, D. J. "Surlyn," An Ionomer. 1. The Effect of Ionic Bonding on Polymer Structure. *ACS Polym. Prepr.* **1965**, *6*, 287–295.

(67) Winey, K. I. Designing Tougher Elastomers with Ionomers. *Science.* **2017**, *358* (6362), 449–450.

(68) Wu, D. Y.; Meure, S.; Solomon, D. Self-Healing Polymeric Materials: A Review of Recent Developments. *Prog. Polym. Sci.* **2008**, *33* (5), 479–522.

(69) Herbst, F.; Döhler, D.; Michael, P.; Binder, W. H. Self-Healing Polymers via Supramolecular Forces. *Macromol. Rapid Commun.* **2013**, *34*, 203–220.

(70) Yang, Y.; Urban, M. W. Self-Healing Polymeric Materials. *Chem. Soc. Rev.* **2013**, *42* (17), 7446.

(71) Kalista, S. J.; Pflug, J. R.; Varley, R. J. Effect of Ionic Content on Ballistic Self-Healing in EMAA Copolymers and Ionomers. *Polym. Chem.* **2013**, *4* (18), 4910.

(72) Varley, R. J.; van der Zwaag, S. Towards an Understanding of Thermally Activated Self-Healing of an Ionomer System during Ballistic Penetration. *Acta Mater.* **2008**, *56* (19), 5737–5750.

(73) Varley, R. J.; Shen, S.; van der Zwaag, S. The Effect of Cluster Plasticisation on the Self Healing Behaviour of Ionomers. *Polymer.* **2010**, *51* (3), 679–686.

(74) Das, A.; Sallat, A.; Böhme, F.; Suckow, M.; Basu, D.; Wießner, S.; Stöckelhuber, K. W.; Voit, B.; Heinrich, G. Ionic Modification Turns Commercial Rubber into a Self-Healing Material. *ACS Appl. Mater. Interfaces* **2015**, *7* (37), 20623–20630.

(75) Xu, C.; Cao, L.; Lin, B.; Liang, X.; Chen, Y. Design of Self-Healing Supramolecular Rubbers by Introducing Ionic Cross-Links into Natural Rubber via a Controlled Vulcanization. *ACS Appl. Mater. Interfaces* **2016**, *8* (27), 17728–17737.

(76) Wang, D.; Guo, J.; Zhang, H.; Cheng, B.; Shen, H.; Zhao, N.; Xu, J. Intelligent Rubber with Tailored Properties for Self-Healing and Shape Memory. *J. Mater. Chem. A* **2015**, *3* (24), 12864–12872.

(77) Filippidi, E.; Cristiani, T. R.; Eisenbach, C. D.; Herbert Waite, J.; Israelachvili, J. N.; Kollbe Ahn, B.; Valentine, M. T. Toughening Elastomers Using Mussel-Inspired Iron-Catechol Complexes. *Science.* **2017**, *358* (6362), 502–505.

(78) Peckham, T. J.; Holdcroft, S. Structure-Morphology-Property Relationships of Non-Perfluorinated Proton-Conducting Membranes. *Adv. Mater.* **2010**, *22* (42), 4667–4690.

(79) Soloveichik, G. L. Flow Batteries : Current Status and Trends. *Chem. Rev.* **2015**, *115*, 11533–11558.

CHAPTER 2

PROGRESSION OF THE MORPHOLOGY IN RANDOM IONOMERS CONTAINING BULKY AMMONIUM COUNTERIONS

2.1. Introduction

Until recently, emulsion polymerizations were the only direct route to synthesize sulfonated ionomers due to the contrasting polarities between the charged monomer and the hydrophobic comonomer.[1,2] The versatility of this polymerization route, however, is limited, and copolymers of high ion content cannot be synthesized.[3] Additionally, heterogeneous distributions of the ionic groups along the polymer chain have been shown.[4–6] To bypass these shortcomings, post-polymerization sulfonation has been widely employed to incorporate the charged functionality into different polymer structures.[7] The library of polymers that can tolerate the harsh sulfonation conditions is limited, and various side reactions, such as cyclization and crosslinking, can occur.[8,9] An alternative synthetic approach using bulky quaternary ammonium counterions was recently reviewed by Cavicchi.[10] These bulky ammonium counterions improve the hydrophobicity of the sulfonated monomer and allow for their copolymerization with nonpolar comonomers in organic solvents. This synthetic method has been employed in various controlled radical polymerization techniques, which has led to the synthesis of new ionomers with a breadth of chemical structures and polymer architectures.[11–13]

In addition to the synthetic advantages, bulky ammonium counterions also provide the ability to alter the thermal and viscoelastic properties of an ionomer. A considerable amount of literature has been devoted to understanding the viscoelastic behavior of ionomers with inorganic counterions. As mentioned previously, the ion aggregates in these

polymers act as physical crosslinks, which increase the polymer-polymer interactions and prolonging their characteristic relaxation times.[14,15] Bulkier counterions, such as alkyl ammoniums, provide steric hinderance that can partially screen the electrostatic interactions and allow for ion cluster dissociation, and consequently flow at shorter time scales (lower temperatures).[16] In sulfonated polystyrene, these organic counterions have been shown to increase the mobility of the polymer, resulting in a reduction in the glass transition temperature and melt viscosity.[17]

With the increased dynamics provided by these organic counterions, the bulk properties of higher ion content copolymers can be evaluated. Particularly, little is known about the structure of copolymers that possess ion contents between the traditional ionomer and polyelectrolyte classifications.[18,19] Understanding the transformation from microphase-separated, ion aggregates to dispersed ionic groups would help guide the future design of new materials for various advanced applications such as actuators,[20,21] shape memory, and self-healing materials.[22] Recently, Colby investigated this transition by plasticizing a poly(oligo(ethylene glycol) methyl ether methacrylate-*co*-styrenesulfonate) with an oligomeric poly(ethylene glycol) oligomer.[18] With sufficient quantities of the plasticizer, the increase in the dielectric constant resulted in dissociation of the ionic groups. Investigations of this transition in systems that do not contain a plasticizer would provide further insight into the structure-property relationships of ion-containing polymers.

In this chapter, two aspects of ion-containing polymer will be addressed. First, exchange of styrenesulfonate's counterion to a bulky ammonium will be used to facilitate the direct copolymerization of styrenesulfonate with isoprene. The second aim of this work is to investigate the morphology of these bulky ammonium-containing copolymers when

increasing the ion content. Thus, a series of novel poly(isoprene-*ran*-dimethyloctylammonium styrenesulfonate) (P(I-*ran*-DMOASS)) copolymers of varying dimethyloctylammonium styrenesulfonate (DMOASS) compositions (30 – 77 wt%) were synthesized. These copolymers possessed moderate glass transition temperatures even at high ionic contents, which enabled for a comprehensive study of their thermal and linear viscoelastic behavior over a broad range of compositions.

2.2. Experimental

2.2.1. Materials

Isoprene (99%, Acros Organic) was distilled at room temperature under vacuum. 3,7-Dioxa-4-aza-6-phosphanonanoic acid, 4,5-bis (1,1-dimethylethyl)-6-ethoxy-2,2-dimethyl-6-oxide (SG1) (BlocBuilder®) was kindly provided by Arkema. Sodium styrenesulfonate (Alfa Aesar), N,N-dimethyloctylamine (97 %, Acros Organic), hydrochloric acid (12 M, VWR), and anisole (99.7 %, Sigma Aldrich) were used without further purification.

2.2.2. Synthesis of N,N-Dimethyloctylammonium Styrenesulfonate (DMOASS)

The synthesis of the DMOASS monomer was based on a previously reported procedure.[13] The N,N-dimethyloctylammonium chloride (DMOACl) was first synthesized by dissolving N,N-dimethyloctylamine (82.24 mL, 400 mmol) in hexanes (320 mL), cooling to 0 ^{o}C, and adding 12M hydrochloric acid (40 mL, 480 mmol) dropwise to the stirring solution. The product precipitated from solution during the addition of the hydrochloric acid. The reaction mixture was stored at -30 ^{o}C overnight. The precipitate was filtered and washed with cold hexanes (3x) to remove excess HCl. The final DMOACl

product was dried in a vacuum oven overnight at room temperature, producing a white solid (95% yield).

For the salt metathesis reaction, DMOACl (77.5 g, 400 mmol) was dissolved in dichloromethane (1 L), and sodium styrenesulfonate (99 g, 480 mmol) was dissolved in deionized water (0.96 L). The two solutions were added to a round bottom flask and stirred for 1 hour at room temperature. The reaction mixture was added to a separation funnel and allowed to settle overnight. The dichloromethane layer was collected, concentrated on a rotovap, and dried overnight at room temperature under vacuum. The dried product was then recrystallized from toluene by heating to 90 ^{o}C and allowed to slowly cool to room temperature. The recrystallized product was subsequently collected through filtration, washed 3 times with toluene, and dried at room temperature under vacuum for 48 hours (74% yield).

2.2.3. Synthesis of Poly(Isoprene-*ran*-N,N-Dimethyloctylammonium Styrenesulfonate) P(I-*ran*-DMOASS) Copolymers

A representative polymerization procedure for the P(I-*ran*-DMOASS) series is described as follows. Isoprene (10 mL, 100 mmol), DMOASS (8.540 g, 25 mmol), SG1 (20 mg, 51.7 μm), and anisole (15.4 mL, 50 wt%) were added to a Teflon screwcap-sealed Schlenk flask charged with a magnetic stirrer. The reaction mixture was subjected to three freeze-pump-thaw cycles to remove oxygen and was backfilled with nitrogen gas following the third cycle. The copolymerization was performed at 125 ^{o}C for 17 hours, and subsequently quenched by placing the reaction flask into an ice bath. The crude product was dissolved in methanol and precipitated twice into excess ethyl acetate to recover the

copolymer as a colorless solid. The comonomer feed ratio was varied to obtain a series of random copolymers of different compositions.

2.2.4. Instrumentation and Characterization

^{1}H NMR was performed using a Bruker Avance III HD 500 MHz spectrometer. Differential scanning calorimetry (DSC) was performed using a TA Instruments DSC Q200 equipped with a refrigerated cooling system (RCS90). Samples of approximately 3-8 mg were loaded into hermetic aluminum pans and subjected to a heat/cool/heat cycle at a heating/cooling rate of 10 K/min over a temperature range of -70 to 80 ^{o}C. The T_g's were determined from the second heating cycle. Dynamic mechanical analysis (DMA) was performed using a TA Instruments DMA Q800 in oscillatory tension mode at a frequency of 1 Hz and a strain amplitude of 0.1 % with a preload force of 0.001N. The samples were heated at a rate of 3 K/min from -70 to 80 ^{o}C. The linear viscoelastic response of the material was characterized using an 8-mm parallel plate fixture in a Malvern Kinexus Pro+ rheometer. Small amplitude oscillatory shear (SAOS) measurement were measured between ω = 1 - 100 rad/s from 0 – 80 ^{o}C in 10K increments at a strain amplitude of 0.1%. In select samples possessing a high T_g, low temperature behavior was not collected due to the sample's stiffness and instrument limitations. Small angle X-ray scattering (SAXS) was performed using a SAXS-LAB Ganesha instrument with a Cu-K_α 0.154 nm line in MAXS mode with scattering profiles collected for 5 minutes.

2.3. Results

2.3.1. Monomer and Polymer Synthesis

Figure 2.1 illustrates the synthesis of the DMOASS monomer and its subsequent nitroxide-mediated polymerization (NMP) with isoprene to obtain P(I-*ran*-DMOASS). ^{1}H NMR spectroscopy confirmed the chemical structure of DMOASS and was used to determine the composition of the copolymers. An overview of the synthesized copolymer series is shown in Table 2.1. The composition of the copolymers was varied between 8 and 40 mol % (30 - 77 wt%) DMOASS. Additionally, polyisoprene (PI) and poly(dimethyloctylammonium styrenesulfonate) (PDMOASS) homopolymers were synthesized to provide the lower and upper compositional bounds.

Due to limitations of conventional molecular weight characterization techniques for partially charged copolymers, the DP of the copolymers was also estimated by ^{1}H NMR spectroscopy. For this estimation, the DMOASS conversion was first determined by integrating the aromatic and the residual vinyl signals in the spectrum of the crude product. The moles of reacted DMOASS was then found by multiplying the initial DMOASS input by its conversion, which was multiplied by the mole ratio of the final copolymer composition to give the moles of reacted isoprene. By summing the moles of reacted DMOASS and isoprene and dividing by the moles of initiator, an estimation of the DP was determined the for the copolymers, which ranged between 670 to 1200.

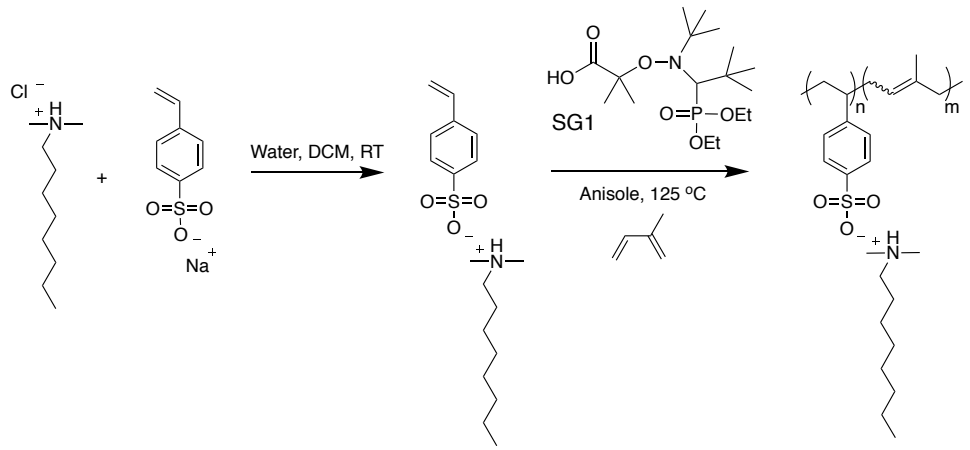

Figure 2.1. Salt metathesis reaction and subsequent nitroxide-mediated polymerization of DMOASS with isoprene

Table 2.1. Overview of the Synthesis and Corresponding Properties of the P(I-*ran*-DMOASS) Copolymer Series

Sample Name	Feed DMOASS	Actual DMOASS[a]		DP[a]	M_n[a]	$T_{g,DSC}$[c]	$T_{g,DMA}$[c]	d-spacing
	(mol %)	(mol %)	(wt %)		(kg/mol)	(°C)	(°C)	(nm)
P(I)	0	0	0	610[b]	41.4[b]	-60		
P(I-*ran*-DMOASS)-8	10	8	30	1200	106.6	-53	-42	5.3
P(I-*ran*-DMOASS)-13	15	13	42	1120	114.8	-46	-35, 0	4.3
P(I-*ran*-DMOASS)-17	20	17	51	670	72.7	-43, -16	-35, 0	3.7
P(I-*ran*-DMOASS)-20	25	20	56	1030	126.8	3		3.1
P(I-*ran*-DMOASS)-28	30	28	66	760	108.9	13		2.9
P(I-*ran*-DMOASS)-34	35	34	72	1040	168.1	25		2.6
P(I-*ran*-DMOASS)-40	40	40	77	1040	183.0	27		2.5
P(DMOASS)	100	100	100			77		2.1

[a] Composition, degree of polymerization, and M_n were determined using ^{1}H NMR. [b] Determined using THF GPC with a PS standard. [c] Comma separated values denote two separate T_g's for the copolymer.

2.3.2. Structural Characterization

Small angle X-ray scattering (SAXS) was used to probe the microstructure of the copolymer series (Figure 2.2). In each scattering profile, a peak appeared in the high q region. With increasing DMOASS content, the peak shifted to higher q values, which corresponded to a change in d-spacing from 5.3 to 2.1 nm over the 30 to 100 wt%

DMOASS range. The decreased d-spacing indicates a smaller distance between scatterers as the ion content is increased. Additionally, the shape of the SAXS peak narrowed and became more Gaussian, signifying a more regular spacing between structures.

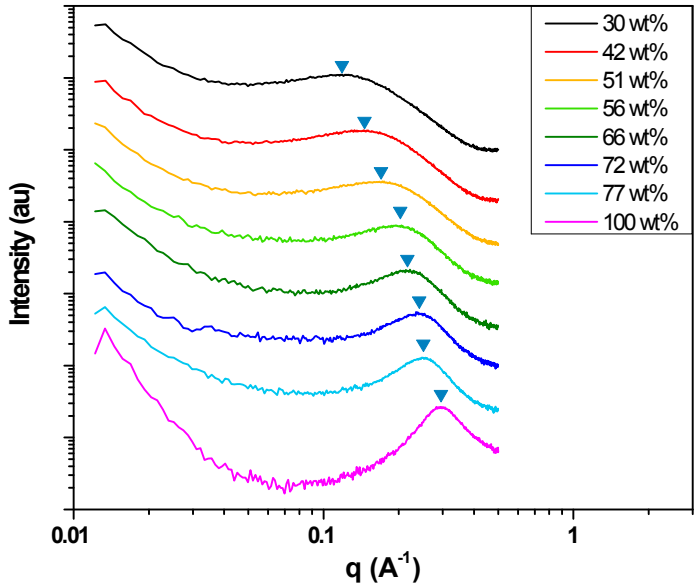

Figure 2.2. Offset SAXS profiles for the P(I-*ran*-DMOASS) copolymers with varying weight percent of DMOASS

2.3.3. Thermal and Viscoelastic Characterization

The glass transition of the P(I-*ran*-DMOASS) copolymer series was probed by DSC (Figure 2.3a). The glass transition temperatures (T_g), tabulated in Table 1, increased from -53 ºC to 27 ºC over a compositional range of 30 - 77 wt% DMOASS. This increase was also accompanied by a broadening of the T_g. At intermediate DMOASS content (42 and 51wt%), two T_g's may be present. The breadth and close proximity of the T_g's in these samples make assigning values difficult; thus, two T_g's were only ascribed for the 51 wt% sample using this characterization method. Additionally, the T_g values of the PI and PDMOASS homopolymers were found to be -60 ºC and 77 ºC, respectively. Figure 2.3b shows the inverse of the T_g as function of weight fraction of DMOASS. The red line

represents the predicted T_g values based on the Fox equation. Above 56 wt%, the T_g followed the Fox equation, while below 56 wt%, the T_g's deviated to lower temperatures.

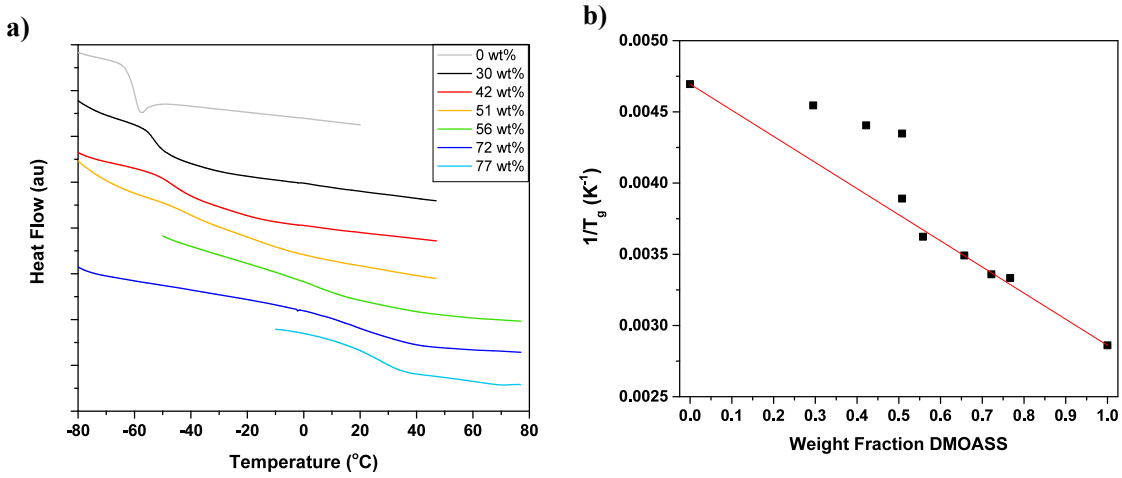

Figure 2.3. a) Offset DSC thermograms for the P(I-*ran*-DMOASS) copolymer series and b) Plot of the $1/T_g$ (determined by DSC) at varying DMOASS weight fraction (Fox Plot). Red line represents the predicted values for a homogenous polymer system calculated from the Fox equation.

For the low ion content copolymers, DMA (Figure 2.4) was used to further investigate the viscoelastic response when proceeding through the T_g. The corresponding T_g values are reported in Table 1. Each copolymer exhibited a glassy modulus of approximately 2 GPa, followed by a three orders of magnitude drop in modulus (E') as the temperature was increased. The 30 wt% DMOASS copolymer exhibited a single T_g at -42 °C marked by a peak in tan δ. As the DMOASS composition was increased to 51 wt%, the transition through the glass extended over a wider temperature range. A slope change also began to appear at 42 wt% DMOASS and became more pronounced at 51 wt%. This feature was amplified in tan δ where an additional inflection point appeared at 0 °C, indicating the presence of a second T_g at these intermediate DMOASS contents.

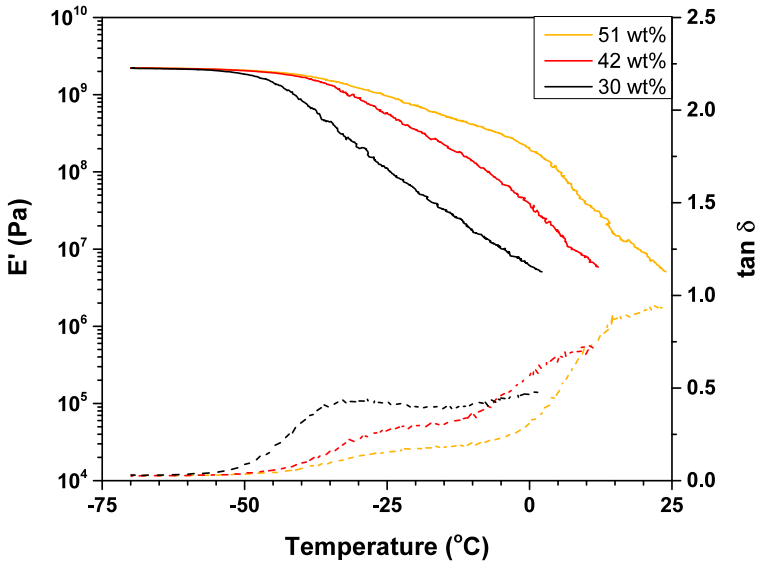

Figure 2.4. DMA single frequency (1 Hz) heating scans (3 K/min): storage modulus (solid lines) and tan δ (dashed lines) as a function of temperature for the low DMOASS content copolymers

Rheology was used to probe the linear viscoelastic response of the copolymer series above their T_g and construct SAOS master curves. The storage modulus and loss modulus are plotted in Figure 2.5a – 2.5d. Time-temperature superposition was applied using free shifting with the horizontal time shift, a_T, dominating over the vertical modulus shift, b_T. It was found that the a_T values followed WLF scaling. The PI homopolymer exhibited behavior typical of a high M_n, linear polymer melt (measured above its T_g) with an entanglement plateau modulus of 7.98 x 10^5 Pa and a terminal flow regime ($G' \sim \omega^2$, $G'' \sim \omega^1$). At low DMOASS compositions (30 - 51 wt%), an extension of the plateau modulus and almost complete suppression of flow occurred. The ability to extend the master curves to lower frequencies was limited due to polyisoprene degradation. At higher compositions (56 – 77 wt%), the entanglement plateau modulus mostly disappeared and the material was able to flow; however, classical terminal flow behavior was not realized.

Normalized δ and storage modulus are plotted in Figures 2.5e and 2.5f, respectively. All of the copolymers are liquids, shown by the increase in δ and decrease in normalized G' at low frequencies. Polyisoprene showed a minimum in δ and elastically dominated normalized storage modulus corresponding to the entanglement plateau modulus at high frequency. At lower frequencies, PI exhibited terminal flow where the viscous component dominates. As the DMOASS content was increased to 30 wt%, an increase in elasticity was introduced that extended the plateau modulus to the lowest accessible frequencies. A second minimum in normalized δ (maximum in the normalized storage modulus) also appeared in this regime, which became less evident when the DMOASS content was increased further to 42 and 51 wt%. At high DMOASS content, above 51 wt%, the high modulus (high frequency) regime was dominated by its proximity to its T_g. As temperature was increased, the polymer began to flow with only a single δ minimum appearing. Additionally, the material's overall elasticity was reduced, represented by the downward shift in the normalized modulus curve, despite more electrostatic interactions being present.

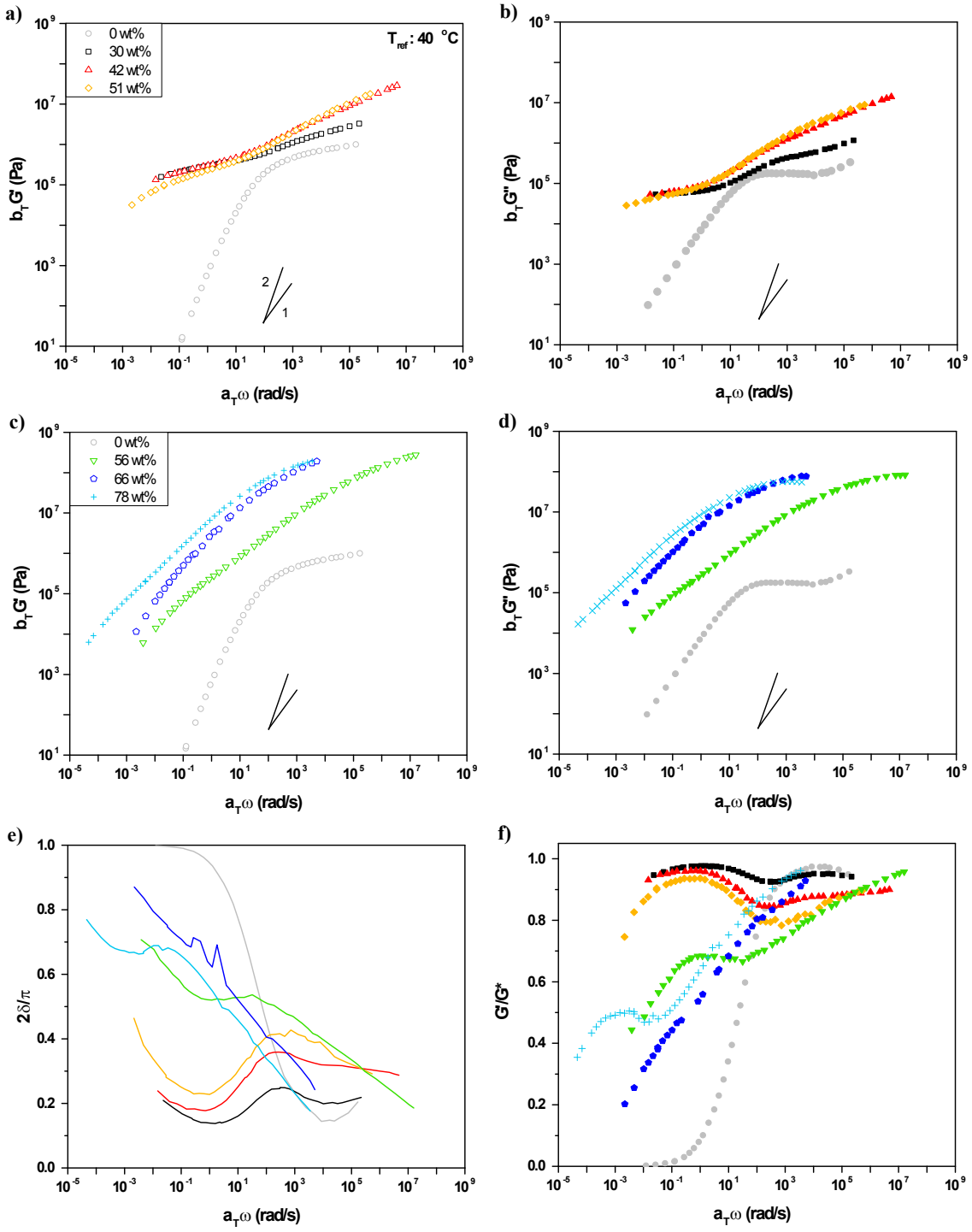

Figure 2.5. Linear viscoelastic response of PI and the P(I-*ran*-DMOASS) copolymer series: a) - d) storage and loss modulus as a function of frequency for the low (a, b) and high (c, d) DMOASS contents; e) normalized δ and f) normalized storage modulus as a function of frequency

Figure 2.6 shows the calculated relaxation spectra for the P(I-*ran*-DMOASS) series.[23] At short times, all of the polymers started to approach the glassy regime where data collection is limited due to the instrument's compliance. At low DMOASS content (Figure 2.6a), each polymer began to flow; however, the full relaxation of the polymer chains was not reached at the highest temperatures. Also, the final relaxation mode indicates an additional long time relaxation process. At high DMOASS content (Figure 2.6b), the polymers' relaxation times were extended. An extension of the relaxation times results from increased interactions being realized at higher DMOASS content, which prevented the polymers' from completely relaxing.

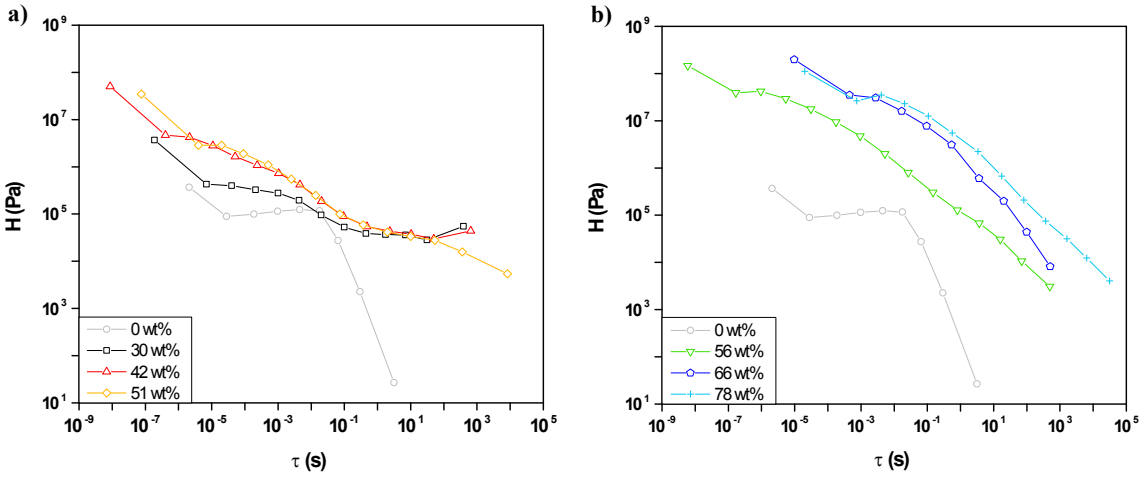

Figure 2.6. Continuous relaxation time spectra calculated from the SAOS data for the a) low and b) high DMOASS content copolymers plotted with the PI homopolymer control

2.4. Discussion

2.4.1. Counterion Exchange and Copolymerization

Due to the incompatibility of polyisoprene with conventional post-polymerization sulfonation techniques, poly(isoprene-*ran*-styrenesulfonate) needed to be synthesized using a direct copolymerization strategy. Direct solution copolymerization of sodium

styrenesulfonate and isoprene cannot be achieved due to their contrasting polarities, thus the styrenesulfonate was modified with a bulky ammonium counterion to enhance its solubility in organic solvents. Various ammonium counterions were screened including different quaternary ammoniums and aniliniums. Protonated ammoniums were found to undergo salt metathesis more easily than their corresponding quaternary ammoniums. This observation presumably stems from the reduced steric hinderance around the nitrogen cation, which allows for closer interaction between the ammonium and sulfonate. The anilinium-based cations were successfully exchanged and polymerized, but rapid discoloration of the monomer and copolymers occurred at ambient conditions due to oxidation of the counterion. The DMOA counterion provided the best results due to its aliphatic, surfactant-like structure, and the corresponding DMOASS possessed the necessary oleophilic character for it solubilization in anisole at elevated temperatures.

The counterion exchange proved to be an efficient and facile method to tune the hydrophobicity of the styrenesulfonate (SS) monomer, and large quantities of DMOASS (~100 grams) were produced with considerable yield (~70%). The critical component for this salt metathesis reaction was the water/dichloromethane solvent system. These two immiscible phases facilitate the formation of the DMOASS and sodium chloride due to favorable hydrophobic-hydrophilic interactions. After vigorous stirring, the DMOASS and sodium chloride separate into the organic and aqueous phase, respectively. This autonomous separation allowed for simple work up of the monomer after the reaction. The ^{1}H NMR spectrum of the recrystallized monomer showed a stoichiometric imbalance between the peak integrations of the vinylic SS protons and the alkyl DMOA protons, indicating the presence of some DMOACl impurities (~ 10 mol%). Additional

recrystallization steps produced no further improvement in purity possibly due to co-crystallization of DMOACl with the monomer. Copolymerization of DMOASS with isoprene was not affected by the excess DMOACl, thus the impure monomer was used and the stoichiometry adjusted appropriately.

Direct copolymerization of DMOASS with isoprene via a nitroxide-mediated polymerization produced the desired P(I-*ran*-DMOASS) copolymers. The composition of each copolymer was determined by comparing the integrations of the aromatic DMOASS peaks with the vinylic isoprene peaks in the ^{1}H NMR spectrum. The aromatic peaks were used as the reference and each integration was normalized by the corresponding number of protons. The isoprene formed three isomers during the polymerization: 1,4-addition, 1,2-addition, and 3,4- addition. Each addition can be identified and the relative ratios of each isomer estimated by analyzing the vinylic proton signals between δ 4.5 – 6 ppm. The quantities 1,2- and 1,4-additions were determined directly from the integrations while the 3,4-addition was calculated by integrating over the entire 1,2- and 3,4-addition overlapping region (δ 4.93 – 4.40 ppm). The two protons corresponding to the 1,2-addition were subtracted out and the remainder was normalized by the two protons to give the quantity of 3,4-addition. For the P(I-*ran*-DMOASS) copolymers series, the isoprene contained relative ratios of 81-86% to 3-4% to 10-16% of the 1,4-, 1,2-, and 3,4- isomers, respectively. The ^{1}H NMR spectra and table with the complete composition of each copolymer (including each isoprene addition) are available in the Appendix.

Based on the compositions determined from the ^{1}H NMR spectra, controlling the comonomer feed ratio allowed for precise control over the copolymer's ion content. The similarity between the feed ratio and copolymer's final composition after moderate

monomer conversion (30 – 40%) suggests the synthesis of statistical copolymers and allowed for targeting of specific DMOASS compositions and DP's. Thus, counterion exchange has been shown to be a versatile route to synthesize isoprene-based ionomers. These low T_g ionomers also provided a model system to explore the effect of the DMOA counterions on the physical properties of these materials with a large range of ionic contents.

2.4.2. Three Structural Regimes

The combination of the SAXS, DSC, DMA, and rheology show distinct differences between the copolymers depending on the DMOASS content. These differences are believed to stem from the organization of the ionic groups within the polymers, which is supported through the various characterization techniques. In this system, three structural regimes were found (Figure 2.7) and ascribed as follows: ion clusters (30 wt%), a continuous ionic phase (≥ 56 wt%), and the coexistence of the two structures (42 – 51 wt%).

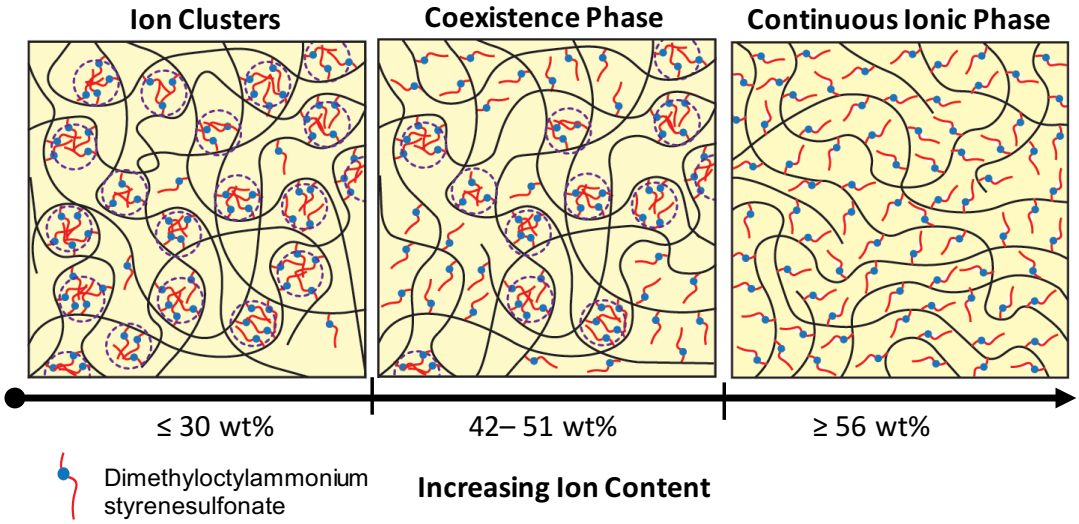

Figure 2.7. Depiction of the three structural regime: Ion Clusters (left), Coexistence Phase (middle), and Continuous Ionic Phase (right)

2.4.2.1. Presence of Ion Clusters at the Lowest Ionic Composition

At the lowest DMOASS composition (30 wt%), the copolymer exhibited a broad asymmetric scattering peak in the high q regime (0.04 – 0.4 $Å^{-1}$) of the SAXS profile (Figure 2.2) in addition to a upturn in scattering intensity at low q. This peak and low q upturn appear in all ionomers and are attributed to the presence of ion cluster structures.[24] The ionomer SAXS feature arises from the electron density contrast between the isoprene matrix and the DMOASS ion clusters with an average 5.3 nm spacing corresponding to the average inter-cluster distance. The breadth of the peak results from the random placement of the ionic group along the polymer backbone, which gives an irregular structure with a range of aggregate spacings. Furthermore, the low q upturn is believed to result from a heterogeneous distribution of the aggregates in the polymer matrix where some regions of the polymer are richer in ion aggregates than others.[25]

The exact shape and size of ionic clusters remain unclear and highly debated. Several models have been proposed to fit the ionomer SAXS peak with the conventional models ascribing the scattering feature to spherical ion clusters in a liquid-like arrangement.[24,26] These models pertain to ionomers possessing ionic groups with single atom counterions. In these P(I-*ran*-DMOASS) ionomers, the steric hindrance of the bulky, organic DMOA counterion may result in differences in the ion cluster shape and size, therefore fitting of the SAXS feature is not appropriate using these models.[27]

The viscoelastic response of the low ion content copolymer provided complementary evidence of ion clusters formation. When compared to the PI control, the incorporation of low quantities of DMOASS into the polymer backbone caused a four orders of magnitude extension of the plateau modulus to lower frequencies (longer times)

and consequently shifted the onset of terminal flow outside of the accessible frequency range. This extension of the plateau modulus can to be attributed to the formation of ion clusters, which introduces more connectivity between the polymer chains. The electrostatic interactions of the ionic moieties within the clusters act as physical crosslinks, suppressing cooperative chain motion and relaxation.[14] It should be noted that these polymers possess high molecular weights and thus entanglements are also present, as in the case of the PI homopolymer.

The dynamic frequency-dependent data were converted to the time domain and expressed in a continuous relaxation spectrum, allowing for analysis of the polymer's relaxation processes.[23] As depicted by the PI homopolymer, the relaxation spectrum is dominated by three relaxation regimes: approaching of the glass transition (short times), entanglements (intermediate times) and terminal flow (long times). With the introduction of ionic clusters, an additional relaxation process arises in the accessible timescales of the rheological experiments. The combination of these clusters and entanglements increases the polymer's characteristic relaxation times as shown by the horizontal extension in the relaxation spectra (Figure 2.6a). These two relaxation processes are further highlighted in the other linear viscoelastic functions.

Specifically, in the dynamic moduli (Figure 2.5a and 2.5b) and normalized δ (Figure 2.5e), these two distinct relaxation processes appear as a double plateau and two local minima, respectively. Each plateau (or local minimum) is believed to correspond to the relaxation of either ion clusters or entanglements. Assigning each phenomenon to a specific relaxation process is difficult. Leibler *et al.* have proposed a theory describing similar dynamics for entangled, physically crosslinked systems. In their model, the

relaxation of the reversible crosslinks occurs prior to the relaxation of entanglements when the molecular weight between reversible crosslinks is less than the molecular weight between entanglements. The additional connectivity from the reversible crosslinks adds another relaxation process, which alters the time scale of the entanglement relaxation.[28,29] Therefore, based on their model, the relaxation at intermediate frequencies (shorter times) results from ion cluster dissociation. On the other hand, the relaxation at intermediate frequencies occurs on similar time scales as the relaxation of entanglement for PI, suggesting the entanglement relaxation process may actually compete with the cluster disassociation. In this case, the electrostatic interactions within a cluster result in the rise of an additional low frequency mode. It is possible that a portion of the polymer chains are not permanently connected through the ion cluster structure due to weakening of the electrostatic interactions with the bulky ammonium counterions. This could allow for chain reptation to occur prior to the complete dissociation of the ion clusters. A very similar phenomenon was seen in the gelation at highly entangled polybutadiene.[23] Based on linear viscoelastic observations, both explanations are plausible, but a definitive assignment cannot be conclusively drawn in this polymer system.

2.4.2.2. High Ion Compositions and Continuous Ionic Phase

When the DMOASS composition is increased to 56 – 77 wt%, the existence of ion clusters becomes less apparent. A scattering peak in the high q region still appears in the SAXS patterns; however, the peak shifts to higher q values while the shape narrows and becomes more Gaussian. These differences indicate a smaller, more regular spacing in the structure. The peak is presumably not due to ion clusters since a similar scattering feature appears in the PDMOASS homopolymer. In this homopolymer, the backbone lacks the

nonpolar spacers (isoprene units) between ionic groups necessary for the organization of ion clusters. The scattering feature instead corresponds to the backbone-backbone spacing as a consequence of the electron density contrast between the ionic pendent groups and the polymer backbone. Various side chain-containing polymers, such as comb-shaped and bottlebrush copolymers, also exhibit a backbone-backbone spacing, with the spacing increased with the side chain length.[30–33] Considering this behavior, the high number of DMOASS repeat units in copolymers results in the distribution of the bulky DMOA counterions in between the polymer backbones as opposed to in discrete ion clusters.

The different polymer structure also has major consequences for the viscoelastic response. The first key difference is the disappearance of a definitive plateau in the storage modulus (Figure 2.5c), despite having high molecular weights. Above 56 wt% DMOASS, these copolymers showed a restricted flow behavior with no evidence of the physical crosslinks present in the low ion content copolymers. Instead, the viscoelastic response resembled more of a constrained, unentangled polymer melt, in which the dynamic moduli decayed but did not achieve terminal flow ($G' \sim \omega^2$, $G'' \sim \omega^1$). The disappearance of the entanglement plateau possibly results from an increase in the polymer chain's persistence length and corresponding decrease in the degree of entanglements with the incorporation of the styrenic monomer and the steric hindrance of the bulky DMOA counterions. Similar results have also been reported for various bottlebrush copolymers.[33–36] Additionally, a local minimum in δ at a higher δ value appears in the low frequency regime, indicative of an additional but unknown relaxation process. The delay in terminal flow (shifted to longer, inaccessible times) is attributed to prolonged relaxations resulting from the persistence of the electrostatic interactions between polymer chains. While these electrostatic interactions

extend the relaxation time, they are not strong enough to result in a plateau modulus as seen in the ionic clusters. Terminal flow is expected to eventually be reached at longer times, but it was not accessible within the experimental range.

2.4.2.3. Transition from Ion Clusters to Continuous Ionic Phase

At a critical composition between 51 and 56 wt% DMOASS, the thermal and viscoelastic properties of the copolymer series diverge. The discontinuity appears clearly when plotting the T_g data according to the Fox equation (Figure 2.3b). The Fox equation asserts that the T_g of a polymer mixture or a statistical copolymer in a homogeneous state depends on the T_g's of each individual component and their corresponding weight fractions within the system. If the criteria for the Fox equation persists across all compositions, the inverse of the copolymers' T_g's should scale with weight fraction (represented by the red line in Figure 2.3b). Below 51 wt% DMOASS, the isoprene content dominates the T_g of the copolymer as a result of the ionic groups microphase-separating from the isoprenic portions of the polymer chains to form the ion clusters. Above 56 wt% DMOASS, the T_g's follow the Fox equation. Therefore, the transition can be attributed to a transformation from the phase-separated ion cluster structure into a phase-mixed continuous ionic structure where DMOASS and isoprene contribute proportionally to the T_g of the system.

At 51 wt% DMOASS, DSC revealed a second T_g that was difficult to distinguish, thus DMA was performed on the 30, 42, and 51 wt% samples to further probe their glass transition. The DMA results confirmed the appearance of a second T_g at the intermediate ion content (42 and 51 wt% DMOASS) copolymers. This finding suggests the presence of macrophase separation where regions of ion clusters ($T_{g,1}$) and the continuous ionic phase ($T_{g,2}$) coexist at intermediate ion content. Additionally, the increase in prominence of the

second T_g feature in DMA indicates a rise of the continuous ionic phase over ion clusters with DMOASS content. Eisenberg reported similar results for poly(styrene-*ran*-sodium methacrylate) ionomers, and first proposed three morphological regimes for these ionomers in relation to percolation theory.[37] The structural and viscoelastic characterization results further support our proposed evolution from ion cluster to coexistence and finally to a continuous ionic phase.

In the SAXS profiles, the gradual transition of the structure peak with increased DMOASS content is unanticipated. The coexistence of the two structures shown by the thermal characterization is expected to exhibit two separate peaks. A convolution of the two competing structures' form factors is believed to occur due to the similarity of their characteristic spacing, thus producing the continuous transformation of the SAXS feature from the ion cluster structure at low DMOASS content to the backbone-backbone spacing seen at high DMOASS content.

Additionally, the scattering profiles at low q values (~0.01 - 0.05 $Å^{-1}$) remain similar across the copolymer series with I(q) scaling varying between -2 and -3. Analysis of scaling in this regime provides information related to the interface of the copolymer's microstructure and has been regularly employed in both polymer blends and block copolymers.[38,39] According to Porod's law, microstructures with sharp, smooth interfaces result in I(q) scaling with q^{-4}. Deviation for Porod's law occurs when phase mixing, diffuse phase boundaries, or rough interfaces are present.[40,41] In the copolymers containing the coexistence of ion clusters and the continuous ionic phase, this region coincides with the low q upturn observed with ion clusters, and does not change significantly with the altered morphologies. Thus, this deviation from Porod's law is believed to also result from the

heterogeneous distributions of the ionic groups in the copolymer where the continuous ionic phase possesses higher ionic group concentrations than the ion cluster phase.[42] Due to the similarity between the scattering of the two phases and the fluctuations of the ionic groups in these random copolymers, the nature of the interface between these two phases cannot be definitively determined using SAXS.

When reviewing the relaxation spectra of the 30, 42, and 51 wt% DMOASS copolymers, minor distinctions become apparent. In Figure 2.6a, the last relaxation mode trends upwards for the 30 and 42 wt% DMOASS copolymers. The combination of entanglements and ion clusters in these polymers adds increased elasticity even at the longest time and lowest temperatures accessed. Despite this, the samples are still liquids based on the low frequency upturn in the normalized δ (Figure 2.5e). In the case of the 51 wt% sample, the last relaxation mode trends downwards, indicating the beginning of flow. The appearance of flow suggests that some portions of the chains begin to adopt an extended chain configuration with longer persistence lengths (decreased degree of entanglement), however the clusters still dominate the viscoelastic response of the copolymer. The extension of these chains reduces, and may prevent, possible entanglements and allows the material to flow after ion cluster dissociation, but in a restricted fashion. This proposed chain structure is also reflected in the storage and loss modulus downward trend, which scales as $G' \sim \omega^{1.15}$ and $G'' \sim \omega^{0.95}$ opposed to $G' \sim \omega^2$ and $G'' \sim \omega^1$ as expected for terminal flow.

A final overview of the viscoelastic response in the context of the three structural regimes is highlighted in the Winter Plot (Figure 2.8). In a Winter Plot, a typical entangled polymer melt response portrays the polymer entanglement plateau modulus (elastically

dominated behavior) as a vertical line in the high frequency regime and terminal flow as a horizontal line in the low frequency regime, as demonstrated by the PI (grey circles) sample. The horizontal curvature at low frequencies (low modulus) highlights the liquid behavior of all samples while still showing the unique viscoelastic response of the copolymer series.[27] The 30 wt% DMOASS copolymer exhibits elastic behavior with modulus values exceeding that of the neat PI and a less evident flow regime. At intermediate ionic content (42 and 51 wt% DMOASS), the ion cluster structure still dictates the viscoelastic response but the characteristics of the continuous ionic phase begin to appear and introduce a slight slope to the plateau regime. At high ion contents (> 51 wt% DMOASS), the high modulus regime is dominated by its proximity to its T_g, and the copolymers flow as a result of the extend chain configuration but do not fully relax (become horizontal) due to the presence of the electrostatic interactions.

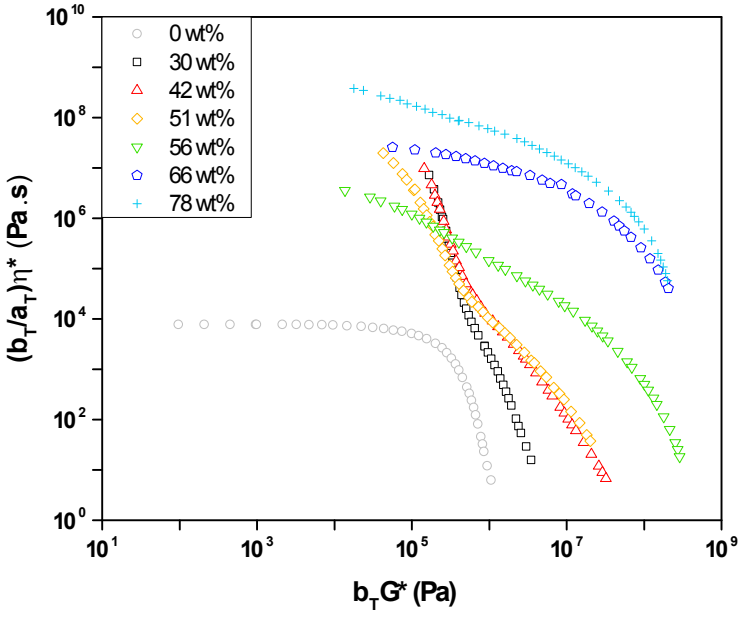

Figure 2.8. Winter Plot of the P(I-*ran*-DMOASS) copolymers series

2.5. Conclusion

High molecular weight, random ionomers with controlled ion content were synthesized through direct nitroxide-mediated copolymerization of DMOASS with isoprene. Through a combination of thermal, viscoelastic, and X-ray scattering experiments, three structural regimes were identified within the copolymer series: ion clusters, continuous ionic phase, and the coexistence of both structures. With the ion cluster structure, the copolymer's T_g was dominated by the isoprene matrix, and the viscoelastic properties showed increased connectivity between the polymer chains due to physical crosslinking reinforcement provided by the clusters. For the continuous ionic phase, the elasticity of the system was reduced and the copolymers behaved as unentangled polymer melts with restricted flow characteristics as a result of the electrostatic interactions. At intermediate DMOASS content, a coexistence of both structures was evident with the appearance of two T_g in the DMA in addition to the minor distinctions in the viscoelastic response. Considering these three structural regimes, further variation of the polymer structure and counterion will allow for tailoring of the ionomer morphologies and dynamics for improved transport membranes, self-healing materials, or soft actuators.

2.6. References

(1) Siadat, B.; Oster, B.; Lenz, R. W. Preparation of Ion-containing Elastomers by Emulsion Copolymerization of Dienes with Olefinic Sulfonic Acid Salts. *J. Appl. Polym. Sci.* **1981**, *26* (3), 1027–1037.

(2) Siadat, B.; Lundberg, R. D.; Lenz, R. W. Solubility Behavior of Copolymers of Isoprene and Sodium Styrenesulfonate. *Macromolecules* **1981**, *14*, 773–776.

(3) Turner, S. R.; Weiss, R. A.; Lundberg, R. D. The Emulsion Copolymerization of Styrene and Sodium Styrene Sulfonate. *J. Polym. Sci. Polym. Chem. Ed.* **1985**, *23* (2), 535–548.

(4) Siadat, B.; Oster, B.; Lenz, R. W. Preparation of Ion-Containing Elastomers by Emulsion Copolymerization of Dienes with Olefinic Sulfonic Acid Salts. *J. Appl.*

Polym. Sci. **1981**, *26*, 1027–1037.

(5) Weiss, R. A.; Lundberg, R. D.; Turner, S. R. Comparisons of Styrene Ionomers Prepared by Sulfonating Polystyrene and Copolymerizing Styrene with Styrene Sulfonate. *J. Polym. Sci. Polym. Chem. Ed.* **1985**, *23* (2), 549–568.

(6) Blosch, S. E.; Orler, E. B.; Talley, S. J.; Moore, R. B.; Turner, S. R. Effect of Ion Concentration on the Properties of Polyisoprene-Sodium Styrene Sulfonate Elastomeric Ionomers Prepared by Emulsion Polymerization. *Polymer.* **2019**, *172*, 126–132.

(7) Hickner, M. A.; Ghassemi, H.; Kim, Y. S.; Einsla, B. R.; McGrath, J. E. Alternative Polymer Systems for Proton Exchange Membranes (PEMs). *Chem. Rev.* **2004**, *104*, 4587–4611.

(8) Kucera, F.; Jancar, J. Homogeneous and Heterogeneous Sulfonation of Polymers: A Review. *Polym. Eng. Sci.* **1998**, *38* (5), 783–792.

(9) Fitzgerald, J. J.; Weiss, R. A. Synthesis, Properties, and Structure of Sulfonate Ionomers. *J. Macromol. Sci. Part C Polym. Rev.* **1988**, *28* (1), 99–185.

(10) Cavicchi, K. A. Synthesis and Polymerization of Substituted Ammonium Sulfonate Monomers for Advanced Materials Applications. *ACS Appl. Mater. Interfaces* **2012**, *4* (2), 518–526.

(11) McCullough, L. A.; Dufour, B.; Matyjaszewski, K. Incorporation of Poly(2-Acryloamido-2-Methyl-N-Propanesulfonic Acid) Segments into Block and Brush Copolymers by ATRP. *J. Polym. Sci. Part A Polym. Chem.* **2009**, *47* (20), 5386–5396.

(12) Consolante, V.; Marić, M. Nitroxide-Mediated Polymerization of an Organo-Soluble Protected Styrene Sulfonate: Development of Homo- and Random Copolymers. *Macromol. React. Eng.* **2011**, *5* (11–12), 575–586.

(13) Liu, Y.; Pollock, K. L.; Cavicchi, K. A. Synthesis of Poly(Trioctylammonium p-Styrenesulfonate) Homopolymers and Block Copolymers by RAFT Polymerization. *Polymer.* **2009**, *50* (26), 6212–6217.

(14) Weiss, R. A.; Fitzgerald, J. J.; Kim, D. Viscoelastic Behavior of Lightly Sulfonated Polystyrene Ionomers. *Macromolecules* **1991**, *24* (5), 1071–1076.

(15) Kim, J. S.; Yoshikawa, K.; Eisenberg, A. Molecular Weight Dependence of the Viscoelastic Properties of Polystyrene-Based Ionomers. *Macromolecules* **1994**, *27* (22), 6347–6357.

(16) Chen, Q.; Liang, S.; Shiau, H. S.; Colby, R. H. Linear Viscoelastic and Dielectric Properties of Phosphonium Siloxane Ionomers. *ACS Macro Lett.* **2013**, *2* (11), 970–974.

(17) Weiss, R. A.; Agarwal, P. K.; Lundberg, R. D. Control of Ionic Interactions in Sulfonated Polystyrene Ionomers by the Use of Alkyl- Substituted Ammonium Counterions. *J. Appl. Polym. Sci.* **1984**, *29*, 2719–2734.

(18) Chen, Q.; Bao, N.; Wang, J. H.; Tunic, T.; Liang, S.; Colby, R. H. Linear

Viscoelasticity and Dielectric Spectroscopy of Ionomer / Plasticizer Mixtures : A Transition from Ionomer to Polyelectrolyte. *Macromolecules* **2015**, *48*, 8240–8252.

(19) Eisenberg, A.; Rinaudo, M. Polymer Bulletin. *Polym. Bull.* **1990**, *24*, 671.

(20) Ricks-Laskoski, H. L.; Snow, A. W. Synthesis and Electric Field Actuation of an Ionic Liquid Polymer. *J. Am. Chem. Soc.* **2006**, *128* (38), 12402–12403.

(21) Jo, C.; Pugal, D.; Oh, I. K.; Kim, K. J.; Asaka, K. Recent Advances in Ionic Polymer-Metal Composite Actuators and Their Modeling and Applications. *Prog. Polym. Sci.* **2013**, *38* (7), 1037–1066.

(22) Zhang, L.; Brostowitz, N. R.; Cavicchi, K. A.; Weiss, R. A. Perspective : Ionomer Research and Applications. *Macromol. React. Eng.* **2014**, *8*, 81–99.

(23) Baumgaertel, M.; Winter, H. H. Determination of Discrete Relaxation and Retardation Time Spectra from Dynamic Mechanical Data. *Rheol. Acta* **1989**, *28* (6), 511–519.

(24) Yarusso, D. J.; Cooper, S. L. Microstructure of Ionomers: Interpretation of Small-Angle X-Ray Scattering Data. *Macromolecules* **1983**, *16* (12), 1871–1880.

(25) Grady, B. P. Review and Critical Analysis of the Morphology of Random Ionomers Across Many Length Scales. *Polym. Eng. Sci.* **2008**, *48* (6), 1029–1051.

(26) Kinning, D. J.; Thomas, E. L. Hard-Sphere Interactions between Spherical Domains in Diblock Copolymers. *Macromolecules* **1984**, *17* (9), 1712–1718.

(27) Zhou, N. C.; Chan, C. D.; Winey, K. I. Reconciling STEM and X-Ray Scattering Data To Determine the Nanoscale Ionic Aggregate Morphology in Sulfonated Polystyrene. *Macromolecules* **2008**, *41* (16), 6134–6140.

(28) Leibler, L.; Rubinstein, M.; Colby, R. H. Dynamics of Reversible Networks. *Macromolecules* **1991**, *24* (16), 4701–4707.

(29) Chen, Q.; Zhang, Z.; Colby, R. H. Viscoelasticity of Entangled Random Polystyrene Ionomers. *J. Rheol.* **2016**, *60* (6), 1031–1040.

(30) Plate, N. A.; Shibaev, V. P. Comb-Like Polymers. Structure and Properties. *J. Polym. Sci. Macromol. Rev.* **1974**, *8*, 117–253.

(31) Arbe, A.; Genix, A.-C.; Colmenero, J.; Richter, D.; Fouquet, P. Anomalous Relaxation of Self-Assembled Alkyl Nanodomains in High-Order Poly(n-Alkyl Methacrylates). *Soft Matter* **2008**, *4*, 1792–1795.

(32) Salas-De La Cruz, D.; Green, M. D.; Ye, Y.; Elabd, Y. A.; Long, T. E.; Winey, K. I. Correlating Backbone-to-Backbone Distance to Ionic Conductivity in Amorphous Polymerized Ionic Liquids. *J. Polym. Sci. Part B Polym. Phys.* **2012**, *50* (5), 338–346.

(33) López-Barrón, C. R.; Brant, P.; Eberle, A. P. R.; Crowther, D. J. Linear Rheology and Structure of Molecular Bottlebrushes with Short Side Chains. *J. Rheol.* **2015**, *59* (3), 865–883.

(34) Zhang, Z.; Liu, C.; Cao, X.; Wang, J. H.; Chen, Q.; Colby, R. H. Morphological Evolution of Ionomer / Plasticizer Mixtures during a Transition from Ionomer to

Polyelectrolyte. *Macromolecules* **2017**, *50*, 963–971.

(35) Daniel, W. F. M.; Burdyńska, J.; Vatankhah-varnoosfaderani, M.; Matyjaszewski, K.; Paturej, J.; Rubinstein, M.; Dobrynin, A. V; Sheiko, S. S. Solvent-Free , Supersoft and Superelastic Bottlebrush Melts and Networks. **2016**, *15* (February), 183–190.

(36) Paturej, J.; Sheiko, S. S.; Panyukov, S.; Rubinstein, M. Molecular Structure of Bottlebrush Polymers in Melts. *Sci. Adv.* **2016**, *2* (11).

(37) Kim, J.; Jackman, R. J.; Eisenberg, A. Filler and Percolation Behavior. *Macromolecules* **1994**, *27* (10), 2789–2803.

(38) Russell, T. P.; Ito, H.; Wignall, G. D. Neutron and X-Ray Scattering Studies on Semicrystalline Polymer Blends. *Macromolecules* **1988**, *21* (6), 1703–1709.

(39) Perrin, P.; Prud'homme, R. E. SAXS Measurements of Interfacial Thickness in Amorphous Polymer Blends Containing a Diblock Copolymer. *Macromolecules* **1994**, *27* (7), 1852–1860.

(40) Koberstein, J. T.; Morra, B.; Stein, R. S. The Determination of Diffuse-Boundary Thicknesses of Polymers by Small-Angle X-Ray Scattering. *J. Appl. Crysta.* **1980**, *13* (1), 34–45.

(41) Martin, J. E.; Hurd, A. J. Scattering from Fractals. *J. Appl. Crystal.* **1987**, *20* (2), 61–78.

(42) Elliott, J. A.; Hanna, S.; Elliott, A. M. S.; Cooley, G. E. Interpretation of the Small-Angle X-Ray Scattering from Swollen and Oriented Perfluorinated Ionomer Membranes. *Macromolecules* **2000**, *33* (11), 4161–4171.

CHAPTER 3

MODIFYING THE STRUCTURE AND DYNAMICS OF ELASTOMERIC IONOMERS THROUGH COUNTERION STERICS

3.1. Introduction

Developing a fundamental understanding of ionomers has been a goal since the inception of ionomers, and countless studies have been performed to uncover the factors that drive their unique structure and physical properties.[1,2] Two general concepts that emerged from these investigations are: 1) ionomers possess a microphase-separated morphology consisting of nanometer-sized ion aggregates within a nonpolar, polymer matrix, and 2) the ion aggregates act as physical crosslinks that hold the polymer chains together. Based on these conclusions, controlling the structure and the corresponding interaction dynamics is critical for the future development of these polymeric materials.

In the majority of these studies, the counterion identity has been a critical molecular parameter of interest due to its ability to tune the ionomer's properties without altering any of the polymer's covalent bonds. In other words, different counterions can be ionically attached to polymers with identical chemical structures and ion compositions with relative ease. Depending on the neutralizing reagent, a variety of counterions can be employed, the majority being either alkali or alkaline earth metal ions. Based on X-ray scattering and electron microscopy, the majority of these metal neutralized ionomers exhibit a structure comprised of spherical ion clusters in a liquid-like arrangement.[3–5] These spherical ion clusters range in diameter from 1.5 to 2.8 nm, and a minimal change in cluster size was shown with varying ion content, degree of neutralization, and counterion identity.[6–8] While the structure of the ionomers does not significantly change with counterion identity, the

dynamics depends on the size, valency, and interaction strength of the ionic group/counterion pair. In general, it has been shown that as the counterion radius is decreased, improved interactions between the ionic groups are realized, and the polymers become less dynamic.[9,10]

With advancement of the field, recent works have explored ionomer systems containing alternative counterions, such as organic, multi-atom quaternary ammoniums and phosphoniums.[11–14] These counterions offer great diversity in chemical structure as a result of the various pendent group that can be attached. With bulkier groups, the electrostatic interactions can be tuned through steric screening that allows for ion cluster dissociation and the onset of flow at shorter time scales (lower temperatures).[15] Thus, these organic counterions have been employed in several ionomer and polyelectrolyte systems in order to increase their dynamics.[12,13] For ionomers, the majority of these studies have looked at the effect of the counterion on perfluorosulfonate polymers[11,16–18] and sulfonated polystyrene,[12] and increased counterion sterics resulted in a depression of the T_g. Thus, the bulky counterions acted as a plasticizer, which resulted in increased mobility of the polymer chains.

While the dynamics of ionomers with bulky counterions have been investigated, effects of these counterion on the structure of ion aggregates have generally been overlooked. Employing these counterions in a more dynamic, high mobility polymer would deconvolute the glass transition from the steric effects of the counterion. Thus, in this work, a low glass transition temperature, amorphous poly(isoprene-*ran*-styrenesulfonate) copolymer was synthesized, and the counterions were exchanged to different organic, tetraalkylammonium counterions. The sterics of the ammonium

counterions was systematically altered by increasing the length of the counterions' pendent alkyl chains, and the copolymer's structure and dynamics were evaluated.

3.2. Experimental

3.2.1. Materials

Isoprene (99%, Acros Organic) was distilled at room temperature under vacuum. 3,7-Dioxa-4-aza-6-phosphanonanoic acid, 4,5-bis (1,1-dimethylethyl)-6-ethoxy-2,2-dimethyl-6-oxide (SG1) (BlocBuilder®) was kindly provided by Arkema. Sodium styrenesulfonate (Alfa Aesar), N,N-dimethyloctylamine (97 %, Acros Organic), hydrochloric acid (12 M, VWR), anisole (99.7 %, Sigma Aldrich), tetramethylammonium hydroxide (25 % w/w in methanol, Alfa Aesar), tetraethylammonium hydroxide (25 % w/w in methanol, Alfa Aesar), tetra-n-propylammonium hydroxide (40 % w/w in water, Beantown Chemical), and tetrabutylammonium hydroxide (1M in methanol, Alfa Aesar) were used without further purification.

3.2.2. Synthesis of Poly(Isoprene-*ran*-Tetraalkylammonium Styrenesulfonate) Copolymers

Dimethyloctylammonium styrenesulfonate (DMOASS) and poly(isoprene-*ran*-dimethyloctylammonium styrenesulfonate) containing 7 mol % DMOASS (P(I-*ran*-DMOASS)-7) were synthesized following our previously reported procedure.[19] After the synthesis of the P(I-*ran*-DMOASS)-7 copolymer, exchange of the DMOA counterion to the tetraalkylammonium was achieved by treating the copolymer with the corresponding tetraalkylammonium hydroxide. A representative counterion exchange procedure is described as follows. The P(I-*ran*-DMOASS)-7 copolymer (200 mg, 0.165 mmol

DMOASS) was dissolved into a solution of tetrahydrofuran and methanol (6 mL, 2:1, v/v). Tetraethylammonium hydroxide (25% w/w in methanol, 0.22 mL, 0.33 mmol) was added dropwise to the stirring polymer solution and allowed to react for 1 hour at room temperature. The P(I-*ran*-SS)-7-TEA copolymer was isolated from the reaction solution by precipitating into 300 mL of ethyl acetate and decanting off the liquid phase. The polymer was then collected and dried overnight under vacuum. For the more hydrophilic tetramethylammonium and sodium counterions, the amount and ratio of the tetrahydrofuran:methanol solvent was adjusted (9 mL, 1:5, v/v) to prevent precipitation of the hydroxide, and the removal of excess base was achieved through membrane dialysis (Spectra/Pro® 4, MWCO: 12k – 14kDa) in methanol. Films of the copolymers were then obtained by dissolving the copolymer into chloroform:methanol (7:3, v/v) at a concentration of 100 mg/mL and casting into a Teflon® dish. The cast polymer solutions were then covered with a glass dish and allowed to dry in a fume hood overnight. For the sodium cation-containing copolymer a chloroform:N,N-dimethylformamide (1:1, v/v) solvent system was used, which required a longer drying time (~7 days).

3.2.3. Characterization

Solution ^{1}H NMR and solid-state NMR experiments were performed using Bruker Avance III HD 500 MHz and 600 MHz spectrometers, respectively. For $T_{1\rho}$ relaxation measurements, a pulse sequence with a variable-length spin-lock pulse followed by a ^{1}H-^{13}C cross polarization (CP) was used, with 10 to 16 spin-lock data points for each experiment. The spin-lock field strength was 79 kHz, and a temperature window of 263K – 283K was probed. Most experiments used a short CP time of 0.3 ms to optimally retain the component with short $T_{1\rho}$ times, except for $T_{1\rho}$ measurement of the TMA moiety in

P(I-*ran*-SS)-7-TMA, in which a CP time of 1.5 ms was used due to the fast dynamics of the TMA cation. For the polyisoprene homopolymer, the pulse sequence was simply a ^{1}H 90° excitation followed by a variable-length spin-lock pulse followed by ^{1}H detection.

For X-ray scattering, copolymer films were melt pressed into metal washers at 80 °C and fixed in place using Kapton® tape. X-ray scattering experiments were performed using a SAXS-LAB Ganesha instrument with a Cu-K_α 0.154 nm line in MAXS mode with scattering profiles collected over a 5 minute time interval. The scattering from an empty washer covered in Kapton® tape was subtracted from the scattering data prior to fitting with the Kinning-Thomas (K-T) modified hard sphere model.[20]

Differential scanning calorimetry (DSC) was performed on a TA Instruments DSC Q200 equipped with a refrigerated cooling system (RCS90). Samples of approximately 3-5 mg were loaded into hermetic aluminum pans and subjected to a heat/cool/heat cycle at a heating/cooling rate of 10 K/min over a temperature range of -70 to 80 °C. The T_g's were determined from the second heating cycle. Dynamic mechanical analysis (DMA) was performed on a TA Instruments DMA Q800 in oscillatory tension mode at a frequency of 10 Hz and a strain amplitude of 0.3 % with a preload force of 0.01N. The samples were heated at a rate of 3 K/min from -80 to 80 °C. For rheology, the copolymers were molded into disk shapes by melt pressing into metal washers (I.D. = 8 mm, t = 1.6) at 80 °C. The linear viscoelastic response of the material was characterized using an 8-mm parallel plate fixture in a Malvern Kinexus Pro+ rheometer. Small amplitude oscillatory shear (SAOS) measurement were measured between 1 rad/s < ω < 100 rad/s from -20 to 80 °C in 10K increments at a strain amplitude of 0.1%.

3.3. Results and Discussion

3.3.1. Polymer Synthesis and Counterion Exchange

As previously reported, P(I-*ran*-DMOASS) copolymers can be directly synthesized through a nitroxide-mediated copolymerization of isoprene and DMOASS in anisole.[19] For this study, a P(I-*ran*-DMOASS) copolymer containing 7 mol% DMOASS was synthesized. The copolymer's DMOASS mol% was kept low to ensure the formation of ion aggregate structures. The degree of polymerization can be estimated from ^{1}H NMR spectroscopy as discussed in Chapter 2, and was found to be approximately 1260. Following the polymerization, the initial copolymer was divided into separate batches, and the DMOA counter was exchanged. Five different counterion of varying bulkiness were selected to evaluate their effect on the structure and dynamics of the low T_g, amorphous P(I-*ran*-SS)-7 ionomer. The counterions in this series include: sodium (Na^+), tetramethylammonium (TMA), tetraethylammonium (TEA), tetrapropylammonium (TPA), and tetrabutylammonium (TBA). The sodium cation offered a control alkali metal counterion that possessed minimal steric hinderance while the tetraalkylammonium series provided a platform to vary the counterion sterics systematically by increasing the length of the pendent alkyl chains attached to the ammonium counterion.[11,16] Exchange of the counterion was performed by treating the P(I-*ran*-SS)-7-DMOA copolymer with the sodium or tetraalkylammonium hydroxide as shown in Figure 3.1. This synthetic methodology deprotonated the DMOA, consequently removing its charge and depositing the tetraalkylammonium onto the polymer backbone.

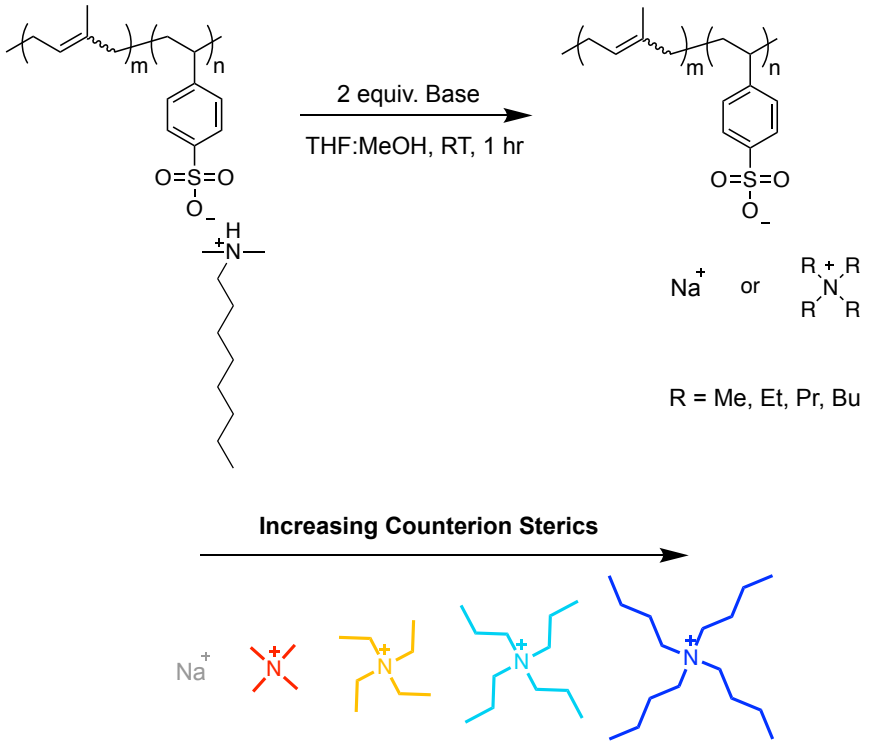

Figure 3.1. Counterion exchange via deprotonation of DMOA

The counterion exchange of the copolymers was monitored using ^{1}H NMR spectroscopy (Figure 3.2). In the spectra, the protons on the carbon alpha to the nitrogen appeared between δ 2.5 – 3.5 ppm for all of the counterions. Signals appearing at δ 3.00 and δ 2.80 ppm for the DMOA counterion correspond to the 2 methylene protons and the 6 methyl protons, respectively. After counterion exchange, these signals disappeared and were replaced by one signal between δ 3.10 and δ 3.30 ppm corresponding to 12 methyl protons for the TMA-containing copolymer or 8 methylene protons for the TEA, TPA, and TBA-containing copolymers. For the Na-containing copolymer, no peak appears in the δ 2.5 – 3.5 ppm range due to a lack of protons.

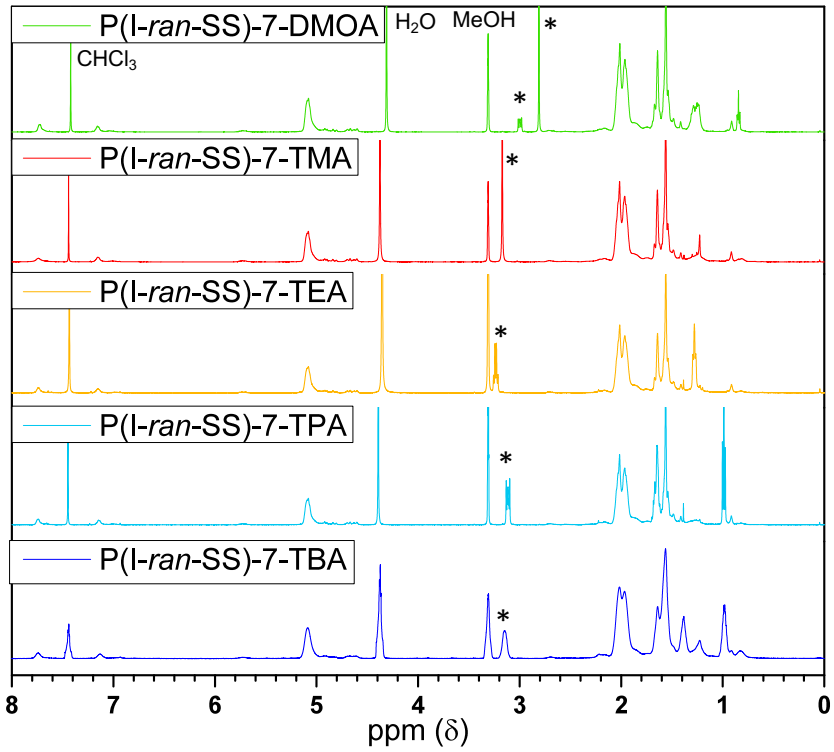

Figure 3.2. Comparison of the ^{1}H NMR spectrum for the P(I-*ran*-SS)-7-x copolymer series (x = Na^{+}, TMA, TEA, TPA, and TBA). The asterisk marks the counterion methyl(ene) protons adjacent to the nitrogen.

3.3.2. Effect of Counterion Sterics on the Ion Aggregates

The structure of the copolymers with the different counterions was probed using SAXS. Figure 3.3 shows the X-ray scattering profiles of the copolymer with the various counterions. The peak in the high q regime indicates the presence of ion aggregate structures in all of the samples.[21] For each copolymer, the q value at the peak maximum was converted to a domain spacing (d-spacing) that corresponds to the average distance between neighboring ion aggregates. These d-spacing values, which are reported in Table 1, gradually increase from 5.1 nm to 7.3 nm with the size of the counterion.

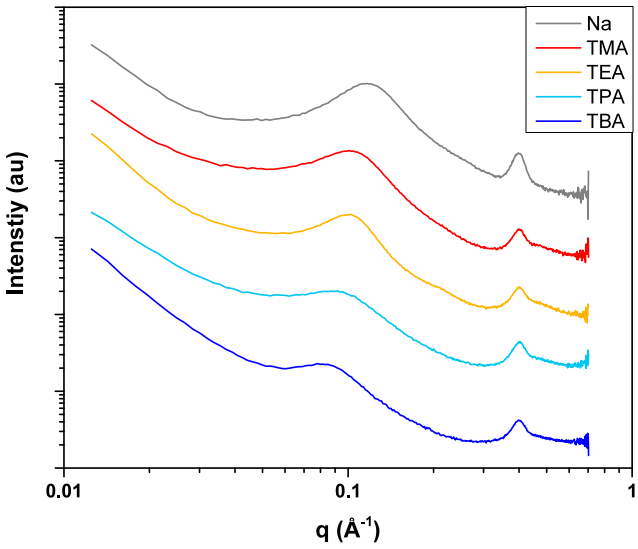

Figure 3.3. Offset SAXS profiles for the P(I-*ran*-SS)-7-x copolymers with different counterions (x = Na^+, TMA, TEA, TPA, and TBA). The peak at 0.4 $Å^{-1}$ in all of the spectra corresponds to Kapton®.

To extract additional structural information from the SAXS profiles, the Kinning-Thomas (K-T) model was used to fit the scattering peaks. From this model, the ion aggregates are assumed to be spherical structures in a liquid-like arrangement. The scattering intensity (*I(q)*) is defined by the hard-sphere form factor (*Φ(x)*) and a Percus-Yevick function that accounts for inter-cluster scattering interference.[20] The equation is shown below.

$$\boldsymbol{I(q) = A\Phi^2(x)\left(\frac{1}{1+24\eta\left(\frac{G(B)}{B}\right)}\right)} \tag{3.1}$$

where

$$\Phi(x) = 3\frac{\sin(x)-x\cos(x)}{x^3}, \tag{3.2}$$

$$x = qR_1, \tag{3.3}$$

$$\eta = \frac{4}{3}\pi {R_{ca}}^3\left(\frac{1}{V_p}\right), \tag{3.4}$$

$$B = 2qR_{ca}\ , \tag{3.5}$$

and

$$G(B) = \frac{(1+2\eta)^2}{B^2(1-\eta)^4}(sinB - BcosB) - \frac{6\eta\left(1+\frac{\eta}{2}\right)^2}{B^3(1-\eta)^4}[2BsinB + (2-B^2)cosB - 2] +$$

$$\frac{\eta(1+2\eta)^2}{2B^5(1-\eta)^4}\{-B^4cosB + 4[(3B^2-6)cosB + (B^3-6B)sinB + 6]\} \qquad (3.6)$$

Four parameters are adjusted to obtain the best fit. These parameters are A, R_1, R_{ca}, and V_p; where A is a scaling factor, R_1 is the radius of the ion aggregate, R_{ca} is the radius of closest approach, and V_p is the sample volume per ion aggregate. As shown in the equation, R_1 is associated with the radius of the hard sphere form factor, while R_{ca} and V_p are determined from the inter-clustering scattering interference. Figure 3.4a and 3.4b show the SAXS profiles fitted with the K-T model and the plot of the fitting parameters as a function of the counterion radius, respectively. The corresponding parameter values are displayed in Table 3.1. It is important to note that the information obtained from scattering models is limited when direct visualization of the aggregate structures is not available.[22] However, the K-T scattering model still provided a useful framework to begin to explore these ion aggregate structures.

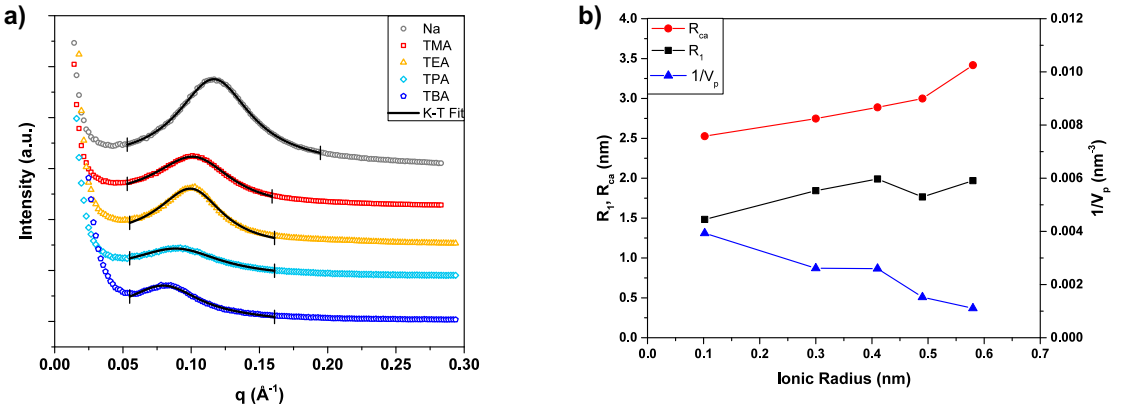

Figure 3.4. a) Kinning-Thomas fitting of the SAXS profiles for P(I-*ran*-SS)-7-x copolymers and b) the plot of the R_1, R_{ca}, and $1/V_p$ as a function of the counterion radius (lines are plotted to guide the eye)

Table 3.1. Summary of the Kinning-Thomas Fitting Parameters and Calculated Ion Aggregate Compositions

Sample	D-spacing (nm)	R_1 (nm)	R_{ca} (nm)	V_p (nm^3)	$N_{agg}(R_1)$	$N_{agg}(V_p)$	$N_{agg}(V_p)/N_{agg}(R_1)$
Na	5.4	1.5	2.5	254 ± 1	224	119	0.53
TMA	5.9	1.8	2.7	383 ± 4	141	188	1.33
TEA	6.1	2	2.9	385 ± 6	123	182	1.48
TPA	6.8	1.8	3	656 ± 12	65	298	4.57
TBA	7.4	2	3.4	902 ± 18	73	394	5.39

Additionally, the number of ionic groups per aggregate were calculated using two different methods previously reported in the literature.[8] Both methods assume that all of the ionic groups reside within an aggregate. The first method divides the spherical aggregate volume, determined from R_1, by the volume of the sulfonate-cation pair ($V_{acid-ion}$) to give the number of ion-pairs per aggregate. The second method uses V_p, the volume fraction of the styrenesulfonate-cation (ϕ_{SS}), and the number of styrenesulfonate-cation pairs per volume (η_{SS}). The equations associated with these calculations are shown below:

$$N_{agg}(R_1) = \frac{\frac{4}{3}\pi R_1^3}{V_{acid-ion}} \quad (1)$$

$$N_{agg}(V_p) = \phi_{SS} V_p \eta_{SS} \quad (2)$$

For the $V_{acid-ion}$ for each sulfonate-counterion pair, the volume of the corresponding tetraalkylammonium chloride was calculated from their respective molecular weights and densities. To account for the difference in volume of a chloride and sulfonate ion, a volume 0.018 nm^3 was added to each of these values. This volumetric difference was calculated using a model system involving the corresponding sodium salts (sodium chloride and sodium sulfonate), in which the volume of a sodium sulfonate was approximated by multiplying the volume of a sodium sulfate by a factor of 5/7 to account for the additional

oxygen and sodium.[5,8] These values are available in the appendix. For the determination of the number of styrenesulfonate groups per volume, assuming the density of the styrenesulfonate unit does not change significantly between the different counterions, the density of styrenesulfonate-counterion should scale with the molecular weight increase due to the counterion. Further explanation of the calculations is available in the supporting information.

From these calculations, the values of $N_{agg}(R_1)$, $N_{agg}(V_p)$, and $N_{agg}(V_p)/N_{agg}(R_1)$ are reported in the Table 1 and plotted in Figure 3.5. The $N_{agg}(V_p)/N_{agg}(R_1)$ is the occupancy ratio, which estimates the composition of the ion aggregates. An occupancy ratio of 1 indicates that the ion aggregates contain only ionic groups, while an occupancy ratio less than 1 suggests that there are not sufficient ionic groups to completely occupy the spherical aggregate volume. Thus, other portions of the polymer chain exist within the electron-dense aggregate structure. On the other hand, when the occupancy ratio is greater than 1, not all ionic groups are present within the ion cluster, and some of the ionic groups must reside in the polymer matrix.[8]

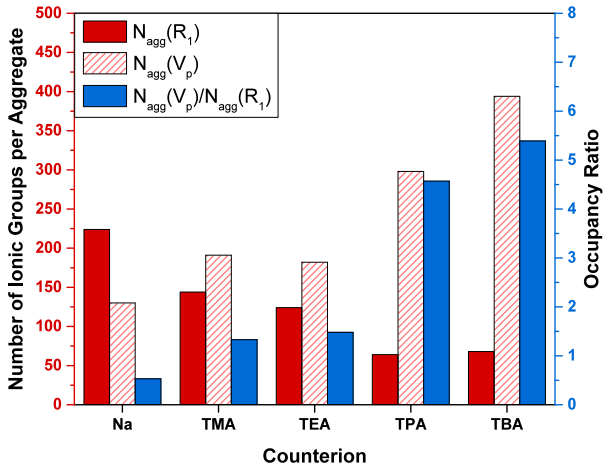

Figure 3.5. Comparison of the estimated number of ion pairs per aggregate ($N_{agg}(R_1)$, $N_{agg}(V_p)$) calculated from the K-T fitting parameters (left y-axis) and the occupancy ratio ($N_{agg}(V_p)/ N_{agg}(R_1)$, right y-axis)

From both the parameters obtained from the K-T fitting and the aggregate composition calculations, a comprehensive depiction of the ion aggregates arises. First, the sodium counterion, which offers the smallest cation radius of the series, exhibited an ion aggregate radius of approximately 1.5 nm. This large aggregate radius results from both the strong ionic interaction of the sulfonate moieties and the flexible, low T_g isoprene matrix, and further confirms the role of the polymer backbone and ionic group on the structure of the ion aggregates.[1,23] Based on the $N_{agg}(R_1)$ value for the P(I-*ran*-SS)-7-Na, the ion aggregates consist of a high number of ionic groups (~220). Additionally, the occupancy ratio of 0.53 indicates a fraction of nonionic material present within the ion aggregates, which has also been seen in other ionomer systems.[6,8]

Increasing the counterion bulkiness from sodium to TMA or TEA, both R_1 and R_{ca} increase, and the aggregates appear to swell with the presence of the larger counterions. As shown by $1/V_p$, a decrease in the number density of the aggregates also results. Furthermore, the occupancy ratio of 1.36 and 1.46 for the P(I-*ran*-SS)-7-TMA and P(I-*ran*-SS)-7-TEA, respectively, suggests that not all of the ionic group are present in the ion cluster, thus some fraction of the ionic groups are distributed into the isoprene matrix.

When increasing the counterion sterics further to TPA or TBA, R_1 initially decreases followed by an increase back to approximately 2 nm. In addition, R_{ca} continues to increase along with a large decrease in $1/V_p$. Upon further inspection, a large increase in the occupancy ratio occurs that greatly exceeds 1, and it appears that a significant structural change results once sufficient steric hinderance is achieved.

Two important details to consider when understanding the structure in these copolymers are: (1) the steric screening provided by the pendent alkyl chains effectively

decreases the dipole-dipole interactions between neighboring ion pairs and (2) less efficient packing of the ion pairs into electron-dense aggregates occurs due to the additional volume. The combination of these two phenomena are believed to limit the number of ionic groups in the scattering structure that results in some ion pairs being excluded to region surrounding the ion cluster. These regions would then correspond with the increase in R_{ca}. Additionally, the ionic groups become more oleophilic as the counterion's alkyl chain lengths increases, favoring additional mixing with the isoprenic portions of the polymer chains. Thus, these surrounding regions are expected to consist of a combination of ionic groups and isoprenic polymer chain segments.

3.3.3. Molecular Dynamics of P(I-*ran*-SS)-7-TMA and P(I-*ran*-SS)-7-TBA

To further understand the morphology and molecular dynamics in the copolymer samples, ^{1}H $T_{1\rho}$ relaxation behaviors of P(I-*ran*-SS)-7-TMA and P(I-*ran*-SS)-7-TPA were studied by solid-state NMR. Two example spectra of P(I-*ran*-SS)-7-TPA at different spin-lock times are shown in Figure 3.6. The $T_{1\rho}$ relaxation is sensitive to molecular dynamics in the 10^4 – 10^5 s^{-1} range, and based on the temperature dependence of the $T_{1\rho}$, the segmental motion can be determined relative to the spin-lock field strength of 79 kHz.

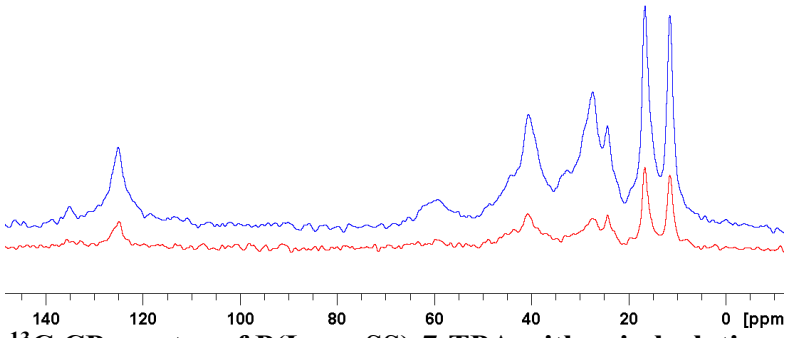

Figure 3.6. ^{13}C CP spectra of P(I-*ran*-SS)-7-TPA with spin lock times of 0.01 ms (blue) and 1 ms (red)

The decay of the isoprene signal at δ 28ppm was tracked for $T_{1\rho}$ measurements of the isoprene moiety. For all the temperatures probed, a bi-exponential model provided the best fit for both P(I-*ran*-SS)-7-TMA and P(I-*ran*-SS)-7-TPA (Table 3.2). The decay constants of the two components differed by a factor of approximately 3 and 10 for P(I-*ran*-SS)-7-TPA and P(I-*ran*-SS)-7-TMA, respectively. Such large difference suggests that the two components belong to separate domains with differing molecular dynamics. The relatively large error values partially reflect the relatively broad signals, which produce low signal-to-noise ratios. To verify the reliability of the curve fitting, $T_{1\rho}$ relaxations of the isoprene backbone signals at δ 17 and δ 41 ppm for the P(I-*ran*-SS)-7-TMA copolymer were also calculated. The results, shown in Table S1, are consistent with those of the δ 28 ppm peak.

Table 3.2. Fitting results for $T_{1\rho}$ relaxation experiments for P(I-*ran*-SS)-7-TPA and P(I-*ran*-SS)-7-TMA (contact time = 0.3 ms). The superscripts s and l stand for short and long, respectively. The δ 28 ppm peak is from the isoprene backbone, and the δ 11 ppm peak is from the methyl group of the TPA cation.

T (K)	P(I-*ran*-SS)-7-TPA			P(I-*ran*-SS)-7-TMA	
	$T_{1\rho}^{s}$ (28ppm)	$T_{1\rho}^{l}$ (28ppm)	$T_{1\rho}$ (11ppm)	$T_{1\rho}^{s}$ (28ppm)	$T_{1\rho}^{l}$ (28ppm)
263K	0.28 ± 0.03	1.1 ± 0.1	1.20 ± 0.02	0.64 ± 0.09	6.7 ± 0.7
273K	0.35 ± 0.08	0.9 ± 0.1	0.87 ± 0.02	0.63 ± 0.04	6.5 ± 0.3
283K	0.48 ± 0.09	1.5 ± 0.4	0.69 ± 0.02	0.71 ± 0.04	6.1 ± 0.3

$T_{1\rho}$ of the methyl group in the TPA counterion moiety at δ 11 ppm was calculated from the same experimental data as those for the δ 28 ppm peak. For the temperature range probed, $T_{1\rho}$ relaxation curves could be fit with a single exponential model. Aided by the

intensity and sharpness of its peak, small fitting errors of its $T_{1\rho}$ results were obtained, as seen in Table 3.2. As temperature increases from 263K to 283K, its $T_{1\rho}$ decreased from 1.20 s to 0.69 s. The temperature dependence of the TPA methyl group indicates that its dynamics are in the slow motion regime, with average segmental motion slower than the spin-lock field strength of 79 kHz. On the other hand, $T_{1\rho}$ of the short-$T_{1\rho}$ component of the isoprene moiety exhibits the opposite temperature dependence, and its dynamics are in the fast motion regime throughout the 263K – 283K window. These results suggest that the counterions reside in lower-mobility domains while the short-$T_{1\rho}$ component of the isoprene moiety resides in higher-mobility domains. The long-$T_{1\rho}$ component of P(I-*ran*-SS)-7-TPA, as well as both components of P(I-*ran*-SS)-7-TMA, in columns 3, 5, and 6 of Table 1, have larger fitting errors and their temperature dependence is not clear.

$T_{1\rho}$ of the N-methyl moiety in P(I-*ran*-SS)-7-TMA was measured in a separate series of experiments. The high signal strength of the N-methyl group requires longer contact time due to its low CP efficiency, likely as a result of the rotational freedom of the TMA cation. Therefore, 1.5 ms of contact time was used to track its $T_{1\rho}$ relaxation behavior. Similar to the TPA methyl signal of the P(I-*ran*-SS)-7-TPA sample, the relaxation curves of N-methyl in P(I-*ran*-SS)-7-TMA at δ 55 ppm are best fit by a single-exponential model for the entire temperature window studied (Table 3.3). To eliminate the possibility of the long contact time concealing a possible short-$T_{1\rho}$ component, $T_{1\rho}$ of the isoprene signal at δ 28 ppm signal was calculated from the same experiment. The peak decay could only be well fitted by a bi-exponential model, thus confirming that the $T_{1\rho}$ of the N-methyl group signal is indeed single-exponential. Additionally, the fitting results for the δ 28 ppm peak

differ slightly between the two contact times used, resulting from somewhat different selection of the population contributing to the signals.

Table 3.3. Fitting results for $T_{1\rho}$ relaxation experiments for P(I-*ran*-SS)-7-TMA (contact time = 1.5 ms). The superscripts s and l stand for short and long, respectively. The δ 28 ppm peak is from the isoprene backbone, and the δ 55 ppm peak is from the methyl group of the TPA cation.

T (K)	$T_{1\rho}^{s}$ (28ppm)	$T_{1\rho}^{l}$ (28ppm)	$T_{1\rho}$ (55ppm)
263	0.8 ± 0.2	7.5 ± 0.4	6.1 ± 0.4
273	1.2 ± 0.3	9.4 ± 1.6	6.2 ± 0.3
283	1.3 ± 0.3	8.5 ± 2.7	4.9 ± 0.4

$T_{1\rho}$ relaxation of the polyisoprene homopolymer synthesized by the same method was measured for comparison. The $T_{1\rho}$ of the homopolymer increased sharply with temperature, indicative of the fast motion regime. A number of different behaviors arise between the homopolymer and the isoprene matrix in the copolymers. First, at 263 – 283K, cross polarization yields little signal intensity for the homopolymer while generating strong signal intensity for the copolymers. This indicates that the homopolymer has much faster and more isotropic segmental mobility than the isoprene matrix phase in the copolymers, resulting in low CP efficiency. Second, $T_{1\rho}$ of the homopolymer exhibits much stronger temperature dependence, increasing almost four-fold from 263K to 283K, than that of the isoprene matrix in copolymers (the short $T_{1\rho}$ component), which increases by less than 60% in the same temperature window for both P(I-*ran*-SS)-7-TPA and P(I-*ran*-SS)-7-TMA. This is a result of the different widths of segmental rotation correlation time distribution. The homopolymer has a narrow distribution of correlation time, while that of the

copolymers is much broader due to the spatial constraints exerted by adjacent ion aggregate domains.

The copolymers discussed in this report have an isoprene-based, non-polar matrix, in which polar interactions between the ionic groups must be minimized. Thus, the ionic groups should reside within the same domain and spatially arrange in such a way that the Coulombic as well as the higher-order multipole interactions are appropriately minimized. Based on the Eisenberg-Hird-Moore model, the isoprene units that are adjacent to the styrene units reside in the regions of restricted mobility and are expected to have lower segmental mobility due to their proximity to the high-T_g styrenesulfonic units, as compared to longer sequences of isoprene units that form the matrix.[24]

It follows that two types of domains exist: higher-mobility, lower-T_g domains formed by longer-sequence isoprene units, and lower-mobility, higher-T_g domains formed by the styrenesulfonate units, counterions, and adjacent isoprene units. The two $T_{1\rho}$ components in both P(I-*ran*-SS)-7-TPA and P(I-*ran*-SS)-7-TMA support this picture. The higher-mobility isoprene matrix has short $T_{1\rho}$ while the lower-mobility ionic clusters have long $T_{1\rho}$. In P(I-*ran*-SS)-7-TPA, the values of the TPA methyl groups are similar to those of the long-$T_{1\rho}$ component of isoprene, which is a result of both "communicative" averaging due to spin diffusion and physical averaging due to close contact within the same domain. In Table 3, it is clear that in P(I-*ran*-SS)-7-TMA, across all the temperatures probed, $T_{1\rho}$ of the N-methyl group is much closer to the long-$T_{1\rho}$ component of the isoprene than to the short-$T_{1\rho}$ component. This supports the assignment of the long-$T_{1\rho}$ component to the domains with styrenesulfonate groups, isoprene units adjacent to them, and counterions. $T_{1\rho}$ of the N-methyl signal decreases with increasing temperature, indicative

of being in the slow-motion regime. The assignments of the two relaxation components to the two types of domains in P(I-*ran*-SS)-7-TPA and P(I-*ran*-SS)-7-TMA are consistent with each other.

The relaxation behaviors of P(I-*ran*-SS)-7-TPA and P(I-*ran*-SS)-7-TMA are qualitatively similar, both having two components for the isoprene population. On the other hand, the $T_{1\rho}$ of the ionic clusters in P(I-*ran*-SS)-7-TMA (ca. 6 ms) is much longer than that in P(I-*ran*-SS)-7-TPA (ca. 1 ms). Since they are both in the slow motion regime, the segmental mobility in the ionic clusters of P(I-*ran*-SS)-7-TMA is much lower than in P(I-*ran*-SS)-7-TPA. This is consistent with the prediction based on the different ion size and ionic strength between TMA and TPA.

Additionally, the different $T_{1\rho}$ relaxation behaviors between the rigid ion clusters and the mobile matrix offers a possibility to conduct spin diffusion experiments with a gradient created by a $T_{1\rho}$ filter. A plot of the spin diffusion spectra for the P(I-*ran*-SS)-7-TPA is available in the Appendix. By monitoring the intensity of both the counterion peaks and the isoprene signals, the diffusion of the magnetization between the two domains can be observed. The counterion signals (δ 11, 16, and 60 ppm) decrease in intensity at increasing diffusion time, as their magnetization diffuse away to surrounding domains. In the meantime, the isoprene signals at δ 28 and δ 41 ppm gain strengths by receiving magnetization from the counterions and the long-$T_{1\rho}$ isoprene units. The equilibrium is reached between 3 and 10 ms. Based on the information, estimate of separation between the counterion cluster and the matrix is likely in the order of 3 – 5 nm.

3.3.4. Effect of Counterion Sterics on the Polymer Dynamics

The glass transition temperature (T_g) of the copolymer, determined via DSC, was -53 ^oC for all of the copolymer samples, while the PI homopolymer possessed a T_g at -60 ^oC. The difference between the T_g of the copolymers and the homopolymer is attributed to decreased polymer chain mobility from a combination of the incorporation of the styrenic copolymer and their ionic groups. As previously reported, the microphase separation of the ionic groups into discrete aggregates causes only a moderate increase in T_g relative to the PI homopolymer and a deviation from the Fox equation prediction due to the heterogeneous distribution of the ionic groups.[19] In these samples, the isoprene matrix dominates the T_g of the copolymer with the ion clusters providing some restrictions in the polymer chain segmental mobility.

To elucidate the thermal transitions of the copolymers further, DMA was performed on each sample. Figure 3.7a and 3.7b shows the storage modulus (E') and tan δ as a function of temperature, respectively. For all of the copolymers, a thermal transition appears between -30 and -25 ^oC marked by a drop in the E' and a peak in tan δ. This transition corresponds with the T_g of the isoprene matrix, which was also observed in the DSC thermograms. At temperatures above 0 ^oC, E' decreased at a more rapid rate as the counterion steric hindrance increased, and a second peak appeared in the plot of tan δ. Additionally, a plateau modulus was present in the thermograms for all samples. Thus, as temperature increases, the copolymers first undergoes the glass transition of the isoprene matrix followed by the mobility associated with the ion aggregates.[25,26]

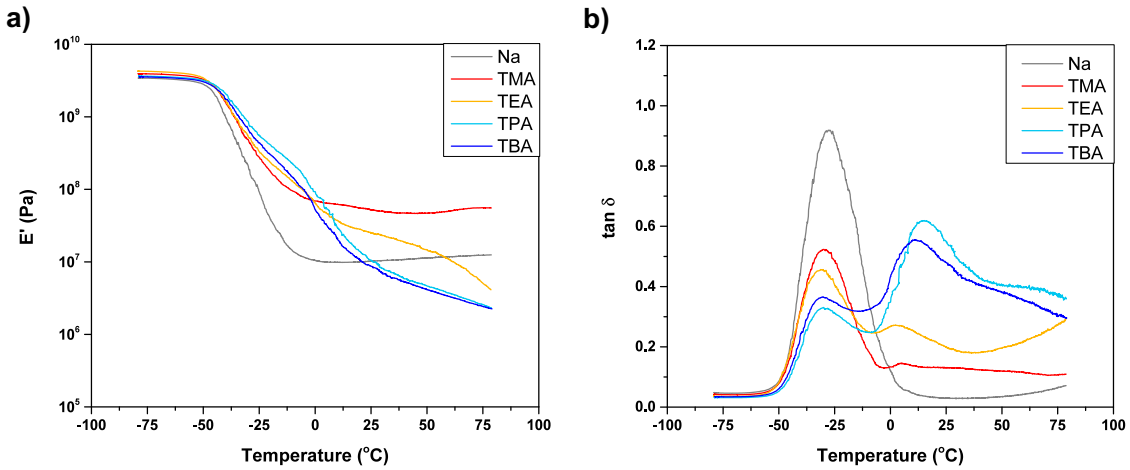

Figure 3.7. DMA single frequency (10 Hz) heating scans (3 K/min): a) storage modulus and b) tan δ as a function of temperature for the P(I-*ran*-SS)-7-x copolymers

For the least sterically hindered sodium and TMA counterions, the stronger dipole-dipole interactions produce static ion aggregate structures as indicated by the persistence of the plateau modulus to 80 °C. Surprisingly, P(I-*ran*-SS)-7-TMA exhibited a plateau modulus that was an order of magnitude higher than the sodium-containing copolymer. This increase in plateau moduli was unexpected since the sodium counterion possesses a higher number density of cluster ($1/V_p$), which decreases the molecular weight between the ionic physical crosslinks and should increase the plateau modulus. This discrepancy is believed to be caused by the presence of ionic groups within the isoprene matrix in the TMA copolymer (as indicated by the occupancy ratio > 1) that can still interact with other nearby ionic groups outside of the ion aggregates.

For TEA, the effect of the counterion sterics begins to appear, as shown by the decrease in the plateau modulus and the onset of long-range segmental mobility at high temperatures. For the TPA and TBA, the large counterion sterics results in weak dipole-dipole interactions, and the ionic groups gain mobility at temperatures above 0 °C. As

shown by the $T_{1\rho}$ relaxation experiments, the larger counterions possess faster molecular dynamics, thus the mobility of the ionic groups in the aggregate structures occurs at lower temperatures. Based on the presence of the plateau, it appears that not all of the TPA and TBA become mobile, and some fraction of the ionic groups remain associated within a cluster. With this understanding of the polymer dynamics, a clearer picture of the aggregate structures observed through SAXS arises.

By rheology, SAOS master curves were constructed and the linear viscoelastic behavior of the copolymers was evaluated. Figure 3.8a and 3.8b show the storage modulus (G') and loss modulus (G") as a function of frequency, respectively. A PI homopolymer, shown in black, represents a typical entangled polymer melt, containing both a plateau modulus and a terminal regime. With the incorporation of the ionic groups, an extension of the plateau modulus was realized for all of the copolymers. This extension to lower frequencies results from the increased polymer connectivity due to the physical bonds provided by the ion aggregates.[9] At high frequencies, the G' and G" both increased with the counterion size. This correlation agrees with the results from the DMA where further restriction of the copolymer's dynamics at temperature near the polymer matrix glass transition occurred. Based on the SAXS results, this restriction is believed to result from ionic groups that reside in the areas surrounding the ion aggregate.

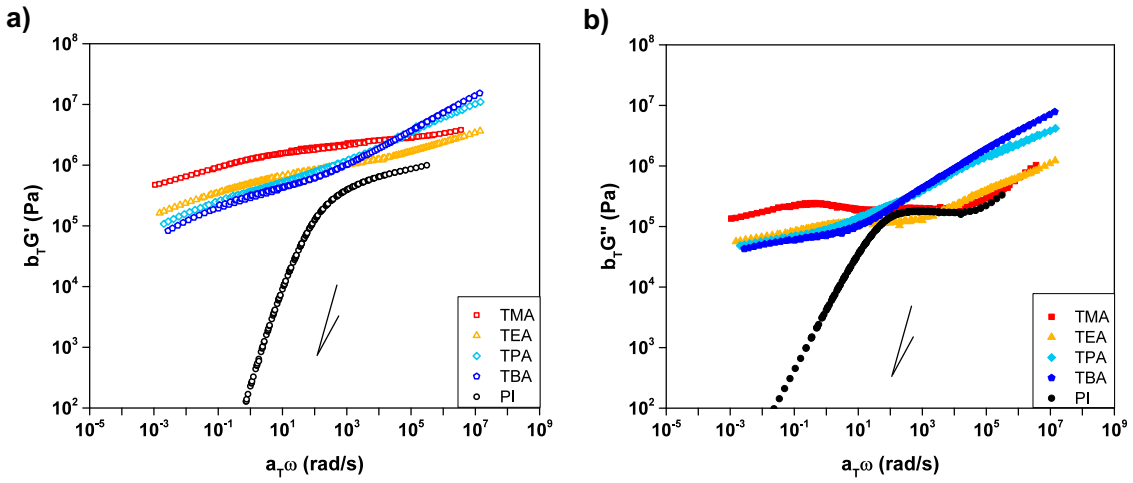

Figure 3.8. a) Storage and b) loss modulus as a function of frequency for PI and the P(I-*ran*-SS)-7-x copolymer series (T_{ref} = 50 °C)

At intermediate frequencies, the storage modulus decreased for the TEA, TPA, and TBA copolymers and gradually reached plateau moduli of similar magnitude. For the TMA copolymer, the plateau modulus began at higher frequencies with a larger modulus value than the other samples. This higher plateau modulus results from the higher number density of ion aggregates and the stronger electrostatic interactions of the smaller TMA counterion, which persist over a wider frequency range. At low frequencies, the storage modulus decreased with the counterions size. In this frequency regime, the steric screening effect of the larger counterions arises. The steric hinderance of the counterion reduced the ability of the dipole-dipole interactions to approach each other, thus weakening electrostatic interactions and causing the copolymer to have a more viscous response at elevated temperatures.

Similar tends are observed with additional viscoelastic functions. Figure 3.9 shows the plot of the normalized δ as a function of the frequency. In this plot, normalized δ generally increases with the counterion sterics throughout the frequency range. Thus, the linear viscoelastic behavior of the ionomers exhibits a larger contribution of the viscous

component as a result of the weakened dipole-dipole interactions with the more sterically hindered counterions. Additionally, as noted in the dynamic moduli, the onset of the terminal regime at the lowest frequencies becomes more prevalent as the counterion size is increased. Specifically, all of the copolymers, except for the TMA-containing sample, are liquids as shown by the upturn in δ at the lowest frequencies. The TMA-containing copolymer shows more elastic behavior throughout the entire frequency window as a consequence of the strong electrostatic interactions; however, the copolymer is expected to exhibit a terminal regime at lower frequencies due to the presence of only physical crosslinks.

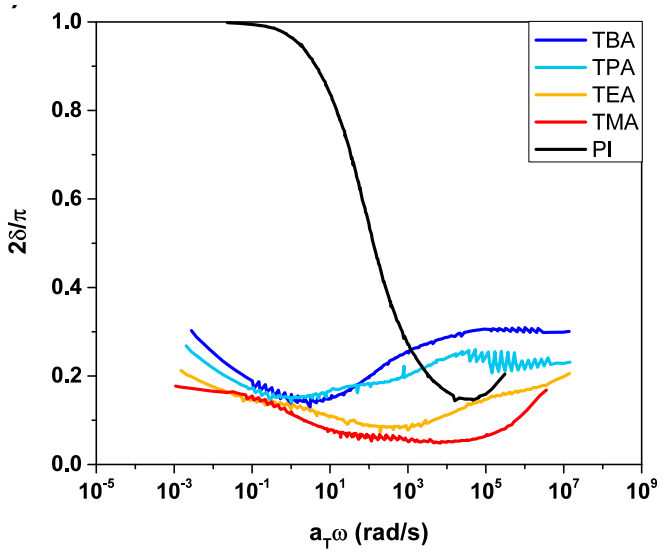

Figure 3.9. Normalized δ as a function of frequency in for PI and the P(I-*ran*-SS)-7-x copolymer series (T_{ref} = 50 °C)

Figure 3.10 shows the continuous relaxation spectra of the copolymer series, which were calculated for the TTS master curves using a method developed Baumgaertel and Winter.[27] For the copolymers, an increase in the relaxation modes at the shortest times results from approach of the glass transition. For the less sterically hindered TMA and TEA counterions, minimal changes occur in H(τ) throughout the relaxation spectra indicating

only slight relaxations of the polymer chains. Compared to the TMA or TEA, the larger TPA or TBA counterions cause an increase in the relaxation modes at short times. At longer times, the relaxation modes of the TPA or TBA counterions decrease and eventually plateau at long times. In these ionomers, the more sterically hindered counterions introduce a new relaxation process. This relaxation process result from the larger, disrupted ion aggregate structures, which allow for the polymer chains to relax. This observation further confirms the increased molecular dynamics and polymer chain mobility that was identified in the solid-state NMR and DMA, respectively. For the smaller counterions, following the relaxation of the isoprene matrix, the stronger electrostatic interactions prevent further relaxation of the polymer chains. Additionally, the relaxation modes at the longest times increase, indicating additional relaxation process at long times.

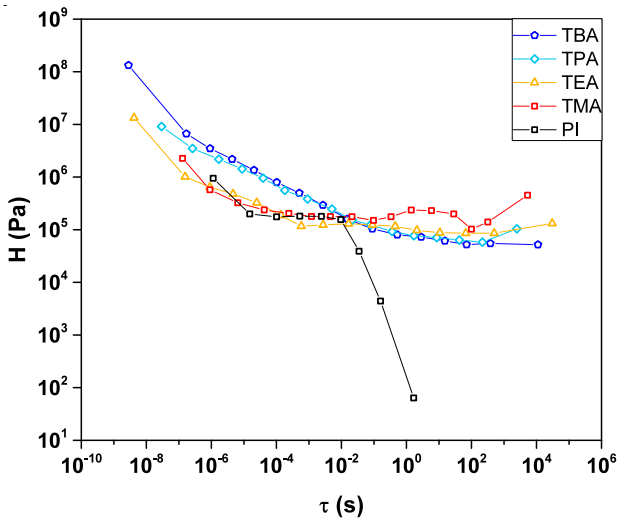

Figure 3.10. Continuous relaxation time spectra calculated from the SAOS data for PI and the P(I-*ran*-SS)-7-x copolymer series

3.4. Conclusion

Counterion sterics were evaluated on the structure and dynamics of low T_g, amorphous P(I-*ran*-SS)-7 copolymers. When collectively reviewing the structural and

dynamic characterization results of the entire P(I-*ran*-SS)-7 series, the role of counterion sterics becomes apparent. The sodium counterion provides minimal steric hinderance, and forms large ion aggregates (radius of ~1.5 nm) due to the strong sulfonate ionic moieties and the flexible, low T_g isoprene polymer backbone. These aggregates possess a high number of ionic groups (~220) with a small fraction of nonionic material also present.

The TMA and TEA counterions appear to swell the ion aggregates in addition to decreasing the number density of the aggregates. The occupancy ratio greater than unity suggests that not all of the ionic group are present in the ion cluster, thus some fraction of the ionic groups are distributed into the isoprene matrix. This slight change in the structure causes the plateau modulus to increase an order of magnitude higher than the sodium ion-containing copolymer, presumably due to interactions between neighboring ionic groups outside of the discrete ion aggregates.

When increasing the counterion sterics further to TPA or TBA, the K-T fitting parameters suggest a lower number density of ion aggregates with larger regions of restricted mobility. In addition, the occupancy ratio greatly exceeds unity. It appears that a significant structural change results once sufficient steric hinderance is achieved. The high steric hinderance of these counterions most likely impede the formation of typical ion aggregate structures and a large fraction of the ionic groups may reside in the isoprene matrix due to the increased oleophilic nature of the counterion.

In the dynamics of these copolymer, increased counterion sterics resulted in weakening of the ionic physical crosslinks and a more rapid decrease in the dynamic moduli at elevated temperatures. At lower temperatures, the dynamic moduli increased with the counterion sterics, further indicating the modification of the copolymer structure.

3.5. References

(1) Eisenberg, A.; Kim, J.-S. *Introduction to Ionomers*; Wiley: New York, 1998.

(2) *Ionomers: Synthesis, Structure, Properties and Applications*; Tant, M. R., Mauritz, K. A., Wilkes, G. L., Eds.; Chapman & Hall: New York, 1997.

(3) Grady, B. P. Review and Critical Analysis of the Morphology of Random Ionomers Across Many Length Scales. *Polym. Eng. Sci.* **2008**, *48* (6), 1029–1051.

(4) Winey, K. I.; Laurer, J. H.; Kirkmeyer, B. P. Ionic Aggregates in Partially Zn-Neutralized Poly(Ethylene-Ran-Methacrylic Acid) Ionomers: Shape, Size, and Size Distribution. *Macromolecules* **2000**, *33* (2), 507–513.

(5) Benetatos, N. M.; Chan, C. D.; Winey, K. I. Quantitative Morphology Study of Cu-Neutralized Poly(Styrene-Ran- Methacrylic Acid) Ionomers: STEM Imaging, X-Ray Scattering, and Real-Space Structural Modeling. *Macromolecules* **2007**, *40* (4), 1081–1088.

(6) Castagna, A. M.; Wang, W.; Winey, K. I.; Runt, J. Structure and Dynamics of Zinc-Neutralized Sulfonated Polystyrene Ionomers. *Macromolecules* **2011**, *44* (8), 2791–2798.

(7) Taubert, A.; Winey, K. I. Imaging and X-Ray Microanalysis of a Poly(Ethylene-Ran-Methacrylic Acid) Ionomer Melt Neutralized with Sodium. *Macromolecules* **2002**, *35* (19), 7419–7426.

(8) Zhou, N. C.; Chan, C. D.; Winey, K. I. Reconciling STEM and X-Ray Scattering Data To Determine the Nanoscale Ionic Aggregate Morphology in Sulfonated Polystyrene. *Macromolecules* **2008**, *41* (16), 6134–6140.

(9) Weiss, R. A.; Fitzgerald, J. J.; Kim, D. Viscoelastic Behavior of Lightly Sulfonated Polystyrene Ionomers. *Macromolecules* **1991**, *24* (5), 1071–1076.

(10) Weiss, R. A.; Zhao, H. Rheological Behavior of Oligomeric Ionomers. *J. Rheol.* **2009**, *53* (1), 191–213.

(11) Page, K. A.; Landis, F. A.; Phillips, A. K.; Moore, R. B. SAXS Analysis of the Thermal Relaxation of Anisotropic Morphologies in Oriented Nafion Membranes. *Macromolecules* **2006**, *39* (11), 3939–3946.

(12) Weiss, R. A.; Agarwal, P. K.; Lundberg, R. D. Control of Ionic Interactions in Sulfonated Polystyrene Ionomers by the Use of Alkyl- Substituted Ammonium Counterions. *J. Appl. Polym. Sci.* **1984**, *29*, 2719–2734.

(13) Tudryn, G. J.; Liu, W.; Wang, S. W.; Colby, R. H. Counterion Dynamics in Polyester-Sulfonate Ionomers with Ionic Liquid Counterions. *Macromolecules* **2011**, *44* (9), 3572–3582.

(14) Zander, Z. K.; Wang, F.; Becker, M. L.; Weiss, R. A. Ionomers for Tunable Softening of Thermoplastic Polyurethane. *Macromolecules* **2016**, *49*, 926–934.

(15) Chen, Q.; Liang, S.; Shiau, H. S.; Colby, R. H. Linear Viscoelastic and Dielectric Properties of Phosphonium Siloxane Ionomers. *ACS Macro Lett.* **2013**, *2* (11), 970–

974.

(16) Page, K. A.; Cable, K. M.; Moore, R. B. Molecular Origins of the Thermal Transitions and Dynamic Mechanical Relaxations in Perfluorosulfonate Ionomers. *Macromolecules* **2005**, *38* (15), 6472–6484.

(17) Osborn, S. J.; Hassan, M. K.; Divoux, G. M.; Rhoades, D. W.; Mauritz, K. A.; Moore, R. B. Glass Transition Temperature of Perfluorosulfonic Acid Ionomers. *Macromolecules* **2007**, *40* (10), 3886–3890.

(18) Phillips, A. K.; Moore, R. B. Mechanical and Transport Property Modifications of Perfluorosulfonate Ionomer Membranes Prepared with Mixed Organic and Inorganic Counterions. *J. Polym. Sci. Part B Polym. Phys.* **2006**, *44*, 2267–2277.

(19) Enokida, J. S.; Tanna, V. A.; Winter, H. H.; Bryan Coughlin, E. Progression of the Morphology in Random Ionomers Containing Bulky Ammonium Counterions. *Macromolecules* **2018**, *51* (18), 7377–7385.

(20) Kinning, D. J.; Thomas, E. L. Hard-Sphere Interactions between Spherical Domains in Diblock Copolymers. *Macromolecules* **1984**, *17* (9), 1712–1718.

(21) Yarusso, D. J.; Cooper, S. L. Microstructure of Ionomers: Interpretation of Small-Angle X-Ray Scattering Data. *Macromolecules* **1983**, *16* (12), 1871–1880.

(22) Middleton, L. R.; Winey, K. I. Nanoscale Aggregation in Acid- and Ion-Containing Polymers. *Annu. Rev. Chem. Biomol. Eng.* **2017**, *8* (1), 499–523.

(23) Castagna, A. M.; Wang, W.; Winey, K. I.; Runt, J. Influence of Cation Type on Structure and Dynamics in Sulfonated Polystyrene Ionomers. *Macromolecules* **2011**, *44* (13), 5420–5426.

(24) Eisenberg, A.; Hird, B.; Moore, R. B. A New Multiplet-Cluster Model for the Morphology of Random Ionomers. *Macromolecules* **1990**, *23* (18), 4098–4107.

(25) Agarwal, P. K.; Makowski, H. S.; Lundberg, R. D. Viscoelastic Behavior of Sulfonated Polymers: Sulfonated Ethylene-Propylene Terpolymer. *Macromolecules* **1980**, *13* (6), 1679–1687.

(26) Nishida, M.; Eisenberg, A. Dynamic Mechanical Study of Sodium Sulfonated Random Ionomers Based on Hydrogenated Styrene-Butadiene Copolymer. *Macromolecules* **1996**, *29* (5), 1507–1515.

(27) Baumgaertel, M.; Winter, H. H. Determination of Discrete Relaxation and Retardation Time Spectra from Dynamic Mechanical Data. *Rheol. Acta* **1989**, *28* (6), 511–519.

CHAPTER 4

MIXED COUNTERION IONOMERS WITH CONTROLLED DYNAMICS AND MECHANICAL PROPERTIES

4.1. Introduction

Ionomers containing mixtures of two counterions have been employed for some industrial applications such as golf ball covers.[1] These mixed counterions allow for easy modification of the ionomer's stiffness, yield strength, and water absorption. The majority of the studies have investigated poly(ethylene-*co*-methacrylic acid) ionomers with binary blends of metal counterions.[2–4] Based on these studies, it was found that ion aggregate structures consisting of both counterions formed, resulting in altered interactions between ionic groups within the aggregates.

As presented in Chapter 3, bulky counterions can greatly affect both the structure and dynamics of an ionomer. However, there has been minimal work focused on mixed ammonium counterion systems. Moore and coworkers investigated the thermal and transport properties of Nafion® possessing a mixture of sodium and tetrabutylammonium (TBA) counterions.[5] In this high T_g, semicrystalline perfluorosulfonate copolymer, a gradual transition of the thermomechanical properties between the 100% sodium ion and 100% TBA samples occurred, where both the α- and β-relaxations decreased to lower temperatures as more TBA counterions were incorporated into the polymer structure. Thus, the TBA counterions contributed to both the plasticization of the polymer chains (β-relaxation) and the ionic network structures (α-relaxation). Additionally, in this system the ^{23}Na NMR and SAXS data suggested ion aggregates consisting of both sodium ions and TBA. Analysis of these mixed counterion systems, however, are complicated by complex

branched chemical structure of Nafion® in addition to the presence of crystalline domains. A more in-depth investigation of the effect of mixed counterion systems in a model system would provide more information regarding their structure and interactions at different ratios.

Specifically, the poly(isoprene-*ran*-styrenesulfonate) (P(I-*ran*-SS)) copolymer offers a model polymer system to further investigate these mixed counterion systems due to its low T_g amorphous structure. In this chapter, binary mixtures of tetramethylammonium (TMA) and tetrabutylammonium (TBA) P(I-*ran*-SS) copolymers were synthesized and a detailed characterization of the resulting ionomer structure, polymer dynamics, and corresponding mechanical properties was performed.

4.2. Experimental

4.2.1. Materials

Isoprene (99%, Acros Organic) was distilled at room temperature under vacuum. 3,7-Dioxa-4-aza-6-phosphanonanoic acid, 4,5-bis (1,1-dimethylethyl)-6-ethoxy-2,2-dimethyl-6-oxide (SG1) (BlocBuilder®) was kindly provided by Arkema. Sodium styrenesulfonate (Alfa Aesar), N,N-dimethyloctylamine (97 %, Acros Organic), hydrochloric acid (12 M, VWR), anisole (99.7 %, Sigma Aldrich), tetramethylammonium hydroxide (25 % w/w in methanol, Alfa Aesar), and tetrabutylammonium hydroxide (1M in methanol, Alfa Aesar) were used without further purification.

4.2.2. Scaled-Up Synthesis of P(I-*ran*-DMOASS)

The synthesis DMOASS and P(I-*ran*-DMOASS)-8.3 was based on our previously reported procedure.[6] The copolymerization was further modified to accommodate a larger

scale reaction. This modified synthetic procedure used a bench top Parr 4560 Mini reactor with a 600 mL stainless steel pressure vessel. DMOASS (57.88 g, 150 mmol, weight adjusted for 11.5 wt% impurity), isoprene (165 mL, 1350 mmol, volume adjusted with 30 mL excess), anisole (150 mL), and SG1 (240 mg, 0.62 mmol) were added to the pressure vessel. The reaction mixture was degassed at 0 °C for 45 minutes with a nitrogen gas flow of 0.5 L/min. The polymerization was then performed at 125 °C for 17 hours and subsequently quenched by placing the pressure vessel in to an ice bath. Methanol was added to the crude reaction mixture to obtain a homogenous solution, which was then precipitated twice into ethyl acetate (2x, 7 L each). The copolymer was collected by dissolving in a mixture of chloroform and methanol, concentrating on a rotovap, and drying in a vacuum oven overnight at room temperature. Approximately 20 g of clear, rubbery polymer were recovered.

4.2.3. Counterion Exchange of P(I-*ran*-DMOASS)

Exchange of the DMOA counterion to the tetraalkylammonium was achieved by treating the copolymer with the corresponding tetraalkylammonium hydroxide. A representative counterion exchange procedure is described as follows. The P(I-*ran*-DMOASS)-8.3 copolymer (6 g, 5.48 mmol DMOASS) was dissolved into a solution of tetrahydrofuran and methanol (225 mL, 2:1, v/v). Tetrabutylammonium hydroxide (11 mL, 2 equiv., 1M in methanol) was added dropwise to the stirring polymer solution at 0 °C and allowed to react for 3 hours. The polymer solution was then concentrated on the rotovap and precipitated twice into 1 L of ethyl acetate. For the more hydrophilic tetramethylammonium (TMA), the amount and ratio of the tetrahydrofuran:methanol solvent was adjusted (360 mL, 1:4, v/v) to prevent precipitation of the

tetramethylammonium hydroxide. The removal of excess TMA hydroxide was achieved through membrane dialysis (Spectra/Pro® 4, MWCO: 12k – 14kDa) in methanol.

4.2.4. Solution Blending to Afford Mixed TMA:TBA P(I-*ran*-SS) Copolymers

The mixed counterion systems were obtained through a solution blending procedure. Different weight percentages of the TMA- and TBA-containing copolymers (TMA:TBA; 100:0, 75:25, 50:50, 25:75, and 0:100) were blended to give a total of 1 gram of sample. The samples were dissolved into 10 mL of chloroform:methanol (7:3 , v/v) solution by mixing the polymer and solvent in a vortex until a homogenous, clear solution was obtained. The solutions were then cast into 7 cm diameter Teflon dishes, placed into a fume hood, and covered with a petri dish. The solvent was allowed to evaporate overnight. The polymer films were them placed into a vacuum oven at room temperature for 24 hours.

4.2.5. Characterization

^{1}H NMR spectroscopy was performed on a Bruker Avance III HD 500 MHz spectrometer with the samples dissolved in a mixture of deuterated chloroform and deuterated methanol (0.6 mL, 2:1, v/v). Thermogravimetric analysis (TGA) was performed on a TA Instruments TGA Q500, and the samples were heated at a rate of 10 K/min from 25 – 700 ^{o}C under a nitrogen atmosphere. X-ray scattering experiments were performed using a SAXS-LAB Ganesha instrument with a Cu-K_{α} 0.154 nm line in MAXS mode with scattering profiles collected over a 5 minute time interval. The X-ray scattering samples were melt pressed into metal washers at 80 ^{o}C and fixed in place by Kapton® tape. The scattering from an empty washer covered in Kapton® tape was subtracted from the scattering data prior to fitting with the Kinning-Thomas (K-T) modified hard sphere model.[7] Dynamic mechanical analysis (DMA) was performed on a TA Instruments DMA

Q800 in oscillatory tension mode at a frequency of 10 Hz and a strain amplitude of 0.3 % with a preload force of 0.01N. The samples were heated at a rate of 3 K/min from -80 to 80 ^{o}C. For rheology, the copolymers were molded into disks by melt pressing into metal washers (I.D. = 8 mm, t = 1.6) at 80 ^{o}C for approximately 30 minutes. The linear viscoelastic response of the material was characterized using an 8-mm parallel plate fixture in a Malvern Kinexus Pro+ rheometer. Small amplitude oscillatory shear (SAOS) measurement were measured between ω = 1 - 100 rad/s from -20 – 80 ^{o}C in 10K increments at a strain amplitude of 0.1%. For tensile testing, dogbone test samples (length: 22 mm, width: 5 mm) were punched from the copolymer films (thickness: 0.22 – 0.12 mm) and tested using Instron 4468 with a 50 N load cell. Samples were tested at a rate of 100 mm/min until failure.

4.3. Results and Discussion

4.3.1. Polymer Synthesis and Counterion Exchange

In this study the P(I-*ran*-DMOASS)-8.3 copolymer was synthesized in a single batch to prevent variations in the chemical structure. Thus, the scaled-up polymerization was performed in a 600 mL metal pressure reactor. With the metal container, degassing of the reaction mixture could not be performed via the typical freeze-pump-thaw cycle. Instead, the solution was purged with nitrogen gas for 45 minutes. The high volatility of the isoprene results in isoprene loss during the purging process, thus a 30 mL excess of isoprene was used. Addition of the excess isoprene proved sufficient, and targeted composition were consistently obtained. Using this synthetic procedure, P(I-*ran*-DMOASS) copolymer containing 8.3 mol% DMOASS and an estimated degree of polymerization of 1170 (determined from ^{1}H NMR) was synthesized.

After the scaled-up synthesis, the base P(I-*ran*-DMOASS)-8.3 was divided into two different batches for counterion exchange. Using the counterion exchange synthetic methodology, the DMOA was exchanged with TMA or TBA as previously outlined in Chapter 3. Figure 4.1 shows the ^{1}H NMR spectra of the two unmixed copolymers with the peaks associated with the counterion protons labeled. In both copolymer spectra, the vinylic isoprene and the aromatic styrene signals appear in the δ 4.5 - 6.0 pmm and δ 7.0 – 8.0 ppm range, respectively. For P(I-ran-SS)-8.3-TMA, a single peak appeared at 3.20 ppm corresponding to the 12 methyl protons. The NMR spectrum of P(I-ran-SS)-8.3-TBA, on the other hand, possessed 4 separate peaks corresponding to the protons on the 3 methylene carbons and the 1 methyl carbon. Additionally, the 1:1 ratio between the normalized integrations of the aromatic styrene peaks and alkyl counterion peaks was found. With the TMA- and TBA-containing copolymers, solution blending allowed for the generation of mixed counterion ionomers.

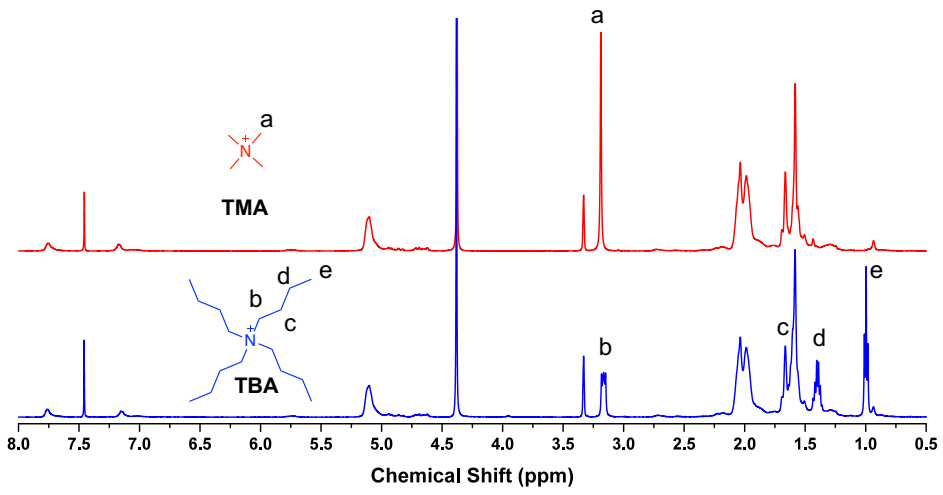

Figure 4.1. ^{1}H NMR spectra for P(I-*ran*-SS)-8.3-TMA (top) and P(I-*ran*-SS)-8.3-TBA (bottom)

Solution blending allowed for easy control of the counterion compositions. The counterion composition of the blended copolymers was monitored using both ^{1}H NMR

spectroscopy and TGA. The ^{1}H NMR spectra of the solution blended copolymers are shown in Figure 4.2. In the mixed counterion systems, the protons on the carbon alpha to the nitrogen appeared at similar ppm for both counterions, thus overlapping of the peaks occurred. Confirmation of the counterion compositions was achieved by first setting the TBA methyl groups as a reference since no other peaks overlapped in this ppm range. With the TBA methyl signal set to 12 protons, the 8 methylene protons of TBA were subtracted from the total integration of signals between δ 3.1 and 3.3 ppm to give the TMA contribution, and the TMA:TBA ratio was determined. As shown in Table 4.1, the mole percentage of each counterion, calculated from the weight percent of each copolymer blend, and the actual composition determined through NMR were in excellent agreement.

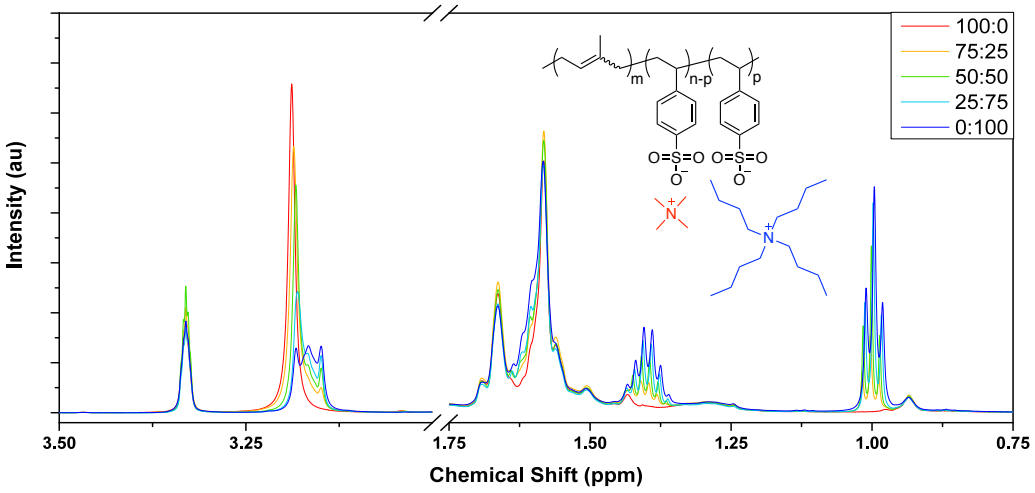

Figure 4.2. Superimposed ^{1}H NMR spectra of the mixed TMA:TBA P(I-*ran*-SS)-8.3 copolymers

Table 4.1. Comparison of the Calculated and Measured Counterion Compositions

Sample Weight Percent (TMA:TBA)	Expected Composition (mol%)		Actual Composition (mol%)	
	TMA	TBA	TMA	TBA
100:0	100	0	100	0
75:25	78	22	77	23
50:50	54	46	54	46
25:75	28	72	30	70
0:100	0	100	0	100

The degradation of the two counterions was monitored by TGA. Figure 4.3a and 4.3b show the percent weight loss and first derivative of the percent weight loss as a function of temperature, respectively. The corresponding temperature at 5% weight loss ($T_{d,5\%}$) is reported in Table 4.2. For all of the copolymers, the degradation of the polymer backbone occurred at ~ 425 ^{o}C. Additionally, the TMA counterion clearly exhibited better thermal stability than the TBA counterion, and a 70 K difference between their corresponding $T_{d,5\%}$ appeared. The decreased thermal stability of the TBA counterion resulted from the presence of beta protons. These beta protons provided an additional Hoffman elimination degradation pathways, with extraction of a beta proton leading to cleaving of the nitrogen-carbon bond and forming of a tertiary amine and an alpha-olefin. Since the TMA does not possess these beta protons, the only degradation pathway that could lead to the production of volatile organic molecules is through substitution.[8] Due to their difference in degradation pathways, the degradation of each counterion can be distinguished, and a gradual transition between the two counterion degradation profiles occurred as the weight ratios were altered.

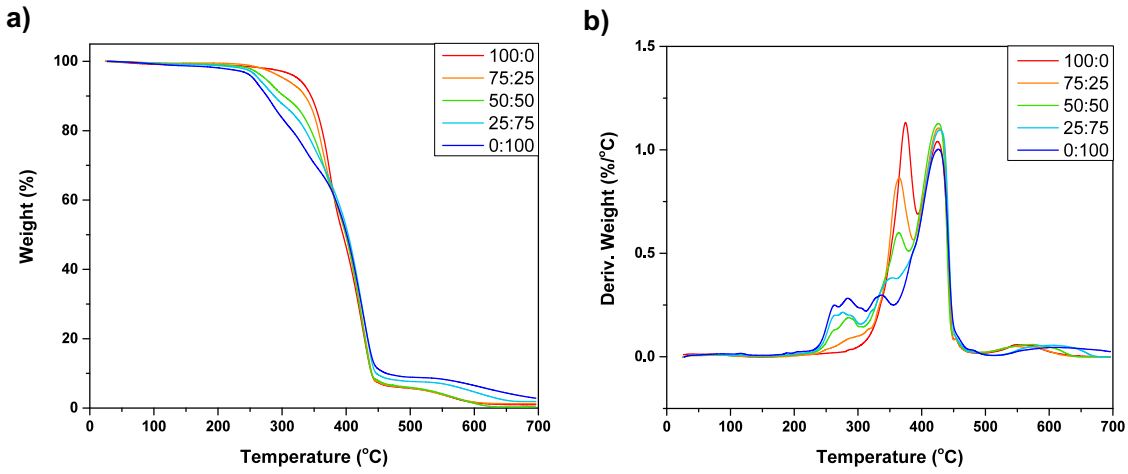

Figure 4.3. a) Weight percent loss and b) its first derivative as a function of temperature of mixed TMA:TBA P(I-*ran*-SS)-8.3 copolymers

Table 4.2. Summary of TGA and SAXS Results

Sample (TMA:TBA)	$T_{d,5\%}$ (°C)	d-spacing (nm)	R_1 (nm)	R_{ca} (nm)	V_p (nm^3)
100:0	325	5.8	2.1	2.8	300 ± 6
75:25	304	5.8	2.0	2.7	298 ± 6
50:50	274	6.1	1.8	2.7	389 ± 8
25:75	264	6.8	1.8	3.0	616 ± 9
0:100	256	7.1	1.8	3.3	1000 ± 32

4.3.2. SAXS Analysis of the Ion Aggregate Structure

The ion aggregate structure was probed by SAXS. As detailed in Chapter 3, structural changes occur when more sterically hindered counterions are present in the ionomer chemical structure. Figure 4.4 shows the scattering profiles for the copolymer with different ratios of TMA and TBA. With the incorporation of more TBA counterion, the ion aggregate d-spacing increased from 5.8 to 7.1 nm (Table 4.2). The d-spacing, however, did

not directly correlate with the TMA:TBA ratio. A considerable increase in d-spacing only occurred when TBA became the majority counterion, suggesting an alteration to the ion aggregate structure at these counterion compositions.

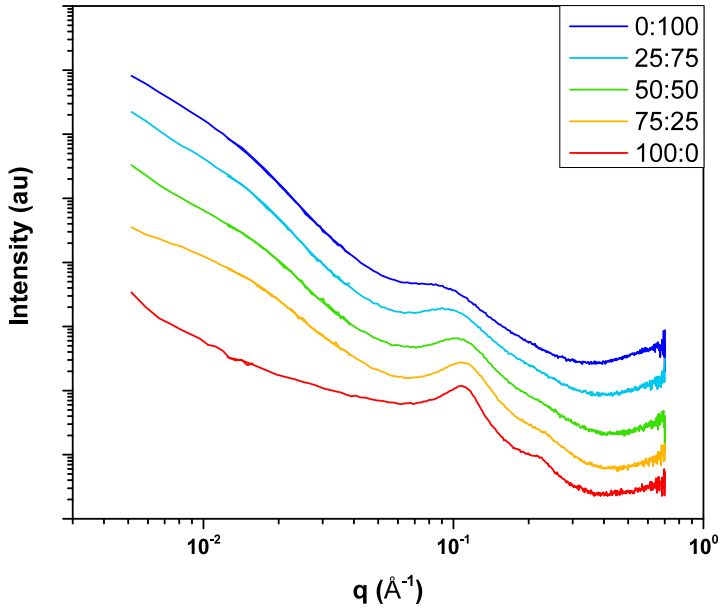

Figure 4.4. Offset SAXS profiles of the mixed TMA:TBA P(I-*ran*-SS)-8.3 copolymers

The scattering profiles of the different copolymers were fitted by the Kinning-Thomas model to further understand the effect of the different weight ratios of the counterions.[7] Figure 4.5a and 4.5b shows the scattering data with the K-T fitting and a plot of the R_1, R_{ca}, and $1/V_p$ as a function of TBA weight percent, respectively. The K-T fitting parameters are also displayed in Table 4.2. Several parameter trends persist throughout the mixed counterion series. First, minimal changes in the parameters appear between the 100:0 and 50:50 copolymers, which agrees with the trend observed in the d-spacing, and further suggests a similar structure for these mixed counterion ionomers. A slight decrease in R_1 occurred with increasing TBA counterion weight ratios. Thus, the formation of smaller electron-dense, ion aggregates occurs. With the increase in the volume of the ionic

species, the observation of smaller ion aggregates is unexpected and suggest that some of the ion pairs may be excluded from the ion aggregate structure. The exclusion of the bulkier TBA-associated ionic groups is presumably due to the increased aliphatic nature of the ionic group. In addition, the 50:50 TMA:TBA copolymer shows a slight increase in V_p, indicating a decrease in the number density of the ion aggregates. Upon further incorporation of the TBA counterion (25:75 and 0:100), major structural changes occur as shown by the increase in both R_{ca} and V_p. At these counterion compositions, R_1 remains constant. With these two results combined with findings from Chapter 3, the steric hindrance imposed by the bulky TBA counterions leads to a disruption of the ion aggregate structure. Additionally, these results suggest the formation of mixed counterion aggregates in which the majority counterion dictates the structure.

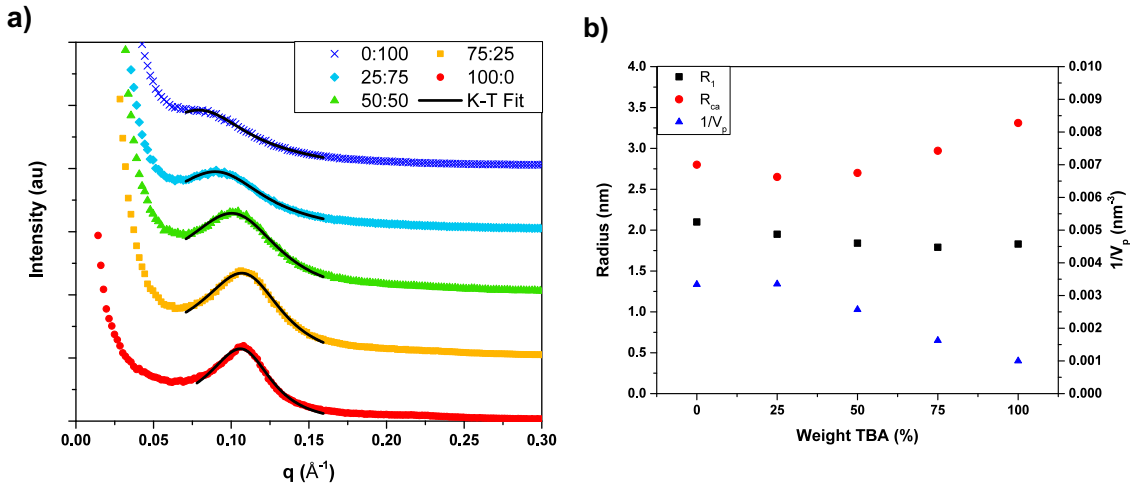

Figure 4.5. a) Kinning-Thomas fits for the scattering profiles of the mixed TMA:TBA P(I-*ran*-SS)-8.3 copolymer series and b) the R_1, R_{ca}, and $1/V_p$ plotted as a function of TBA wt%

4.3.3. Thermal and Viscoelastic Behavior of the Mixed Counterion Copolymers

As discussed in the previous chapter, the identity of the ammonium counterion does not alter the T_g of these P(I-*ran*-SS) ionomers. Thus, DMA was used to probe the thermal

transitions above the copolymers' T_g's. Figure 4.6a and 4.6b shows the E' and tan δ as a function of temperature, respectively.

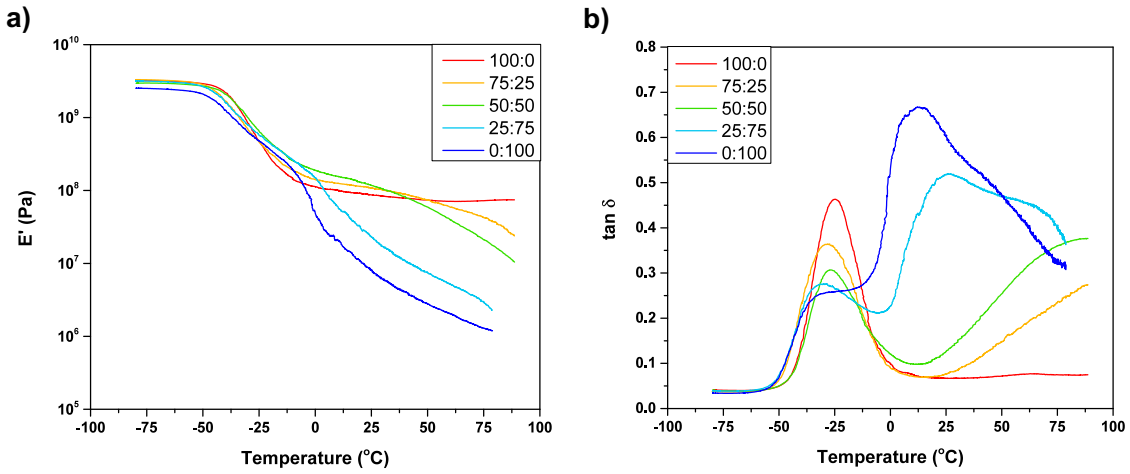

Figure 4.6. a) Storage modulus and b) tan δ as a function of temperature for the mixed TMA:TBA P(I-*ran*-SS)-8.3 copolymer series (10 Hz, 3K/min)

For all of the ionomers in the series, a rapid decrease in E' occurs followed by a plateau at higher temperatures. This initial drop in E' and the associated peak in tan δ corresponds to the T_g of the isoprenic matrix, and the polymer segments within this domain gain mobility. Due to the ion aggregates, the three order magnitude decrease in E' (typically seen when proceeding through the T_g in entangled polymers) does not occur. Instead, a plateau in E' results due to the ion aggregates acting as physical crosslinks, which impedes further motion of the polymer chains. The value of the plateau modulus and the temperature range in which it persists depends heavily on the counterion composition.

For the 100:0 copolymer, the plateau modulus continues throughout the temperature ranged probed due to the strong dipole-dipole interactions of the TMA counterion. When increasing the ratio from 100:0 to 50:50, the plateau modulus increases in the 0 – 50 °C temperature range, indicating increased restriction of the polymer with the

incorporation of more bulky TBA counterions. Additionally, the presence of some TBA counterions results in a second drop in E' appears at temperatures above 50 ^{o}C, and the onset shifts to lower temperatures with the incorporation of more TBA counterions. From these observations, two phenomena appear. First, the restriction in mobility between 0 – 50 ^{o}C is believed to be caused by a fraction of the ion pairs residing in the matrix, which can interact with other ion pairs not associated to a specific ion aggregate. At higher temperatures, these "free" ion pairs can facilitate increased dynamics of the aggregated ionic groups, thus weakening the ionic physical crosslinks and allowing for longer-range rearrangement of the polymer chains.[9] Above the 50:50 TMA:TBA ratio, considerable mobility of the polymer results, and the plateau modulus decreases and becomes less distinct. Additionally, a peak arises in tan δ. These features in the DMA data indicated further weakening of the ionic physical crosslinks. In these copolymers, the sterically hindered TBA counterion prevent the close interaction of the ion pairs from interacting, and the copolymer moduli becomes more temperature dependent.

Master curves were constructed through rheology, and the linear viscoelastic behavior of the mixed counterion copolymers was evaluated. Figure 4.7a - 4.7c show the storage moduli, loss moduli, and normalized δ of the master curves plotted as a function of frequency. Free shifting was used in time-temperature superposition, with the horizontal shift factor a_T dominating over the vertical shift factor b_T. Additionally, a polyisoprene homopolymer is plotted for comparison. As seen in the plot of the viscoelastic functions, the polyisoprene control exhibits a plateau in the dynamic moduli and a minimum in the normalized δ, corresponding to entanglements. Following this plateau at lower frequencies, the terminal regime appears as shown by $G' \sim \omega^2$, $G'' \sim \omega^1$, and normalized $\delta = 1$. With the

incorporation of the ionic moieties, the dynamic moduli increases, and the terminal regime shifts to lower frequencies. For all of the counterion ratios, the terminal regime was not reached at 80 °C.

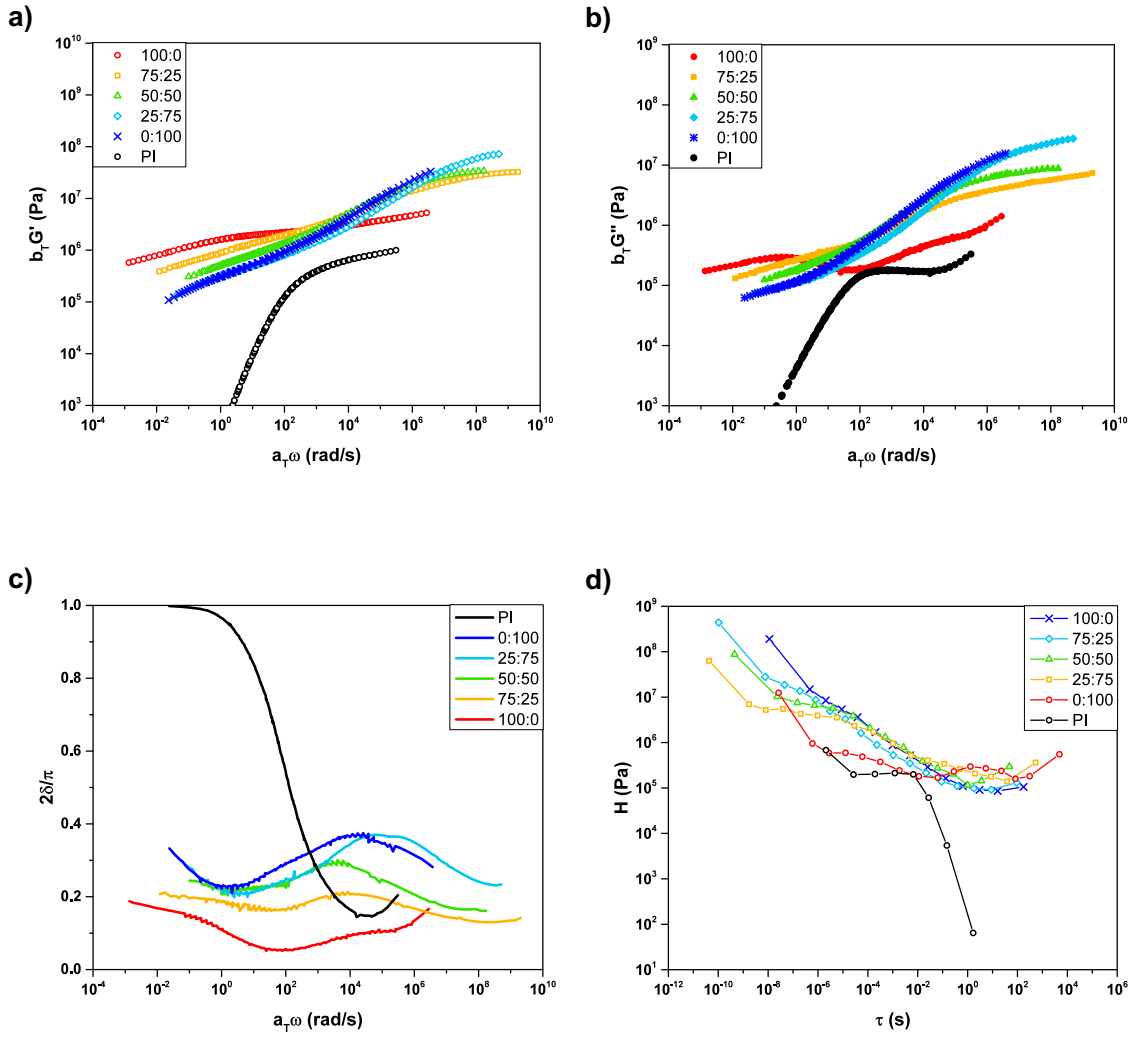

Figure 4.7. Linear viscoelastic response of PI and the mixed TMA:TBA P(I-*ran*-SS)-8.3 copolymer series (T_{ref} = 50 °C): a) storage and b) loss modulus as a function of frequency; c) normalized δ and d) continuous relaxation time spectra calculated from the SAOS data.

For the 100% TMA copolymer, the dynamic moduli changes the least throughout the frequency range, and elastic behavior dominates. This elasticity originates from the strong dipole-dipole interactions that holds the ion aggregates together, providing more

polymer-polymer connectivity. With the presences of the TBA counterion, the copolymers exhibited an increase in the dynamic moduli at high frequencies (low temperatures), and the polymer chains become more restricted due to the larger aggregates. At lower frequencies (high temperatures), the opposite trend is observed, and the dynamics increase with the TBA counterion incorporation. Additionally, the extent of these changes became more pronounced with the presence of more TBA counterions, and the copolymers exhibit more viscous behavior as shown by the increase in normalized δ. These trends are consistent with the DMA data, and the role of the bulky TBA counterion on both the structure and dynamics becomes apparent.

Figure 4.7d shows the continuous relaxation spectra for the mixed counterion copolymer series. These relaxation spectra were calculated from the dynamic data using a method developed by Baumgaertel and Winter.[10] All of the copolymers exhibit a single relaxation process. The number of relaxation events at short time scales increases with the incorporation of the bulky TBA counterions as shown by the increase in H. These relaxation events are believed to correspond with the relaxation of regions possessing both the isoprene and ionic groups. The relaxation becomes more rapid with increasing TBA counterion incorporation. Additionally, the relaxation process extends to longer times when more TMA counterions are present in the ion aggregate structures. The final relaxation mode indicates additional relaxation processes at long times.

4.3.4. Mechanical Properties of the Mixed Counterion Copolymer Series

The mechanical properties of the copolymer series was evaluated by performing tensile tests. Figure 4.8 shows stress-strain curves for the 100:0 to 25:75 TMA:TBA copolymers, and the reported Young's modulus, tensile stress, and tensile strain are

reported in Table 4.3. Tensile tests could not be performed on the 100% TBA copolymer due to its more viscous character, which made preparation of the dogbone tensile samples difficult.

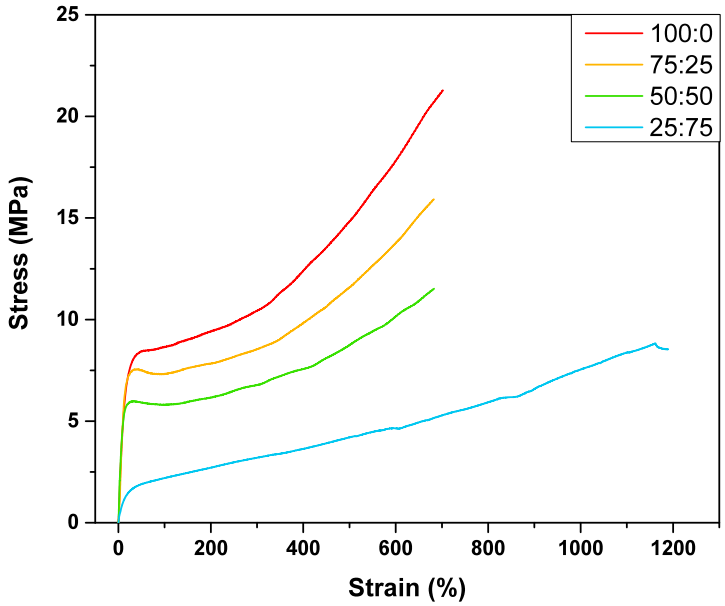

Figure 4.8. Stress-strain curves of the mixed TMA:TBA P(I-*ran*-SS)-8.3 copolymers (crosshead speed = 100 mm/min)

Table 4.3. Summary of the Young's Modulus, Tensile Stress and Tensile Strain of the mixed TMA:TBA P(I-*ran*-SS)-8.3 copolymers

Sample (TMA:TBA)	Young's Modulus (MPa)	Tensile Strength (MPa)	Elongation at Break (%)
100:0	61	21	700
75:25	57	16	680
50:50	62	12	680
25:75	11	9	1180

During the tensile tests, the copolymers deformed homogeneously, with strain whitening at high strain. As shown by the stress-strain curves, all of the copolymers exhibit

plastic-like behavior where, after the elastic deformation at low strain, the polymer yielded. With further strain, strain hardening was observed until failure occurred. The tensile strength and the stress required for yielding increased with the presence of more TMA counterions. Thus, the strong electrostatic interactions of the TMA counterion produced a more robust physically crosslinked network that required higher stress for plastic deformation and failure. These values were obtained from one sample, and more testing is required to obtain statistically relevant values. Subsequent experiments were performed; however, increased relative humidity in the laboratory prevented the collection of repeatable data.

Figure 4.9a and 4.9b show multiple stress strain curves for the 100:0 and 50:50 P(I-*ran*-SS)-8.3 samples, respectively. The different colors signify when the tests were performed, and the legend indicates the thickness of each sample. The red data set were performed at higher relative humidity due to conditions of the testing facility. This increase in the humidity caused a plasticization of the ion aggregates, resulting in a decrease in the sample's mechanical properties. The degree of plasticization was found to correlate with the thickness of the sample, and thinner samples were able to absorb moisture at a more rapid rate. With these findings, subsequent tensile test should be performed under dry testing conditions in order to obtain reproducible data.

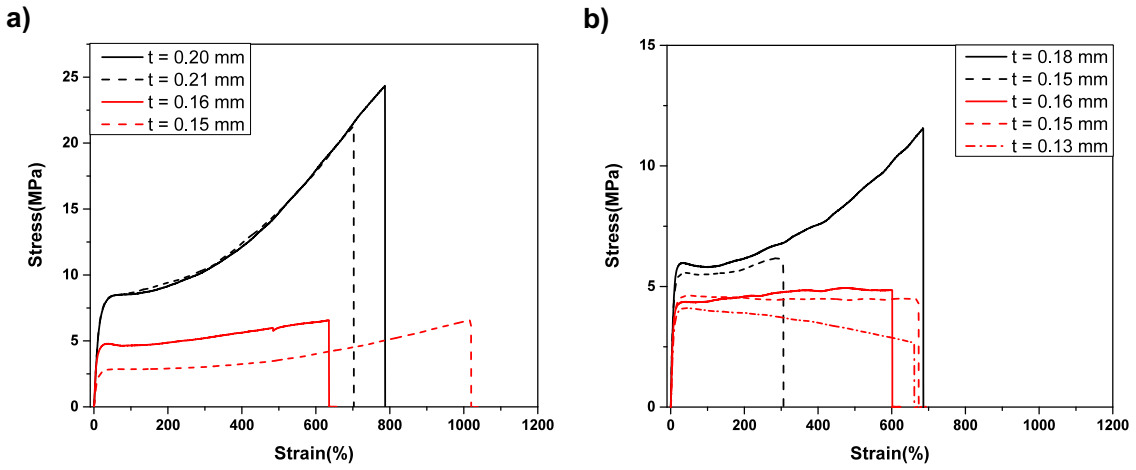

Figure 4.9. Stress-strain curves of a) 100:0 and b) 50:50 mixed TMA:TBA P(I-*ran*-SS)-8.3 copolymers (crosshead speed = 100 mm/min). The legend displays the thickness of each sample. The black and red colors correspond to different days of testing.

4.3.5. Correlating the Structure, Dynamics, and Mechanical Properties

From the SAXS, DMA, rheology, and tensile tests, insight into the role of counterion steric on the structure-property relation of these mixed counterion P(I-*ran*-SS)-8.3 copolymers emerges. From SAXS profiles and K-T fitting of the copolymer with counterion ratios between 100:0 – 50:50, the TMA counterions provides sufficient dipole-dipole interactions to maintain the ion aggregates structures at room temperature. Additionally, the increased moduli at low temperatures (DMA) and high frequency (rheology) with increasing TBA incorporation indicates further restriction of the segment dynamics associated with the isoprene matrix. This result suggests that some fraction of the ion pairs are excluded from the ion clusters and reside in the isoprene matrix. In addition, the thermograms from DMA show minimal change in the thermal transition corresponding to the T_g of the isoprene matrix. Thus, these "free" ion pairs are believed to preferentially arrange in the area surrounding the ion aggregates, and regions containing pure isoprene matrix with no counterion pairs are still present within the copolymers.

At high temperatures and low frequencies, the dynamic moduli decreases due to less connectivity between the polymer chain, and the relaxation of the polymer chains occurs over a smaller time interval. Additionally, the onset of the terminal regime shifts to higher frequencies as shown by the upturn in the normalized δ. These observations are believed to result from two separate phenomena within these copolymers. The decrease in dynamic moduli results from the increased dynamics with the TBA counterion that relax on shorter time scales; however, the interactions provided by the TMA counterions persist and a long time-scale relaxation process becomes more distinct as the TBA counterion content is decreased. Thus, it is believed that the TBA counterions relax first and dipole-dipole interactions between the sulfonate-TMA ion pairs are still present. The shift of the onset of terminal flow to higher frequencies indicates that while the sulfonate-TMA ion pairs provide increased connectivity, the presence of the TBA counterions still affect the dynamics of the dipole-dipole interactions and introduces some mobility to the ion aggregates. Once the TBA becomes the majority counterion, disruption of the ion aggregates is achieved and the dynamic behavior of the 25:75 and 0:100 become similar.

4.4. Conclusions

In this chapter, P(I-*ran*-SS)-8.3 containing binary mixtures of TMA and TBA counterions were produced through solution blending. These two quaternary ammonium counterions offered differing degrees of steric hinderance, and the TMA:TBA weight ratios investigated in this study included 100:0, 75:25, 50:50, 25:75, and 0:100. By ^{1}H NMR spectroscopy, integrations of the protons located on the pendent alkyl chains confirmed the TMA:TBA ratios of the solution blended ionomers. The SAXS profiles and K-T fitting showed only slight structural changes between 100:0 and 50:50, while major modification

of the structure appears once the ratio reaches 75:25 and above. The linear viscoelastic properties of the mixed counterion ionomers further confirmed this observation. Therefore, a heterogeneous distribution of the TBA counterion is suggested at low TBA content where some of the sulfonate-TBA ion pairs reside in regions outside of the ion aggregates when sufficient temperatures are reached (> 0 ºC). At equivalent ratios of the two counterions, ion aggregates possessing both counterions appear. Thus, the structure and properties of these low T_g, amorphous ionomers can be specifically tuned by mixing counterions. The conclusions from this investigation offer insight into the role of the counterion, and by applying this knowledge, more complex ionomer systems can be developed for advance applications such as soft actuators and shape memory materials.

4.5. References

(1) Molitor, R. P. Golf Ball Cover Compositions Comprising A Mixture of Ionomer Resins. U.S. Patent 3,819,768, 1974.

(2) Tachino, H.; Hara, H.; Hirasawa, E.; Kutsumizu, S.; Yano, S. Structure and Properties of Ethylene Ionomers Neutralized with Binary Metal Cations. *Macromolecules* **1994**, *27* (2), 372–378.

(3) Kutsumizu, S.; Hara, H.; Tachino, H.; Shimabayashi, K.; Yano, S. Infrared Spectroscopic Study of the Binary Blends of Sodium and Zinc Salt Ionomers Produced from Poly(Ethylene-*co*-Methacrylic Acid) . *Macromolecules* **2002**, *32* (19), 6340–6347.

(4) Grady, B. P. Effect of Coneutralization on Internal Aggregrate Structure in Ethylene-Based Ionomers. *Macromolecules* **1999**, *32* (9), 2983–2988.

(5) Phillips, A. K.; Moore, R. B. Mechanical and Transport Property Modification of Perfluorosulfonate Ionomer Membranes Prepared with Mixed Organic and Inorganic Counterions. *J. Polym. Sci. Part B Polym. Phys.* **2006**, *44*, 2267–2277.

(6) Enokida, J. S.; Tanna, V. A.; Winter, H. H.; Bryan Coughlin, E. Progression of the Morphology in Random Ionomers Containing Bulky Ammonium Counterions. *Macromolecules* **2018**, *51* (18), 7377–7385.

(7) Kinning, D. J.; Thomas, E. L. Hard-Sphere Interactions between Spherical Domains in Diblock Copolymers. *Macromolecules* **1984**, *17* (9), 1712–1718.

(8) Verrall, R. E.; Burns, J. A. The Mass Spectrometry of the Pyrolysis Products of Some Tetraalkylammonium and Bistetraalkylammonium Bromides. *Can. J. Chem.*

2006, *52* (19), 3438–3443.

(9) Phillips, A. K.; Moore, R. B. Mechanical and Transport Property Modifications of Perfluorosulfonate Ionomer Membranes Prepared with Mixed Organic and Inorganic Counterions. *J. Polym. Sci. Part B Polym. Phys.* **2006**, *44*, 2267–2277.

(10) Baumgaertel, M.; Winter, H. H. Determination of Discrete Relaxation and Retardation Time Spectra from Dynamic Mechanical Data. *Rheol. Acta* **1989**, *28* (6), 511–519.

CHAPTER 5

CONCLUSIONS AND PERSPECTIVE

5.1. Introduction

In this final dissertation chapter the conclusions from the three projects presented in this dissertation will be summarized, and the impact of these findings will be integrated into the current understanding of these complex systems. Based on these results, future directions will be proposed to expand upon this work to further the understanding of the structure-property relationship of ionomers, specifically ionomer that utilize these unconventional, bulky ammonium counterions.

5.2. Summary of Conclusions

In Chapter 2, the first reported direct solution copolymerization of isoprene with styrenesulfonate was presented.[1] The solution copolymerization of these two incompatible monomers relied on modification of the styrenesulfonate monomer by exchanging the sodium counterion to DMOA. The DMOA counterion provided styrenesulfonate with sufficient hydrophobicity to dissolve in anisole at elevated temperatures (125 ^{o}C), allowing for its nitroxide mediated copolymerization with isoprene. This synthetic strategy allowed for facile control over the copolymer's ion content by adjusting the feed ratio of the two comonomers. Additionally, the correlation between the feed ratio and the final composition suggested a random arrangement of the two comonomers along the polymer chains. Thus, modification of styrenesulfonate with more hydrophobic, bulky ammonium counterions was shown to be powerful synthetic strategy to directly synthesize sulfonated ionomers.

In addition to developing this synthetic methodology, Chapter 2 also provided a comprehensive evaluation of the morphology as a function of ion content for these P(I-r*an*-

DMOASS) copolymers. Using a combination of SAXS, thermal, and viscoelastic characterization, a transition from ion cluster structures to a continuous ionic phase was observed as the ion content increased. A coexistence of both ion clusters and the continuous ionic phase was also found at intermediate ion contents. This critical assessment of the structure provides great insight into the role of ion content on the organization of the ionic groups particularly at ion content in between traditional ionomers and polyelectrolytes. This work found a correlation between the copolymer's T_g and the Fox equation at high ion contents, indicating a phase-mixed morphology.

Additionally, the SAXS profiles showed a high q scattering feature at all ion contents, including the PDMOASS homopolymer, which is often attributed to an ion cluster structure. For the homopolymer, this scattering feature instead corresponded to a backbone-backbone spacing. The similarity between the ion cluster structure and backbone-backbone spacing in the scattering profiles demonstrates the limitation of SAXS characterization for these copolymers. Thus, consideration of the ion content and the ionic group chemical structure is necessary to prevent misinterpretation of the data, especially when pendent groups are attached to the ionic moiety. Furthermore, other characterization methods should be used in combination with SAXS to confirm the structure of an ionomer.

In Chapter 3, the role of counterion sterics on the structure and dynamics of P(I-*ran*-SS)-7 copolymer at a fixed ion content was explored. This study provided the first comprehensive investigation of counterion sterics in a low T_g, amorphous ionomers. A systematic investigation of the counterion sterics was achieved by using a series of symmetric tetraalkylammonium with the pendent alkyl group varying from methyl to butyl. The characterization of this ionomer system focused on correlating the aggregate structure

to the dynamics on both the molecular and macroscopic scale. From the K-T fitting of the SAXS profiles, an increase in the steric hinderance from sodium to TEA resulted in a fewer number of larger aggregates with some ionic group residing in the isoprene matrix. With the TPA and TBA counterions, the large steric hinderance caused major structure modifications. These changes were reflected in the viscoelastic behavior of the copolymers in which both the changes in structure and dipole-dipole interaction strength appeared at high and low frequencies, respectively. The results from this detailed investigation provide a fundamental understanding of the effect of counterion steric that will help guide future design of ionomers. Specifically, TMA and TEA offer slightly sterically hindered structures that can increase the dynamics of the ion aggregates without excessively weakening the physically crosslinked ion aggregate network.

In Chapter 4, P(I-*ran*-SS)-8 copolymers containing binary mixtures of TMA and TBA counterions were explored. These counterions were selected to investigate the structure and dynamics of ionomers containing multiple counterions of differing steric hinderance. In these P(I-*ran*-SS)-8 ionomers, TMA:TBA ratios of 100:0, 75:25, 50:50, 25:75, and 0:100 were prepared by solution blending. Correlation of the SAXS and linear viscoelastic behavior indicated the formation of mixed counterion systems in which the majority counterion dictates the dynamics of the ionomer. The main finding from this work was the ability to effectively modify the dynamics at both long and short time scales through the appropriate selection of counterions. Specifically, the TBA counterion controlled the short time scale relaxations of the ionomer while the TMA counterion introduced a longer time scale relaxation process due to the stronger dipole-dipole interactions.

5.3. Future Perspective

The work presented in this dissertation provides detailed insight on the role of ion content, counterion sterics, and mixed counterion ionomer with various ammonium counterions and their effect on the structure and dynamics of ionomers. Building off of these results, several future investigations can be performed. These proposed directions involve chemical modification of the P(I-*ran*-SS) ionomers through hydrogenation and chemical crosslinking in addition to further exploration of other ammonium counterions.

5.3.1. Chemical Modification of Polyisoprene-Based Ionomers

The P(I-*ran*-SS) copolymer developed in this dissertation offers several opportunities for further synthetic modification. One major limitation of the current isoprene-based ionomers is their lack of thermal and chemical stability. This instability results from the carbon-carbon double bond present in the polymer backbone, which are prone to thermal oxidation and reactions with strong electrophiles. Hydrogenation of the polyisoprene ionomer would mitigate these issues while maintaining the low T_g, amorphous polymer structure. Several studies have shown that noncatalytic hydrogenation of isoprenic polymers can be achieved using dimide.[2–4] In these reactions, the dimide molecules are typically generated *in situ* through the thermolysis of p-toluenesulfonyl hydrazinedimide at elevated temperatures (~135 - 145 °C). Using this method, the isoprenic portions of the P(I-*ran*-SS) copolymers can be selectively hydrogenated to afford improved thermal stability. With these thermally stable, low T_g ionomers, the linear viscoelastic behavior can be investigated at temperatures above 80 °C. Access to a higher temperature range would allow for the complete characterization of the ionomers' dynamics and the associated relaxation processes arising from the strong dipole-dipole interactions of the

ionic groups. Additionally, the melt processability of these ionomers and the effects of the counterion sterics could be evaluated at elevated temperatures.

Another useful synthetic modification offered by these P(I-*ran*-SS) ionomers is crosslinking. With the available double bonds in the polyisoprene backbone, these polymers can be crosslinked by either controlled thermal oxidation[5] or UV-initiated thiol-ene click chemistry.[6] This crosslinked polymer systems would then possess both a covalently crosslinked network in addition to a physically crosslinked network provided by the ion aggregates. With the presence of both a chemical and physical network, these polymer offer the possibility to develop tough elastomers.[7] Through the appropriate selection of the counterion, the association of the physical ionic network can be tuned to obtain dynamic structures that can increase the strength of the elastomer without sacrificing its extensibility. In addition, as demonstrated in previous studies, these features allow for the development of shape-memory materials.[8] For these materials, the covalent crosslinks provide the permanent network while the ionic crosslinks allow for "programming" of different shapes at elevated temperatures. With the strong ionic bonds, these temporary shape will persist until sufficient temperature is reached that would allow for the reorganization of the ionic groups.

5.3.2. Additional Studies on Ammonium Counterions

As shown throughout this dissertation, the molecular structure of quaternary ammonium counterions plays an important role in dictating the structure and properties of their corresponding ionomers. Specifically, Chapter 3 showed that increasing the alkyl chain length of the tetraalkylammonium counterion from methyl to butyl weakened the electrostatic interactions and altered the organization of the ionic groups in the aggregate

structures. Asymmetric quaternary ammoniums are an alternative series of counterions to explore. Figure 5.1 shows several asymmetric quaternary ammonium counterions of interest. By increasing the length of only one of the alkyl chain, these counterions offer less steric hinderance that may provide some disruption of the ion cluster structure without diminishing the dipole-dipole interactions to the extent of the symmetric counterions. Thus, improved thermomechanical behavior are anticipated at both low and high temperatures. Additionally, the cyclic and adamantylammonium counterions offer more rigid counterions that offer better thermal and chemical stability in addition to different polymer dynamics.

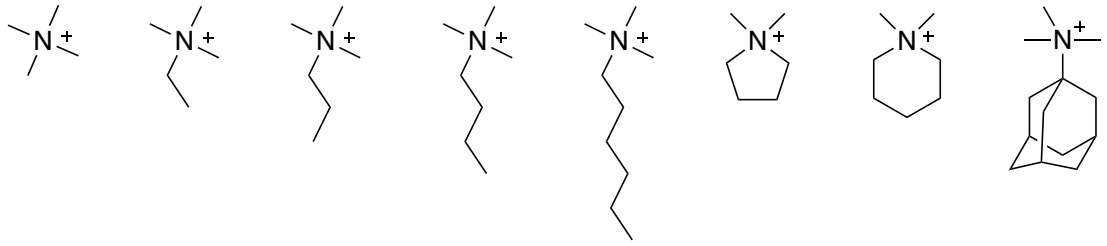

Figure 5.1. Proposed asymmetric quaternary ammonium counterions

As shown in Chapter 4, the mixed counterion systems offer great benefits that cannot be obtained through single counterion systems. With the bulky tetrabutylammonium counterion, significant steric hinderance decreased the thermal and mechanical properties of the copolymers. Blends of TMA with counterions of less steric hinderance such as the TEA should provide better mechanical properties and help decrease the melt viscosity. Thus, these TMA:TEA counterion mixtures would best be investigated in the proposed hydrogenated P(I-ran-SS) ionomer system in which their viscoelastic behavior at elevated temperatures can be evaluated.

5.4. Outlook

With the wealth of knowledge available for these ionomers systems, much work can still done in this field. Particularly, this work should be extended and developed for different advanced applications. Much of the current work on these applications are limited by the availability of the polymer. With the development of these sulfonated, low T_g elastomers, these polymers can have a significant impact in various fields. Some possible applications to explore include membranes, self-healing materials, and actuators.

5.5. References

(1) Enokida, J. S.; Tanna, V. A.; Winter, H. H.; Bryan Coughlin, E. Progression of the Morphology in Random Ionomers Containing Bulky Ammonium Counterions. *Macromolecules* **2018**, *51* (18), 7377–7385.

(2) Hahn, S. F. An Improved Method for the Diimide Hydrogenation of Butadiene and Isoprene Containing Polymers. *J. Polym. Sci. Part A Polym. Chem.* **1992**, *30* (3), 397–408.

(3) Mahittikul, A.; Prasassarakich, P.; Rempel, G. L. Noncatalytic Hydrogenation of Natural Rubber Latex. *J. Appl. Polym. Sci.* **2007**, *103*, 2885–2895.

(4) Phinyocheep, P.; Pasiri, S.; Tavichai, O. Diimide Hydrogenation of Isoprene-Styrene Diblock Copolymers. *J. Appl. Polym. Sci.* **2003**, *87* (1 SPEC.), 76–82.

(5) Tsai, T.-H.; Ertem, S. P.; Maes, A. M.; Seifert, S.; Herring, A. M.; Coughlin, E. B. Thermally Cross-Linked Anion Exchange Membranes from Solvent Processable Isoprene Containing Ionomers. *Macromolecules* **2015**, *48* (3), 655–662.

(6) Ertem, S. P.; Tsai, T.-H.; Donahue, M. M.; Zhang, W.; Sarode, H.; Liu, Y.; Seifert, S.; Herring, A. M.; Coughlin, E. B. Photo-Cross-Linked Anion Exchange Membranes with Improved Water Management and Conductivity. *Macromolecules* **2016**, *49*, 153–161.

(7) Winey, K. I. Designing Tougher Elastomers with Ionomers. *Science.* **2017**, *358* (6362), 449–450.

(8) Zhang, L.; Brostowitz, N. R.; Cavicchi, K. A.; Weiss, R. A. Perspective : Ionomer Research and Applications. *Macromol. React. Eng.* **2014**, *8*, 81–99.

APPENDIX

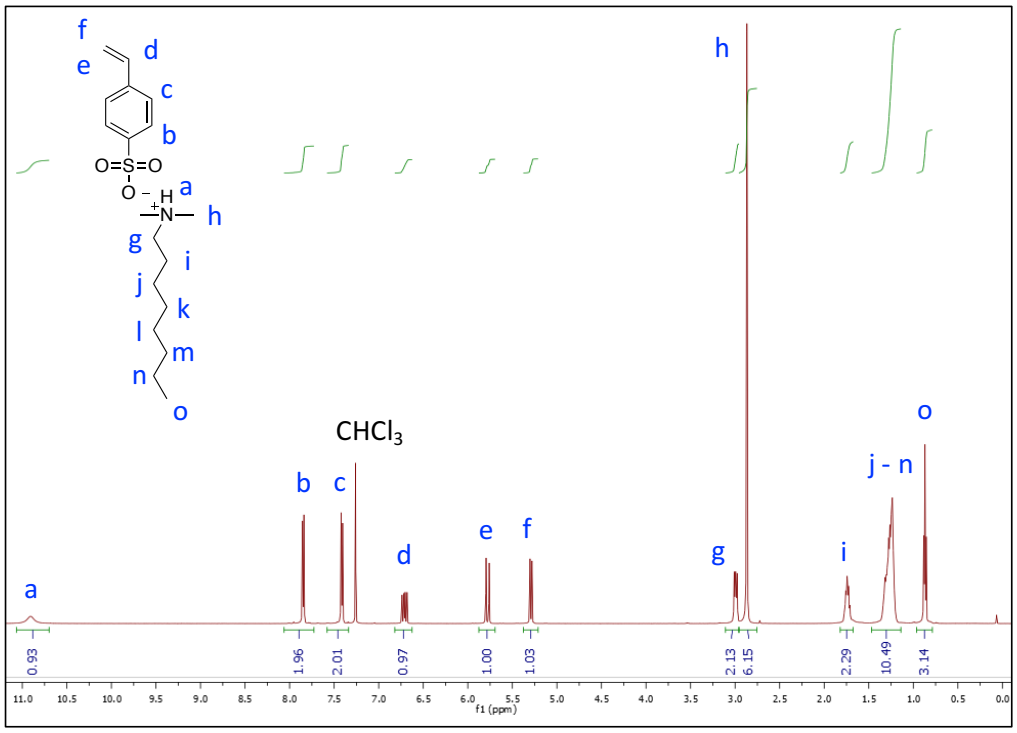

Figure 6.1. ^{1}H NMR spectrum of the DMOASS monomer in chloroform-d

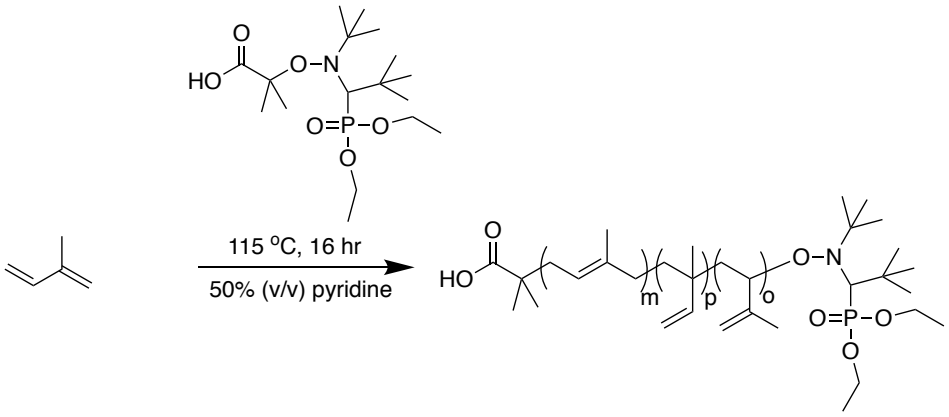

Figure 6.2. Synthesis of polyisoprene (PI) homopolymer

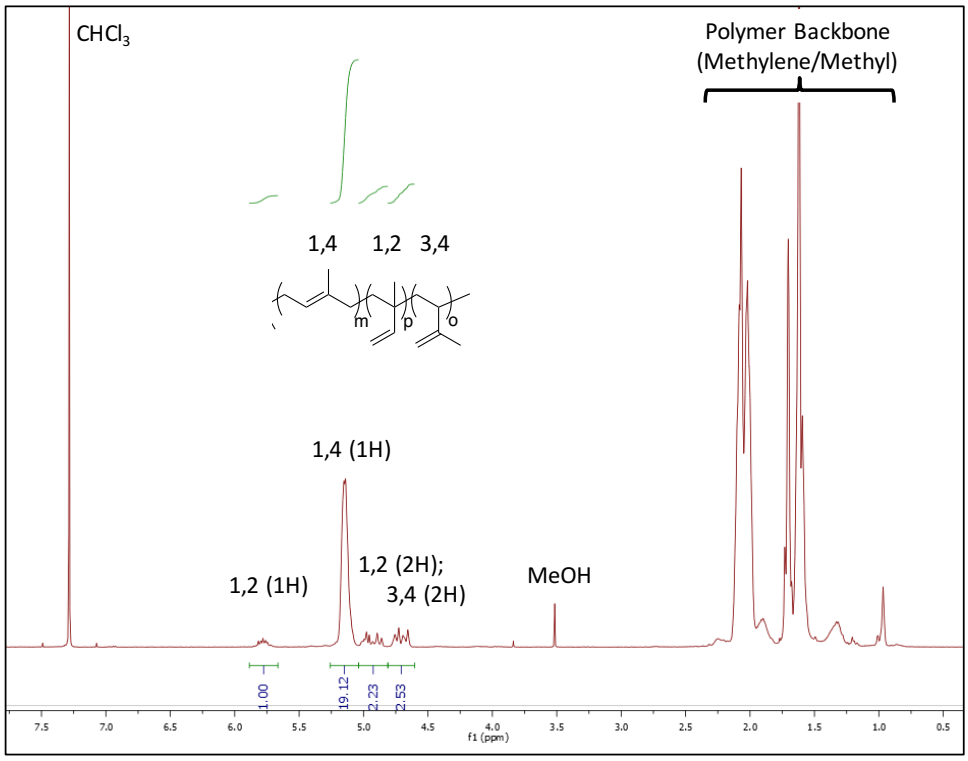

Figure 6.3. ^{1}H NMR spectrum of PI homopolymer in chloroform-d

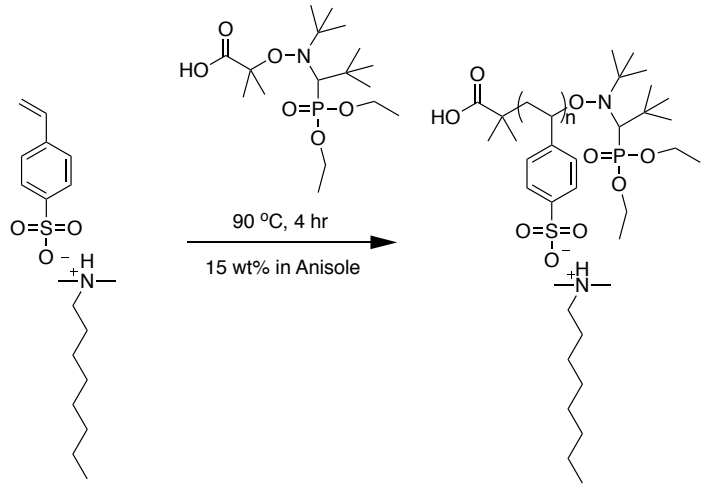

Figure 6.4. Synthesis of poly(N,N-dimethyloctylammonium styrenesulfonate) (PDMOASS)

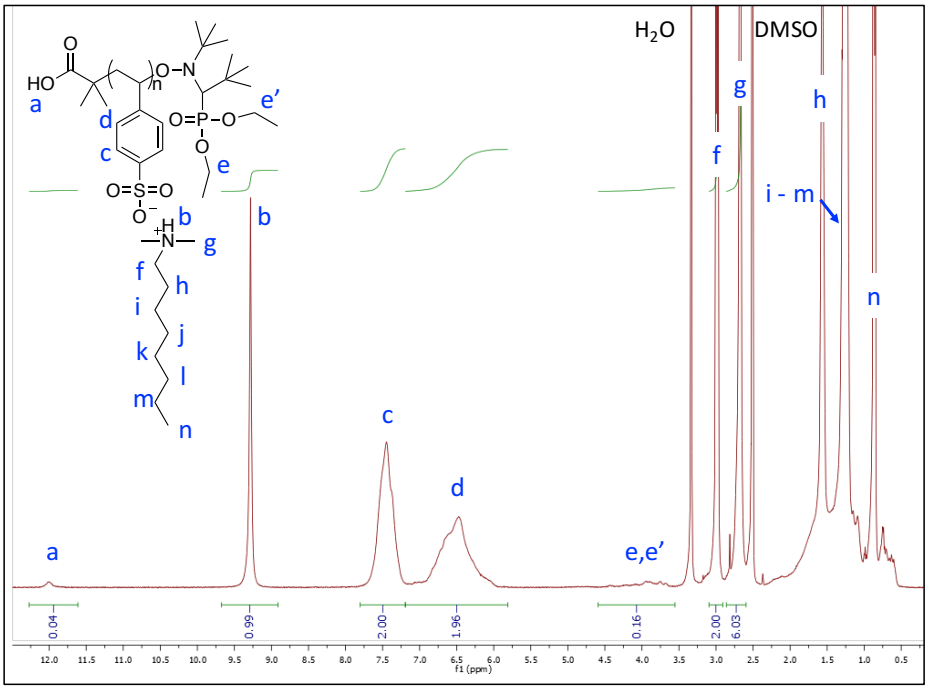

Figure 6.5. ^{1}H NMR spectrum of PDMOASS homopolymer

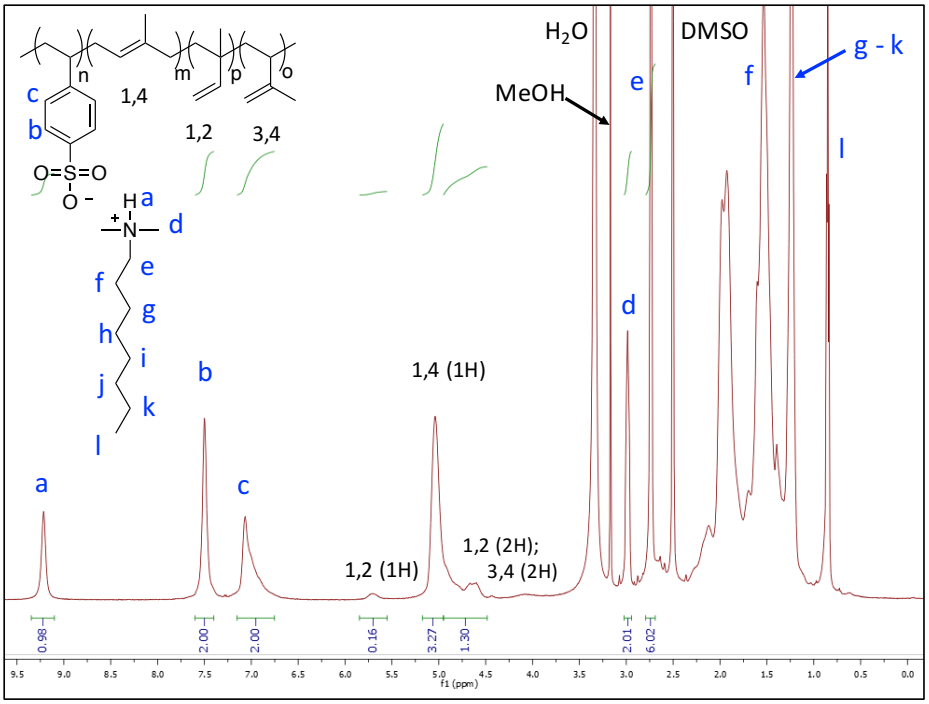

Figure 6.6. Representative ^{1}H NMR spectrum of the P(I-*ran*-DMOASS)-20 copolymer

Table 6.1. Overview of the P(I-*ran*-DMOASS) Synthesis

Sample	DMOASS Conversion	Feed DMOASS	Actual DMOASS[a]		Isoprene Composition (mol %)			
	(%)	(mol %)	(mol %)	(wt %)	1,4	1,2	3,4	Total
P(I-*ran*-DMOASS)-8	38	10	8	30	79.8	3.5	9.8	92
P(I-*ran*-DMOASS)-13	39	15	13	42	71.7	3.5	13.9	87
P(I-*ran*-DMOASS)-17	29	20	17	51	71.5	3.7	7.7	83
P(I-*ran*-DMOASS)-20	34	25	20	56	66.5	3.3	10.0	80
P(I-*ran*-DMOASS)-34	42	35	34	72	55.5	2.0	8.4	66
P(I-*ran*-DMOASS)-40	42	40	40	77	48.9	2.0	9.5	60

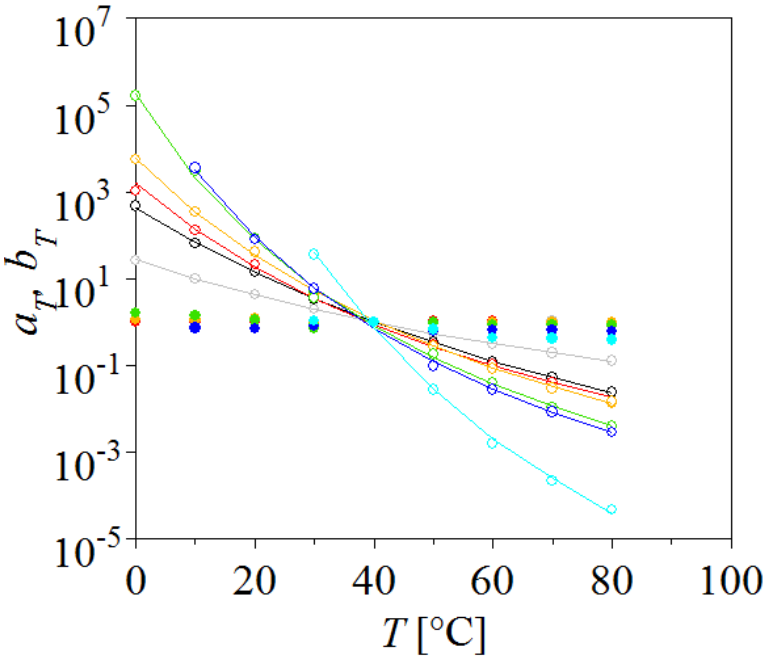

Figure 6.7. Horizontal (a_T, open) and vertical (b_T, closed) shift factors for the P(I-*ran*-DMOASS) master curves along with WLF fits

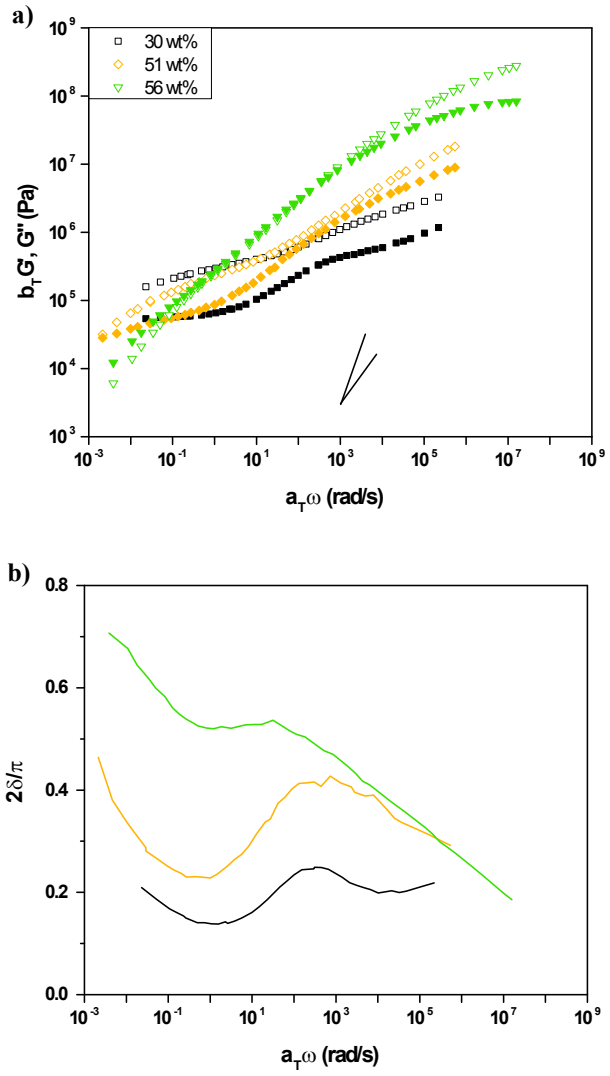

Figure 6.8. Linear viscoelastic responses of the P(I-*ran*-DMOASS) copolymers based on the three structural regimes: ion clusters (30 wt%), continuous ionic phase (56 wt%), and the coexistence of both structures (51 wt%). a) Storage (open) and loss (closed) modulus; b) δ as a function of frequency.

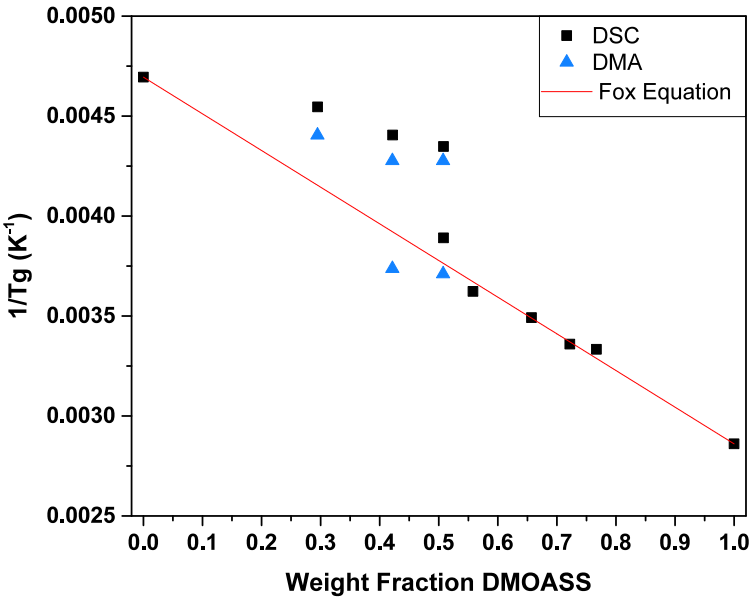

Figure 6.9. Fox Plot with T_g values determined from both DSC (black squares) and DMA (blue triangles). The red line represents the prediction for the Fox equation.

Table 6.2. Volumes of the Tetraalkylammonium Chloride and Adjusted Values for Tetraalkylammonium Sulfonate Estimations

Sample	MW (g/mol)	ρ (g/cm^3)	$V_{cation-Cl}$ (nm^3)	$V_{cation-SO_3}$ (nm^3)
Na_2SO_4	142.04	2.664	0.089	
NaCl	58.44	2.16	0.045	
TMACl	109.06	1.17	0.155	0.173
TEACl	165.71	1.08	0.255	0.273
TPACl	221.81	1.033	0.357	0.375
TBACl	277.92	1.05	0.440	0.458

Table 6.3. Values Used for the Calculation of $N_{agg}(V_p)$

Sample	ϕ_{SS}	η_{SS}	V_p	$N_{agg}(V_p)$
PSSS	0.157	3.24	234	119
PTMASS	0.189	2.60	383	188
PTEASS	0.221	2.13	385	182
PTPASS	0.251	1.81	656	298
PTBASS	0.278	1.57	902	394

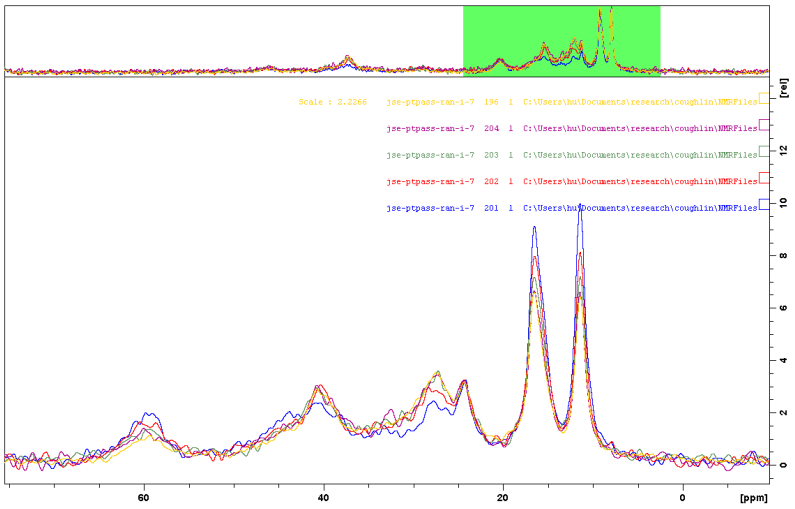

Figure 6.10. Spin diffusion experiments of P(I-*ran*-SS)-7-TPA with a 2 ms $T_{1\rho}$ filter. Experiments were conducted at 263K. Diffusion time: 0.01 (blue), 1 (red), 3 (green), and 10 (purple) ms. The equilibrium spectrum (yellow) is plotted for reference.

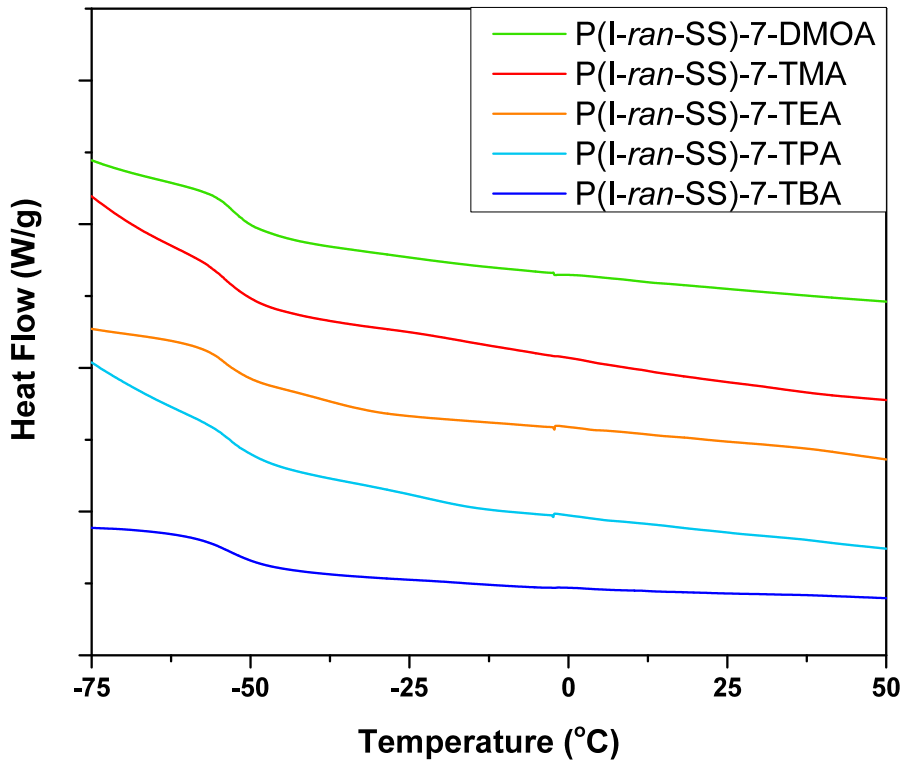

Figure 6.11. DSC thermograms for the P(I-*ran*-SS)-7-x copolymer series.

BIBLIOGRAPHY

Agarwal, P. K.; Makowski, H. S.; Lundberg, R. D. Viscoelastic Behavior of Sulfonated Polymers: Sulfonated Ethylene-Propylene Terpolymer. *Macromolecules* **1980**, *13* (6), 1679–1687.

Arbe, A.; Genix, A.-C.; Colmenero, J.; Richter, D.; Fouquet, P. Anomalous Relaxation of Self-Assembled Alkyl Nanodomains in High-Order Poly(n-Alkyl Methacrylates). *Soft Matter* **2008**, *4*, 1792–1795.

Baumgaertel, M.; Winter, H. H. Determination of Discrete Relaxation and Retardation Time Spectra from Dynamic Mechanical Data. *Rheol. Acta* **1989**, *28* (6), 511–519.

Benetatos, N. M.; Chan, C. D.; Winey, K. I. Quantitative Morphology Study of Cu-Neutralized Poly(Styrene-Ran- Methacrylic Acid) Ionomers: STEM Imaging, X-Ray Scattering, and Real-Space Structural Modeling. *Macromolecules* **2007**, *40* (4), 1081–1088.

Blosch, S. E.; Orler, E. B.; Talley, S. J.; Moore, R. B.; Turner, S. R. Effect of Ion Concentration on the Properties of Polyisoprene-Sodium Styrene Sulfonate Elastomeric Ionomers Prepared by Emulsion Polymerization. *Polymer.* **2019**, *172* (September 2018), 126–132.

Capek, I. Dispersions of Polymer Ionomers: I. *Adv. Colloid Interface Sci.* **2004**, *112* (1–3), 1–29.

Castagna, A. M.; Wang, W.; Winey, K. I.; Runt, J. Influence of Cation Type on Structure and Dynamics in Sulfonated Polystyrene Ionomers. *Macromolecules* **2011**, *44* (13), 5420–5426.

Castagna, A. M.; Wang, W.; Winey, K. I.; Runt, J. Structure and Dynamics of Zinc-Neutralized Sulfonated Polystyrene Ionomers. *Macromolecules* **2011**, *44* (8), 2791–2798.

Cavicchi, K. A. Synthesis and Polymerization of Substituted Ammonium Sulfonate Monomers for Advanced Materials Applications. *ACS Appl. Mater. Interfaces* **2012**, *4* (2), 518–526.

Chang, Y.; Brunello, G. F.; Fuller, J.; Hawley, M.; Kim, Y. S.; Disabb-Miller, M.; Hickner, M. A.; Jang, S. S.; Bae, C. Aromatic Ionomers with Highly Acidic Sulfonate Groups: Acidity, Hydration, and Proton Conductivity. *Macromolecules* **2011**, *44* (21), 8458–8469.

Chen, L.; Hallinan, D. T.; Elabd, Y. A.; Hillmyer, M. A. Highly Selective Polymer Electrolyte Membranes from Reactive Block Polymers. *Macromolecules* **2009**, *42* (16), 6075–6085.

Chen, Q.; Bao, N.; Wang, J. H.; Tunic, T.; Liang, S.; Colby, R. H. Linear Viscoelasticity and Dielectric Spectroscopy of Ionomer / Plasticizer Mixtures : A Transition from Ionomer to Polyelectrolyte. *Macromolecules* **2015**, *48*, 8240–8252.

Chen, Q.; Liang, S.; Shiau, H. S.; Colby, R. H. Linear Viscoelastic and Dielectric

Properties of Phosphonium Siloxane Ionomers. *ACS Macro Lett.* **2013**, *2* (11), 970–974.

Chen, Q.; Tudryn, G. J.; Colby, R. H. Ionomer Dynamics and the Sticky Rouse Model. *J. Rheol.* **2013**, *57* (5), 1441–1462.

Chen, Q.; Zhang, Z.; Colby, R. H. Viscoelasticity of Entangled Random Polystyrene Ionomers. *J. Rheol.* **2016**, *60* (6), 1031–1040.

Consolante, V.; Marić, M. Nitroxide-Mediated Polymerization of an Organo-Soluble Protected Styrene Sulfonate: Development of Homo- and Random Copolymers. *Macromol. React. Eng.* **2011**, *5* (11–12), 575–586.

Daniel, W. F. M.; Burdyńska, J.; Vatankhah-varnoosfaderani, M.; Matyjaszewski, K.; Paturej, J.; Rubinstein, M.; Dobrynin, A. V; Sheiko, S. S. Solvent-Free , Supersoft and Superelastic Bottlebrush Melts and Networks. **2016**, *15* (February), 183–190.

Das, A.; Sallat, A.; Böhme, F.; Suckow, M.; Basu, D.; Wießner, S.; Stöckelhuber, K. W.; Voit, B.; Heinrich, G. Ionic Modification Turns Commercial Rubber into a Self-Healing Material. *ACS Appl. Mater. Interfaces* **2015**, *7* (37), 20623–20630.

Dobrynin, A. V.; Rubinstein, M. Theory of Polyelectrolytes in Solutions and at Surfaces. *Prog. Polym. Sci.* **2005**, *30* (11), 1049–1118.

Eisenberg, A.; Hird, B.; Moore, R. B. A New Multiplet-Cluster Model for the Morphology of Random Ionomers. *Macromolecules* **1990**, *23* (18), 4098–4107.

Eisenberg, A.; Kim, J.-S. *Introduction to Ionomers*; Wiley: New York, 1998.

Eisenberg, A.; Navratil, M. Ion Clustering and Viscoelastic Relaxation in Styrene-Based Ionomers. II. Effect of Ion Concentration. *Macromolecules* **1973**, *6* (4), 604–612.

Eisenberg, A.; Navratil, M. Ion Clustering and Viscoelastic Relaxation in Styrene-Based Ionomers. IV. X-Ray and Dynamic Mechanical Studies. *Macromolecules* **1974**, *7* (1), 90–94.

Eisenberg, A.; Rinaudo, M. Polymer Bulletin. *Polym. Bull.* **1990**, *24*, 671.

Elliott, J. A.; Hanna, S.; Elliott, A. M. S.; Cooley, G. E. Interpretation of the Small-Angle X-Ray Scattering from Swollen and Oriented Perfluorinated Ionomer Membranes. *Macromolecules* **2000**, *33* (11), 4161–4171.

Enokida, J. S.; Tanna, V. A.; Winter, H. H.; Bryan Coughlin, E. Progression of the Morphology in Random Ionomers Containing Bulky Ammonium Counterions. *Macromolecules* **2018**, *51* (18), 7377–7385.

Ertem, S. P.; Tsai, T.-H.; Donahue, M. M.; Zhang, W.; Sarode, H.; Liu, Y.; Seifert, S.; Herring, A. M.; Coughlin, E. B. Photo-Cross-Linked Anion Exchange Membranes with Improved Water Management and Conductivity. *Macromolecules* **2016**, *49*, 153–161.

Filippidi, E.; Cristiani, T. R.; Eisenbach, C. D.; Herbert Waite, J.; Israelachvili, J. N.; Kollbe Ahn, B.; Valentine, M. T. Toughening Elastomers Using Mussel-Inspired Iron-Catechol Complexes. *Science.* **2017**, *358* (6362), 502–505.

Fitzgerald, J. J.; Weiss, R. A. Synthesis, Properties, and Structure of Sulfonate Ionomers.

J. Macromol. Sci. Part C Polym. Rev. **1988**, *28* (1), 99–185.

Geise, G. M.; Freeman, B. D.; Paul, D. R. Characterization of a Sulfonated Pentablock Copolymer for Desalination Applications. *Polymer.* **2010**, *51* (24), 5815–5822.

Grady, B. P. Effect of Coneutralization on Internal Aggregrate Structure in Ethylene-Based Ionomers. *Macromolecules* **1999**, *32* (9), 2983–2988.

Grady, B. P. Review and Critical Analysis of the Morphology of Random Ionomers Across Many Length Scales. *Polym. Eng. Sci.* **2008**, *48* (6), 1029–1051.

Hahn, S. F. An Improved Method for the Diimide Hydrogenation of Butadiene and Isoprene Containing Polymers. *J. Polym. Sci. Part A Polym. Chem.* **1992**, *30* (3), 397–408.

Hall, L. M.; Stevens, M. J.; Frischknecht, A. L. Dynamics of Model Ionomer Melts of Various Architectures. *Macromolecules* **2012**, *45* (19), 8097–8108.

Hara, M.; Jar, P.; Sauer, J. A. Dynamic Mechanical Properties of Sulfonated Polystyrene Ionomers. *Polymer.* **1991**, *32*, 1622–1626.

Herbst, F.; Döhler, D.; Michael, P.; Binder, W. H. Self-Healing Polymers via Supramolecular Forces. *Macromol. Rapid Commun.* **2013**, *34*, 203–220.

Hickner, M. A.; Ghassemi, H.; Kim, Y. S.; Einsla, B. R.; McGrath, J. E. Alternative Polymer Systems for Proton Exchange Membranes (PEMs). *Chem. Rev.* **2004**, *104*, 4587–4611.

Hickner, M. a.; Herring, A. M.; Coughlin, E. B. Anion Exchange Membranes: Current Status and Moving Forward. *J. Polym. Sci. Part B Polym. Phys.* **2013**, *51* (24), 1727–1735.

Hirasawa, E.; Yamamoto, Y.; Tadano, K.; Yano, S. Effect of Metal Cation Type on the Structure and Properties of Ethylene Ionomers. *J. Appl. Polym. Sci.* **1991**, *42*, 351–362.

Hird, B.; Eisenberg, a. Sizes and Stabilities of Multiplets and Clusters in Carboxylated and Sulfonated Styrene Ionomers. *Macromolecules* **1992**, *25*, 6466–6474.

Ionomers: Synthesis, Structure, Properties and Applications; Tant, M. R., Mauritz, K. A., Wilkes, G. L., Eds.; Chapman & Hall: New York, 1997.

Jerome, R.; Mazurek, M. Synthesis and Characterization of Molecular Structure. In *Ionomers: Synthesis, Structure, Properties and Applications*; Tant, M. R., Mauritz, K. A., Wilkes, G. L., Eds.; Chapman & Hall: New York, 1997; pp 1–31.

Jo, C.; Pugal, D.; Oh, I. K.; Kim, K. J.; Asaka, K. Recent Advances in Ionic Polymer-Metal Composite Actuators and Their Modeling and Applications. *Prog. Polym. Sci.* **2013**, *38* (7), 1037–1066.

Kalista, S. J.; Pflug, J. R.; Varley, R. J. Effect of Ionic Content on Ballistic Self-Healing in EMAA Copolymers and Ionomers. *Polym. Chem.* **2013**, *4* (18), 4910.

Kim, J. S.; Yoshikawa, K.; Eisenberg, A. Molecular Weight Dependence of the Viscoelastic Properties of Polystyrene-Based Ionomers. *Macromolecules* **1994**, *27* (22), 6347–6357.

Kim, J.; Jackman, R. J.; Eisenberg, A. Filler and Percolation Behavior. *Macromolecules* **1994**, *27* (10), 2789–2803.

Kinning, D. J.; Thomas, E. L. Hard-Sphere Interactions between Spherical Domains in Diblock Copolymers. *Macromolecules* **1984**, *17* (9), 1712–1718.

Koberstein, J. T.; Morra, B.; Stein, R. S. The Determination of Diffuse-Boundary Thicknesses of Polymers by Small-Angle X-Ray Scattering. *J. Appl. Crysta.* **1980**, *13* (1), 34–45.

Kucera, F.; Jancar, J. Homogeneous and Heterogeneous Sulfonation of Polymers: A Review. *Polym. Eng. Sci.* **1998**, *38* (5), 783–792.

Kutsumizu, S.; Hara, H.; Tachino, H.; Shimabayashi, K.; Yano, S. Infrared Spectroscopic Study of the Binary Blends of Sodium and Zinc Salt Ionomers Produced from Poly(Ethylene-*co*-Methacrylic Acid) . *Macromolecules* **2002**, *32* (19), 6340–6347.

Lefelar, J. A.; Weiss, R. A. Concentration and Counterion Dependence of Cluster Formation in Sulfonated Polystyrene. *Macromolecules* **1984**, *17* (6), 1145–1148.

Leibler, L.; Rubinstein, M.; Colby, R. H. Dynamics of Reversible Networks. *Macromolecules* **1991**, *24* (16), 4701–4707.

Liu, Y.; Pollock, K. L.; Cavicchi, K. A. Synthesis of Poly(Trioctylammonium p-Styrenesulfonate) Homopolymers and Block Copolymers by RAFT Polymerization. *Polymer.* **2009**, *50* (26), 6212–6217.

López-Barrón, C. R.; Brant, P.; Eberle, A. P. R.; Crowther, D. J. Linear Rheology and Structure of Molecular Bottlebrushes with Short Side Chains. *J. Rheol.* **2015**, *59* (3), 865–883.

MacKnight, W. J.; Taggart, W. P.; Stein, R. S. A Model for the Structure of Ionomers. *J. Polym. Sci. Symp.* **1974**, *45* (45), 113–128.

Mahittikul, A.; Prasassarakich, P.; Rempel, G. L. Noncatalytic Hydrogenation of Natural Rubber Latex. *J. Appl. Polym. Sci.* **2007**, *103*, 2885–2895.

Martin, J. E.; Hurd, A. J. Scattering from Fractals. *J. Appl. Crystal.* **1987**, *20* (2), 61–78.

Matsuura, H.; Eisenberg, A. Glass Transitions of Ethyl Acrylate-Based Ionomers. *J. Polym. Sci. Polym. Phys. Ed.* **1976**, *14* (7), 1201–1209.

McCullough, L. A.; Dufour, B.; Matyjaszewski, K. Incorporation of Poly(2-Acryloamido-2-Methyl-N-Propanesulfonic Acid) Segments into Block and Brush Copolymers by ATRP. *J. Polym. Sci. Part A Polym. Chem.* **2009**, *47* (20), 5386–5396.

Middleton, L. R.; Winey, K. I. Nanoscale Aggregation in Acid- and Ion-Containing Polymers. *Annu. Rev. Chem. Biomol. Eng.* **2017**, *8* (1), 499–523.

Molitor, R. P. Golf Ball Cover Compositions Comprising A Mixture of Ionomer Resins. U.S. Patent 3,819,768, 1974.

Mortimer, D. A. Synthetic Polyelect Rolytes-A Review. *Polym. Int.* **1991**, *25*, 29–41.

Navratil, M.; Eisenberg, A. Ion Clustering and Viscoelastic Relaxation in Styrene-Based Ionomers. III. Effect of Counterions, Carboxylic Groups, and Plasticizers.

Macromolecules **1973**, *7* (1), 84–89.

Nishida, M.; Eisenberg, A. Dynamic Mechanical Study of Sodium Sulfonated Random Ionomers Based on Hydrogenated Styrene-Butadiene Copolymer. *Macromolecules* **1996**, *29* (5), 1507–1515.

Okamura, H.; Takatori, Y.; Tsunooka, M.; Shirai, M. Synthesis of Random and Block Copolymers of Styrene and Styrenesulfonic Acid with Low Polydispersity Using Nitroxide-Mediated Living Radical Polymerization Technique. *Polymer.* **2002**, *43* (11), 3155–3162.

Osborn, S. J.; Hassan, M. K.; Divoux, G. M.; Rhoades, D. W.; Mauritz, K. A.; Moore, R. B. Glass Transition Temperature of Perfluorosulfonic Acid Ionomers. *Macromolecules* **2007**, *40* (10), 3886–3890.

Page, K. A.; Cable, K. M.; Moore, R. B. Molecular Origins of the Thermal Transitions and Dynamic Mechanical Relaxations in Perfluorosulfonate Ionomers. *Macromolecules* **2005**, *38* (15), 6472–6484.

Page, K. A.; Landis, F. A.; Phillips, A. K.; Moore, R. B. SAXS Analysis of the Thermal Relaxation of Anisotropic Morphologies in Oriented Nafion Membranes. *Macromolecules* **2006**, *39* (11), 3939–3946.

Paturej, J.; Sheiko, S. S.; Panyukov, S.; Rubinstein, M. Molecular Structure of Bottlebrush Polymers in Melts. *Sci. Adv.* **2016**, *2* (11).

Peckham, T. J.; Holdcroft, S. Structure-Morphology-Property Relationships of Non-Perfluorinated Proton-Conducting Membranes. *Adv. Mater.* **2010**, *22* (42), 4667–4690.

Perrin, P.; Prud'homme, R. E. SAXS Measurements of Interfacial Thickness in Amorphous Polymer Blends Containing a Diblock Copolymer. *Macromolecules* **1994**, *27* (7), 1852–1860.

Phillips, A. K.; Moore, R. B. Mechanical and Transport Property Modifications of Perfluorosulfonate Ionomer Membranes Prepared with Mixed Organic and Inorganic Counterions. *J. Polym. Sci. Part B Polym. Phys.* **2006**, *44*, 2267–2277.

Phillips, A. K.; Moore, R. B. Mechanical and Transport Property Modification of Perfluorosulfonate Ionomer Membranes Prepared with Mixed Organic and Inorganic Counterions. *J. Polym. Sci. Part B Polym. Phys.* **2006**, *44*, 2267–2277.

Phinyocheep, P.; Pasiri, S.; Tavichai, O. Diimide Hydrogenation of Isoprene-Styrene Diblock Copolymers. *J. Appl. Polym. Sci.* **2003**, *87* (1 SPEC.), 76–82.

Plate, N. A.; Shibaev, V. P. Comb-Like Polymers. Structure and Properties. *J. Polym. Sci. Macromol. Rev.* **1974**, *8*, 117–253.

Read, B. B. E.; Carter, E. A.; Connor, T. M.; Macknightt, W. J. Structure and Properties of Ethylene-Methacrylic Acid Copolymers and Their Sodium Salts: Dielectric and Proton Magnetic Relaxation Studies. *Br. Polym. J.* **1969**, *1*, 123–131.

Rees, R. W.; Vaughan, D. J. "Surlyn," An Ionomer. 1. The Effect of Ionic Bonding on Polymer Structure. *ACS Polym. Prepr.* **1965**, *6*, 287–295.

Ricks-Laskoski, H. L.; Snow, A. W. Synthesis and Electric Field Actuation of an Ionic Liquid Polymer. *J. Am. Chem. Soc.* **2006**, *128* (38), 12402–12403.

Russell, T. P.; Ito, H.; Wignall, G. D. Neutron and X-Ray Scattering Studies on Semicrystalline Polymer Blends. *Macromolecules* **1988**, *21* (6), 1703–1709.

Salas-De La Cruz, D.; Green, M. D.; Ye, Y.; Elabd, Y. A.; Long, T. E.; Winey, K. I. Correlating Backbone-to-Backbone Distance to Ionic Conductivity in Amorphous Polymerized Ionic Liquids. *J. Polym. Sci. Part B Polym. Phys.* **2012**, *50* (5), 338–346.

Siadat, B.; Lundberg, R. D.; Lenz, R. W. Solubility Behavior of Copolymers of Isoprene and Sodium Styrenesulfonate. *Macromolecules* **1981**, *14*, 773–776.

Siadat, B.; Oster, B.; Lenz, R. W. Preparation of Ion-Containing Elastomers by Emulsion Copolymerization of Dienes with Olefinic Sulfonic Acid Salts. *J. Appl. Polym. Sci.* **1981**, *26*, 1027–1037.

Siadat, B.; Oster, B.; Lenz, R. W. Preparation of Ion-containing Elastomers by Emulsion Copolymerization of Dienes with Olefinic Sulfonic Acid Salts. *J. Appl. Polym. Sci.* **1981**, *26* (3), 1027–1037.

Soloveichik, G. L. Flow Batteries : Current Status and Trends. *Chem. Rev.* **2015**, *115*, 11533–11558.

Tachino, H.; Hara, H.; Hirasawa, E.; Kutsumizu, S.; Tadano, K.; Yano, S. Dynamic Mechanical Relaxations of Ethylene Ionomers. *Macromolecules* **1993**, *26* (4), 752–757.

Tachino, H.; Hara, H.; Hirasawa, E.; Kutsumizu, S.; Yano, S. Structure and Properties of Ethylene Ionomers Neutralized with Binary Metal Cations. *Macromolecules* **1994**, *27* (2), 372–378.

Tadano, K.; Hirasawa, E.; Yamamoto, H.; Yano, S. Order—Disorder Transition of Ionic Clusters in Ionomers. *Macromolecules* **1989**, *22* (1), 226–233.

Taubert, A.; Winey, K. I. Imaging and X-Ray Microanalysis of a Poly(Ethylene-Ran-Methacrylic Acid) Ionomer Melt Neutralized with Sodium. *Macromolecules* **2002**, *35* (19), 7419–7426.

Tierney, N. K.; Register, R. A. Synthesis and Melt Dynamics of Model Sulfonated Ionomers. *Macromolecules* **2003**, *36* (4), 1170–1177.

Tsai, T.-H.; Ertem, S. P.; Maes, A. M.; Seifert, S.; Herring, A. M.; Coughlin, E. B. Thermally Cross-Linked Anion Exchange Membranes from Solvent Processable Isoprene Containing Ionomers. *Macromolecules* **2015**, *48* (3), 655–662.

Tudryn, G. J.; Liu, W.; Wang, S. W.; Colby, R. H. Counterion Dynamics in Polyester-Sulfonate Ionomers with Ionic Liquid Counterions. *Macromolecules* **2011**, *44* (9), 3572–3582.

Turner, S. R.; Weiss, R. A.; Lundberg, R. D. The Emulsion Copolymerization of Styrene and Sodium Styrene Sulfonate. *J. Polym. Sci. Polym. Chem. Ed.* **1985**, *23* (2), 535–548.

Varley, R. J.; Shen, S.; van der Zwaag, S. The Effect of Cluster Plasticisation on the Self Healing Behaviour of Ionomers. *Polymer.* **2010**, *51* (3), 679–686.

Varley, R. J.; van der Zwaag, S. Towards an Understanding of Thermally Activated Self-Healing of an Ionomer System during Ballistic Penetration. *Acta Mater.* **2008**, *56* (19), 5737–5750.

Verrall, R. E.; Burns, J. A. The Mass Spectrometry of the Pyrolysis Products of Some Tetraalkylammonium and Bistetraalkylammonium Bromides. *Can. J. Chem.* **2006**, *52* (19), 3438–3443.

Wang, D.; Guo, J.; Zhang, H.; Cheng, B.; Shen, H.; Zhao, N.; Xu, J. Intelligent Rubber with Tailored Properties for Self-Healing and Shape Memory. *J. Mater. Chem. A* **2015**, *3* (24), 12864–12872.

Ward, T. C.; Tobolsky, A. V. Viscoelastic Study of Ionomers. *J. Appl. Polym. Sci.* **1967**, *11* (12), 2403–2415.

Weiss, R. A.; Agarwal, P. K.; Lundberg, R. D. Control of Ionic Interactions in Sulfonated Polystyrene Ionomers by the Use of Alkyl- Substituted Ammonium Counterions. *J. Appl. Polym. Sci.* **1984**, *29*, 2719–2734.

Weiss, R. A.; Fitzgerald, J. J.; Kim, D. Viscoelastic Behavior of Lightly Sulfonated Polystyrene Ionomers. *Macromolecules* **1991**, *24* (5), 1071–1076.

Weiss, R. A.; Lundberg, R. D.; Turner, S. R. Comparisons of Styrene Ionomers Prepared by Sulfonating Polystyrene and Copolymerizing Styrene with Styrene Sulfonate. *J. Polym. Sci. Polym. Chem. Ed.* **1985**, *23* (2), 549–568.

Weiss, R. A.; Lundberg, R. D.; Werner, A. The Synthesis of Sulfonated Polymers by Free Radical Copolymerization. Poly(Butadiene-Co-Sodium Styrene Sulfonate). *J. Polym. Sci. Polym. Chem. Ed.* **1980**, *18* (12), 3427–3439.

Weiss, R. A.; Yu, W. Viscoelastic Behavior of Very Lightly Sulfonated Polystyrene Ionomers. *Macromolecules* **2007**, *40* (10), 3640–3643.

Weiss, R. A.; Zhao, H. Rheological Behavior of Oligomeric Ionomers. *J. Rheol.* **2009**, *53* (1), 191–213.

Winey, K. I. Designing Tougher Elastomers with Ionomers. *Science.* **2017**, *358* (6362), 449–450.

Winey, K. I.; Laurer, J. H.; Kirkmeyer, B. P. Ionic Aggregates in Partially Zn-Neutralized Poly(Ethylene-Ran-Methacrylic Acid) Ionomers: Shape, Size, and Size Distribution. *Macromolecules* **2000**, *33* (2), 507–513.

Woeste, G.; Meyer, W. H.; Wegner, G. Copolymers of Ethyl P-Vinylbenzenesulfonate for the Preparation of Polyelectrolytes of Reproducible Ion Content. *Makromol. Chemie* **1993**, *194*, 1237–1248.

Wu, D. Y.; Meure, S.; Solomon, D. Self-Healing Polymeric Materials: A Review of Recent Developments. *Prog. Polym. Sci.* **2008**, *33* (5), 479–522.

Xu, C.; Cao, L.; Lin, B.; Liang, X.; Chen, Y. Design of Self-Healing Supramolecular Rubbers by Introducing Ionic Cross-Links into Natural Rubber via a Controlled

Vulcanization. *ACS Appl. Mater. Interfaces* **2016**, *8* (27), 17728–17737.

Yang, S.; Sun, K.; Risen, W. M. Preparation and Thermal Characterization of the Glass Transition Temperatures of Sulfonated Polystyrene-metal Ionomers. *J. Polym. Sci. Part B Polym. Phys.* **1990**, *28* (10), 1685–1697.

Yang, Y.; Urban, M. W. Self-Healing Polymeric Materials. *Chem. Soc. Rev.* **2013**, *42* (17), 7446.

Yarusso, D. J.; Cooper, S. L. Microstructure of Ionomers: Interpretation of Small-Angle X-Ray Scattering Data. *Macromolecules* **1983**, *16* (12), 1871–1880.

Zander, Z. K.; Wang, F.; Becker, M. L.; Weiss, R. A. Ionomers for Tunable Softening of Thermoplastic Polyurethane. *Macromolecules* **2016**, *49*, 926–934.

Zhang, L.; Brostowitz, N. R.; Cavicchi, K. A.; Weiss, R. A. Perspective : Ionomer Research and Applications. *Macromol. React. Eng.* **2014**, *8*, 81–99.

Zhang, Z.; Liu, C.; Cao, X.; Wang, J. H.; Chen, Q.; Colby, R. H. Morphological Evolution of Ionomer / Plasticizer Mixtures during a Transition from Ionomer to Polyelectrolyte. *Macromolecules* **2017**, *50*, 963–971.

Zhou, N. C.; Chan, C. D.; Winey, K. I. Reconciling STEM and X-Ray Scattering Data To Determine the Nanoscale Ionic Aggregate Morphology in Sulfonated Polystyrene. *Macromolecules* **2008**, *41* (16), 6134–6140.

Zhou, Z. L.; Eisenberg, A. Dynamic Mechanial Properties of Sulfonated Cyclized Cis-1,4-polyisoprene. *J. Appl. Polym. Sci.* **1982**, *27* (2), 657–671.